Preparation and Studies on Polycarbonate Matrix Nanocomposites for Electronic Applications

Ph.D. Thesis

Pramod Kumar Sain
(2010RMT101)

Department of Metallurgical and Materials Engineering
Malaviya National Institute of Technology Jaipur, India

November, 2015

Preparation and Studies on Polycarbonate Matrix Nanocomposites for Electronic Applications

This thesis is submitted as a partial fulfilment of
the Ph.D. programme in Engineering

Pramod Kumar Sain
(2010RMT101)

Department of Metallurgical and Materials Engineering
Malaviya National Institute of Technology Jaipur, India

November, 2015

The thesis is dedicated to my beloved parents for their unconditional love and encouragement.....

MALAVIYA NATIONAL INSTITUTE OF TECHNOLOGY JAIPUR
DEPARTMENT OF MECHANICAL ENGINEERING

CERTIFICATE

This is to certify that the thesis entitled **"Preparation and Studies on Polycarbonate Matrix Nanocomposites for Electronic Applications"** is being submitted by **Mr. Pramod Kumar Sain (ID: 2010RMT101)**, to the Malaviya National Institute of Technology Jaipur for the award of the degree of **Doctor of Philosophy** in **Metallurgical and Materials Engineering**, is a bonafide record of original research work carried out by him. He has worked under our guidance and supervision and has fulfilled the requirement for the submission of this thesis, which has reached the requisite standard.

The results contained in this thesis have not been submitted in part or full, to any other University or Institute for the award of any degree or diploma.

Prof. A. K. Bhargava
Dept. of Met. & Mat. Engineering
MNIT, Jaipur, India

Dr. Y.V.S.S. Prasad
Dept. of Met. & Mat. Engineering
MNIT, Jaipur, India

Dr. R. K. Goyal
Dept. of Met. & Mat. Science
COEP, Pune, India

CERTIFICATE

This is to certify that the thesis entitled "**Preparation and Studies on Polycarbonate Matrix Nanocomposites for Electronic Applications**" is being submitted by me to the Malaviya National Institute of Technology Jaipur for the award of **Doctor of Philosophy** in Metallurgical and Materials Engineering, is a bonafide record of original research work carried out by me. The content of the thesis has been checked using software "Plagiarism Detector".

I have incorporated all the suggestions/queries/changes raised by the Examiner in the Thesis Evaluation Reports.

(Pramod Kumar Sain)

This is to certify that the above statement made by the candidate is true to our knowledge.

(Prof. A. K. Bhargava)	**(Dr. Y. V. S. S. Prasad)**	**(Dr. R. K. Goyal)**
Supervisor	Supervisor	Supervisor

Ph.D. viva-voce examination of Mr. Pramod Kumar Sain, Research Scholar, was held on 26-11-2015 in the seminar hall of the department of Metallurgical and Materials Engineering, MNIT Jaipur. The candidate defended the viva-voce successfully to the satisfaction of Oral Defense Committee. The Committee recommends for the award of Ph.D. Degree.

Signature of Supervisor(s) **Signature of External Examiner**

ACKNOWLEDGEMENTS

First and foremost, I am really indebted to my thesis supervisor **Prof. A. K. Bhargava** who provided me precious opportunity to pursue research under his guidance. His guidance put me on a new platform of wonderful and challenging materials world. His unique guiding quality, interest, working enthusiasm and analytical approach towards the experimental results impressed me so much. It is great honour for me to work with him. I am grateful to **Dr. Y.V.S.S. Prasad**, co-supervisor for my Ph.D. work, for his consistent guidance and encouragement throughout my Ph.D. work. He has been a great source of inspiration for me. My special thanks go to **Dr. R. K. Goyal**, Associate Professor, College of Engineering Pune (COEP), Pune, external joint supervisor, who offered me the opportunity to join his research group and to work in his leading nanotechnology laboratory. His research experience in the nanotechnology field has motivated and benefited me a lot. I would like to express my sincere thanks to **Prof. U. Pandel**, and **Prof. C. P. Sharma** for being in my DREC committee as well as for their encouragement, analytical insights and recommendations.

I further extend my thanks to **Dr. K. B. Sharma**, Principal, Subodh PG College, Jaipur, **Prof. B. K. Shrivastava**, Department of Physics, University of Rajasthan, **Dr. Vibhav Saraswat,** Banasthanli Universtiy for providing characterization facilities. I express my sincere gratitude to **Er. N. Singh,** Principal, Govt. Polytechnic College, Baran and **Er. Neeraj Sharma**, Principal, Govt. Polytechnic College Bharatpur for their cooperation during Ph.D. work**.** Thanks are also due to the researchers from different countries, their valuable discussions through research sites made me confident about the different results. I express my deep appreciation to my friends and co-workers **Dr. Satish Tailor**, **Mr. Ornov Maulik, Mohtashim Reza, Archana Gupta (COEP), Jyoti, Garima Kedawat, Anil**, and all the research scholars from the department of Metallurgical and Materials Engineering, MNIT Jaipur for their moral support and help. I would like to extend my sincere thanks to all the faculty and staff members of MNIT, Jaipur for their support during my Ph.D. life.

I would like to thank my parents and my family members for their unconditional love and support. Without them, this thesis would not be possible.

(Pramod Kumar Sain)

ABSTRACT

The work is undertaken to prepare and study polycarbonate (PC) based nanocomoposites for electronic applications. Polycarbonate has been selected due to the good combination of electrical, mechanical and thermal properties exhibited by it. As filler materials, lead zirconate titanate (PZT), Cu nano particles, multi-walled carbon nanotubes (MWCNT), single-walled carbon nanotubes (SWCNT) and few-layer-graphene (FLG) have been used. The FLG has been prepared using dry ice method. The micro-/nanocomposites have been prepared using solution method. Five two-phase micro-/nanocomposite systems and two three-phase nanocomposite systems have been prepared. X-ray diffractometry (XRD), Raman spectroscopy, differential scanning calorimetry (DSC), transmission electron microscopy (TEM), scanning electron microscopy (SEM), energy dispersive X-ray spectroscopy (EDS) have been used to characterize the matrix, filler and the composite/nanocomposites. The electrical properties have been evaluated using Precision impedance analyzer. X-ray diffraction analysis confirmed the presence of filler in the composite and the induced crystallinity in the PC due to solution mixing. With the help of DSC analysis, the effects of solution treatment, filler addition on glass transition temperature and melting point of the micro-/nanocomposites have been studied. TEM and SEM analyses have revealed out micro-/nanostructural information of the fillers and nanocomposites. EDS study has presented elemental information for Cu-PZT-PC nanocomposite. Among all the studied micro-/nanocomposites, the SWCNT-PC nanocomposite exhibited the percolation at minimum concentration of filler. The percolation threshold was found to occur at 0.5 vol % of SWCNT and the maximum achieved conductivity in this system was 10^{-4} S/cm (at 3 vol % of SWCNT). The highest augment in the dielectric constant, with controlled dissipation factor, was found in FLG/PC nanocomposites. The achieved dielectric constant, in smearing reason, was 70 with 0.07 dissipation factor (at 3 vol % of FLG). At higher filler concentration, i.e at 3.5 vol %, the FLG-PC nanocomposite fully percolated and the maximum achieved conductivity was 10^{-2} S/cm with 4.22 vol % of FLG. The dielectric constant and dissipation factor have been examined with varying frequency and temperature. The FLG-PC nanocomposite is the best output of this research work. It could be used as versatile polymer nanocomposite dielectric material below percolation and as conducting material beyond percolation.

LIST OF FIGURES

LIST OF TABLES

ABBREVIATIONS AND SYMBOLS

E	-	Applied Electrical Field
$\in^*$	-	Complex permittivity
DSC	-	Differential Scanning Calorimetry
Tan δ	-	Dissipation Factor
σ	-	Electrical Conductivity
EMI	-	Electromagnetic Interference
ESD	-	Electrostatic Dissipation
EDS	-	Energy Dispersive X-ray Spectroscopy
EG	-	Expanded Graphite
FLG	-	Few Layer Graphene
f	-	Frequency of Applied Electrical Field
GF	-	Graphite Flakes
HDPE	-	High density polyethylene
$\in''$	-	Imaginary Part of Permittivity
PZT	-	Lead Zirconate Titanate
LLDPE	-	Linear Low-Density Polyethylene
LDPE	-	Low-Density Polyethylene
MWCNT	-	Multi Walled Carbon Nanotube
Φ_c	-	Percolation Threshold
PFCB	-	Perfluorocylcobutene
PMMA	-	Poly methyl methacrylate
PVDF	-	Poly(vinylidene fluoride)
PC	-	Polycarbonate
PEEK	-	Polyetheretherketone
PE	-	Polyethylene
PET	-	Polyethylene terephthalate
PMCs	-	Polymer Matrix Composites
PNCs	-	Polymer Matrix Nanocomposites
PPS	-	Polyphenylene sulphide
PP	-	Polypropylene
PVC	-	Polyvinyl chloride
PCB	-	Printed Circuit Board
RFI	-	Radio Frequency Interference
$\in'$	-	Real Part of Permittivity
rGO	-	Reduced Graphene oxide
SEM	-	Scanning Electron Microscopy
SE	-	Shielding Effectiveness
SWCNT	-	Single Walled Carbon Nanotube
TEM	-	Transmission Electron Microscopy
XRD	-	X-ray Diffractometry

CHAPTER 1

INTRODUCTION

There has been increasing interest in developing new materials those can be successfully used in modern microelectronics. It has been reported that more than 70 percent area of printed circuit board (PCB) is occupied by passive components (i.e. resistors, capacitors and inductors) which are individually mounted on the surface of electronic package [1]. Due to such passives the number of long interconnections and solders point are very high which reduces the reliability and performance of the electronic circuit. Therefore, these mounted passive components restrict the improvement in the reliability, performance and the miniaturization of electronic circuits. Embedding these passive components in the substrate can reduce the solder joints, long interconnections and the size of the circuit which ultimately improves the reliability and performance. Among the passive components, the capacitors, having higher capacitance with shorter distance from the serving component has been the centre of focus due to various important functions including timing, filtering and bypassing.

Ceramics, such as barium titanate ($BaTiO_3$), lead zirconate titanate ($PbZrTiO_3$), barium strontium titanate ($BaSrTiO_3$), $CaCu_3Ti_4O_{12}$ (CCTO), and so on exhibit high dielectric constant and low dissipation factor and hence suitable for capacitor applications. They not only find wide applications in capacitors but also in other devices such as transducers, ultrasound imaging, actuators, data storage devices, thermistors, oscillators, filters, light deflectors, modulators, non-volatile memories, piezoelectric transducers, and heat sensors [1-7]. However, their high processing temperature and brittle behaviour make them not suitable for embedding them in PCB which begins to thermally degrade above the temperature of 250 ^{o}C.

Polymeric materials are the possible candidate for such embedding technology due to the low processing temperatures and flexibility but they possess inherently low dielectric constant in the range of 3-5 [1]. During few last decades there has been trend to improve dielectric constant of polymers by addition of ferroelectric ceramics including $BaTiO_3$, $PbZrTiO_3$, $BaSrTiO_3$, $CaCu_3Ti_4O_{12}$ (CCTO), etc. as filler component. A combination of these two components, in right proportions is expected

to result in a composite with right combination of dielectric constant, dissipation factor and flexibility and hence make these composites interesting for above discussed electronic applications.

It has been observed that to significantly increase the dielectric constant (up to 10 times of base polymer) of the polymer matrix composite, a high concentration (greater than 40 vol %) of ferroelectric ceramic filler is required. However, this makes the composite brittle in nature [8-10]. It has also been reported that the dielectric constant of the ceramic matrix can also be increased by reinforcing/adding metallic filler such as Al, Ni, Cu, Ag, etc. in discrete form [11], but the metallic particles may get oxidized during sintering**.** Though, Platinum and Palladium show very good oxidation resistance but their cost is very high. A combination of both ferroelectric ceramic and conductive filler has also been used in polymer matrix in anticipation of enhancement of dielectric constant of polymer matrix composites [11-16] but in such composites, the required filler concentration is still high. High concentration of filler in the composite might deteriorate the advantageous flexibility, toughness and thermal stability of the base polymer.

In the light of the above, the present research work is an attempt to prepare a light weight flexible polymer matrix composite by introducing a low volume concentration of dielectric ceramic and/or conductive nanosize filler in a high performance polymer matrix. As high performance polymer matrix, Polycarbonate (PC) has been selected. As filler materials PZT, nano-size copper powder, MWCNT, SWCNT, and FLG have been used to make two and three-phase micro-/nanocomposites. PZT is ferroelectric ceramic having dielectric constant value of about 1100 and dissipation factor value of about 0.001. nanocopper powder, MWCNT, SWCNT and FLG are the conductive fillers and due to nano-size they possess high surface area to volume ratio. High surface to volume ratio is beneficial for generating large interfacial area between filler and matrix. The solution method was adopted to prepare the micro-/nanocomposites. The micro-/nanocomposite pellets of 13mm dia, 2 mm thickness were prepared for further studies.

The filler, matrix and micro-/nanocomposites, have been characterized using, XRD, Raman spectroscopy, TEM, SEM, EDS, and DSC methods. Electrical properties were measured/evaluated using Precision impedance analyzer. Among

studied nanocomposites, in SWCNT-PC nanocomposites, the percolation threshold was found at minimum volume concentration of filler (i.e. at 0.5 vol %) and the maximum achieved order of magnitude of conductivity was found to be 10^{-4} S/cm (at 3 vol %). The maximum achieved level of conductivity was also observed in FLG-PC nanocomposite which is 10^{-2} S/cm (at 4.22 vol % of FLG).

The dielectric constant of all the composites was increased as the filler concentration increased. In conductive filler filled nanocomposites, in addition to the increment in the dielectric constant, it was found that below percolation the dissipation factor was remained in tolerable limit. As the filler concentration reached to the level required for percolation, the dissipation factor increased abruptly which is not desirable for a good dielectric material. For instance, the dielectric constant of the SWCNT-PC (at 1 vol % of SWCNT) nanocomposites increased abruptly to the order of 10^3 but at the same time the dissipation factor also increased to the value of about 9, which is very high from application point of view. However, such polymeric composites may find applications for electromagnetic interference (EMI) shielding and electrostatic dissipation (ESD). The significant improvement in the dielectric properties was observed for FLG-PC nanocomposite (at 3 vol %) in which the dielectric constant increased to a value of 70 with dissipation factor of 0.07 (measured at 1 kHz). These data are very interesting for the application point of view in embedded capacitor technology.

The dielectric behaviour of the studied micro-/nanocomposites was examined by varying frequency of applied electrical field and the temperature. As a general trend the value of dielectric constant was decreasing with increasing frequencies. The dissipation factor showed a mixed behaviour, however as a general trend, it was noted that below percolation it showed very slight increasing trend with increasing frequency but beyond percolation it was decreasing almost linearly. The temperature dependence revealed that the dielectric behaviour of micro-/nanocomposite not much affected by the temperature up to 100 °C.

As the output of this research work it is suggested that the FLG-PC nancomposite (at 3 vol %) may be suitable flexible and high dielectric constant material for embedded capacitors. This can be a very good candidate material for various embedded capacitor applications requiring dielectric constant value greater

than 10 [1]. The nanocomposites, beyond percolation, e.g. SWCNT-PC (at greater than 1 vol %) and FLG-PC (greater than 3.6 vol %) nanocomposites, may be good candidate for EMI shielding and ESD applications.

CHAPTER 2

LITERATURE REVIEW

In the present world of modern electronics, everyone is enjoying life with different-different devices in hand. Laptops, mobile phones, tablets, are some common examples of modern electronic devices. Such overwhelming progress in electronics is due to the newer and newer materials which made it possible to reduce the size and performance of electronic circuitry. Due to low cost materials, the devices are now so cost effective that these are approachable to common man. In specific areas like aerospace and medical, performance is of much importance than the cost. So, the research for developing advanced materials is on top worldwide.

2.1 Need of advanced materials in modern electronics

With new technologies the electronic circuits are becoming smaller and smaller in size with increased density of components. According to Moore's law for device density; the number of active components (i.e. transistors) on a single chip is doubling per 1.5 to 2 years as depicted in Figure 2.1[17].

With high density of electronic components for better performance, miniaturization of electronic circuit is in demand for specific areas like aerospace, and medical. Consumer trend towards compact, portable and smarter devices that work faster is attracting the researcher's attention to further miniaturize the electronic components. In mounted component technology, there is a limit of miniaturization of electronic circuits. In a typical electronic circuit, discrete passive components are more than active components by several times and occupy more than 70% area of the substrate [18]. Hence, the discrete passives are the major barrier in the way of miniaturization of the electronic systems. The ratio of the decoupling capacitor to the total passives can be more than 60%. The passives not only occupy the large surface area of the substrate but also lower the performance and reliability of the device due to long interconnections and large number of solder joints [19].

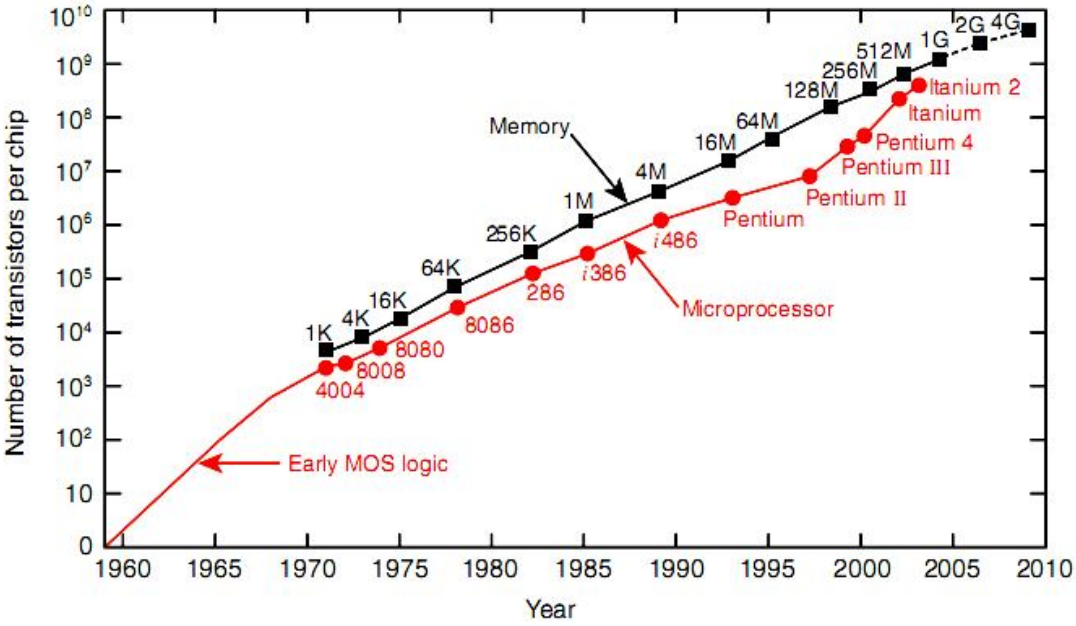

Figure 2.1. Moore's law presenting the transistor's density on a single chip, doubling per 1.5 to 2 year [17]

In order to achieve the desired electrical performance with miniaturization, there have been extensive studies for embedding passive components in microelectronics package. Embedding these components between the interconnecting flexible substrate of a printed wiring board aids better electrical performance, higher reliability due to reduced solder joints, lower cost and improved design options [20]. Among the various embedded passives the embedded capacitors are used in relatively large number of applications such as bypassing, signal decoupling, filtering, switching, tuning and noise suppression, etc. [19]. Hence embedded capacitors call for special attention. In addition, increasing integrated circuit (IC) speed requires decoupling capacitor with higher capacitance and shorter distance from its serving components to increase switch performance [1]. Schematic view for discrete and embedded passives is shown in Figure 2.2 [21].

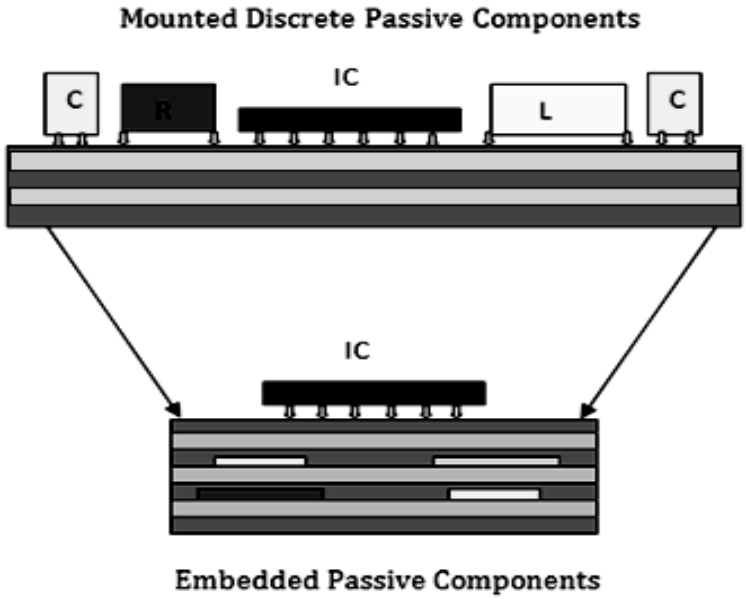

Figure 2.2. Schematic view showing comparison between discrete and embedded passive components [21].

The most challenging task in implementing the embedded capacitor technology is to develop new dielectric materials having good dielectric and mechanical properties coupled with good processabilities and compatibility with flexible organic substrate. For high dielectric constant, several ferroelectric ceramics including $BaTiO_3$, $PbZrTiO_3$, $BaSrTiO_3$, $CaCu_3Ti_4O_{12}$ (CCTO), etc. have been used. These high dielectric constant ceramics are widely used in capacitors and other applications such as transducers, ultrasound imaging, actuators, data storage devices, thermistors, oscillators, filters, light deflectors, modulators, non-volatile memories, piezoelectric transducers, and heat sensors [22-27]. However, their high processing temperature (> 1000 ^{0}C for sintering) increases the cost of the final product. Some ceramic-based systems having lower sintering temperature (< 820 ^{o}C) with good microwave dielectric properties have been reported [28] but still they are not compatible for embedded technology.

The dielectric constant of the ceramic matrix can be increased by reinforcing/adding metallic powder such as Al, Ni, Cu, Ag, etc. [11], but the metallic particles may get oxidized during sintering**.** Though, Platinum and Palladium show very good oxidation resistance but their cost is very high. Hence, newer and advanced dielectric materials are needed for embedded capacitor. In view of above, a brief

account of the dielectric materials and EMI shields is discussed in the subsequent paragraphs.

2.2 Dielectric Materials

Dielectrics are the materials which do not have free or loosely bound electrons that may drift though the material when placed in an electric field. Hence, the dielectrics are insulating materials. However, when the dielectrics are placed in an electric field the positive and negative charges displace slightly with restricted motion so as to make balance with the electric field. This slight displacement of charges stores energy in the form of electrostatic energy.

The force between two electric charges in a dielectric medium is less than it would be in a vacuum, while the quantity of energy stored in an electric field per unit volume of a dielectric medium is greater. The capacitance of a capacitor is related to the dielectric constant of the medium used between the conducting plates of the capacitor. The capacitance of a capacitor filled with a dielectric is greater than it would in the absence of dielectric. The effects of the dielectric on electrical phenomena are described by employing the concepts of polarization, permittivity, dielectric constant and dissipation factor. These concepts are discussed in the following sections.

2.2.1 Polarization

As the name implies, the process of pole making is called the polarization. When it is related to electrical poles i.e. poles due to the negative and positive charges, it is called the electric polarization.

When a dielectric material is placed in an external electric field, the nuclei and electrons related to different atoms/molecules are pushed with the field resulting in an increased positive charge on one side and increased negative charge on the other side. This process is known as electrical polarization and a dielectric material in such a state is said to be electrically polarized. When the field released, the un-relaxed state falls back into a relaxed state. This un-relaxed state of charge distribution increases the

energy of the system and hence the dielectric materials are generally used to store energy in the form of electrostatic energy.

Polarization could be measured by electric **dipole moment (*p*)**, which equals the distance between the slightly shifted centres of positive and negative charge multiplied by the amount of one of the charges. The polarization *P* in a solid is the measure of electric dipole moment per unit volume (*V*) as given in Eq. (2.1).

$$P = p/V \tag{2.1}$$

There are two principal methods by which a dielectric can be polarized: *stretching and rotation*. Dipole moment is induced in every atom/molecule when the atom/molecule stretched by the applied electrical filed. The polarization due to stretching is depicted in the Figure 2.3.

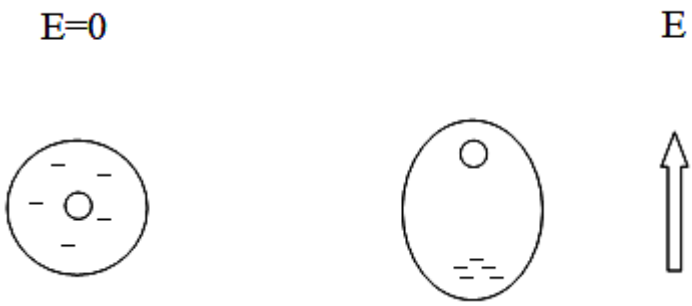

Figure 2.3. Presentation of polarization by stretching [29].

Polarization due to rotation occurs in the polar molecules which possesses permanent dipole moment. The scheme for polarization by rotation is depicted in Figure 2.4 for water molecule.

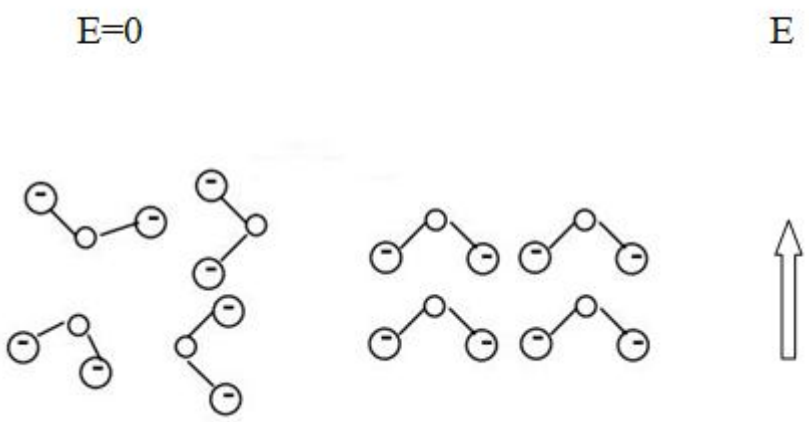

Figure 2.4. Presentation of polarization by rotation [29].

2.2.2 Permittivity

It is a constant of proportionality that relates the electric field in a material to the electric displacement in that material. It characterizes the tendency of the atomic charge in an insulating material to distort in the presence of an electric field. Larger the tendency for charge distortion more is the value of the permittivity. The permittivity of an insulating material is commonly symbolized by the Greek letter epsilon, ε; the permittivity of vacuum, or free space, is symbolized as ε_o.

2.2.3 Dielectric Constant

The ratio of permittivity of any dielectric and the permittivity of free space or vacuum i.e. the ratio $\varepsilon/\varepsilon_0$ is called the dielectric constant, is symbolized by the Greek letter kappa, κ. In the rationalized *mks* and *SI* systems, the magnitude of the permittivity of vacuum ε_0 is 8.854×10^{-12}. The unit of permittivity is square coulombs per Newton square metre or Farad/m. In the mks system, permittivity ε and the dimensionless dielectric constant κ are formally distinct and related by the permittivity of free space $\in_0$; $\in = \kappa \in_0$. In the centimetre-gram-second (cgs) system, the value of the permittivity of free space $\in_0$ is chosen arbitrarily to be 1. Thus, the permittivity ε and the dielectric constant κ in the *cgs* system are identical; both of them are dimensionless numbers. In usual practice some authors symbolize dielectric

constant as k and other symbolize as ε. The symbol ε will be used for the dielectric constant throughout this thesis.

2.2.4 Dissipation Factor

The permittivity is represented as a complex quantity in a manner expressed in Eq. (2.2).

$$\in^* = \in' - \mathbf{j}\in'' \qquad \textbf{(2.2)}$$

Where $\in^*$ is the complex permittivity, $\in'$ is the real part of permittivity and ε" is the imaginary part of permittivity. The real part of permittivity ($\in'$) is a measure of how much energy from an external electric field is stored in a dielectric material. The imaginary part of permittivity ($\in''$) is called the loss part and is a measure of how dissipative or lossy a material is to an external electric field. When complex permittivity is drawn as a simple vector diagram as in Figure 2.5, the real and imaginary components are 90°out of phase. The vector sum forms an aεngle δ with the real part ($\in'$).

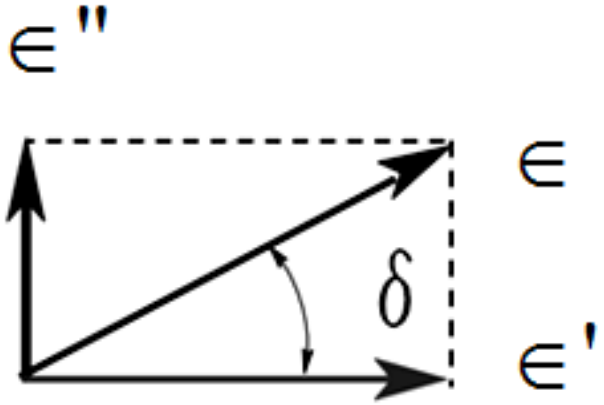

Figure 2.5. Vector representation of real and imaginary part of permittivity

The relative "lossiness" of a material is the ratio of the energy lost to the energy stored. The loss tangent or tan δ or dissipation factor (D) is defined as the ratio of the imaginary part of the dielectric constant to the real part as expressed in Eq. (2.3)

$$D = \tan \delta = \in'' / \in' \quad \textbf{(2.3)}$$

The energy loss (W) in a dielectric material in proportional to the dielectric loss tangent, which can be expressed by the following relation in Eq. (2.4) [29]

$$W \approx \pi \in' E^2 f \tan \delta \quad \textbf{(2.4)}$$

Where, E is the applied field strength and *f* is the frequency. A dissipation factor under 0.1 percent is considered to be quite low and 5 percent is high [29].

2.3 Electromagnetic Interference (EMI) Shielding

EMI shielding is a practice to reduce the electromagnetic field in a space by using specific jamming material. Generally, the field is reduced or blocked due to reflection and/or absorption of electromagnetic radiation by the material [30-31]. Electromagnetic wave e.g. radio waves, emanating from cellular/mobile phones tend to interfere with other nearby electronic devices e.g. computer or television and thereby causes disturbance in proper signal supply. EMI shield of both electronic device and radiation source is needed. EMI shielding mechanisms are illustrated in Figure 2.6.

Reflection is the primary mechanism of EMI shielding. The materials used for EMI shield, must have free charge carriers, which respond to the electromagnetic field in the radiation. That means the material should be electrically conducting. A volume resistivity of the order of 1.0 Ω.cm is typically sufficient [30]. Metals are good materials for EMI shields but they have poor wear and scratch resistance. Secondary mechanism of EMI shielding is absorption. The radiation is significantly absorbed if the shield possesses electric and/or magnetic dipoles which respond to the electromagnetic fields in the radiation.

Third mechanism of shielding is multiple reflections in which the radiation is reflected at various surfaces or interfaces in the shield. This mechanics requires the presence of a large surface area or interface area in the shield. An example of a shield with large surface area is a porous or foam material. An example of a shield material

having large interface area is a composite material containing filler having large surface area. At higher frequencies, the EM radiation penetrates only a limited depth of an electrically conducting material, this effect is known as skin effect and the depth is known as skin depth [30].

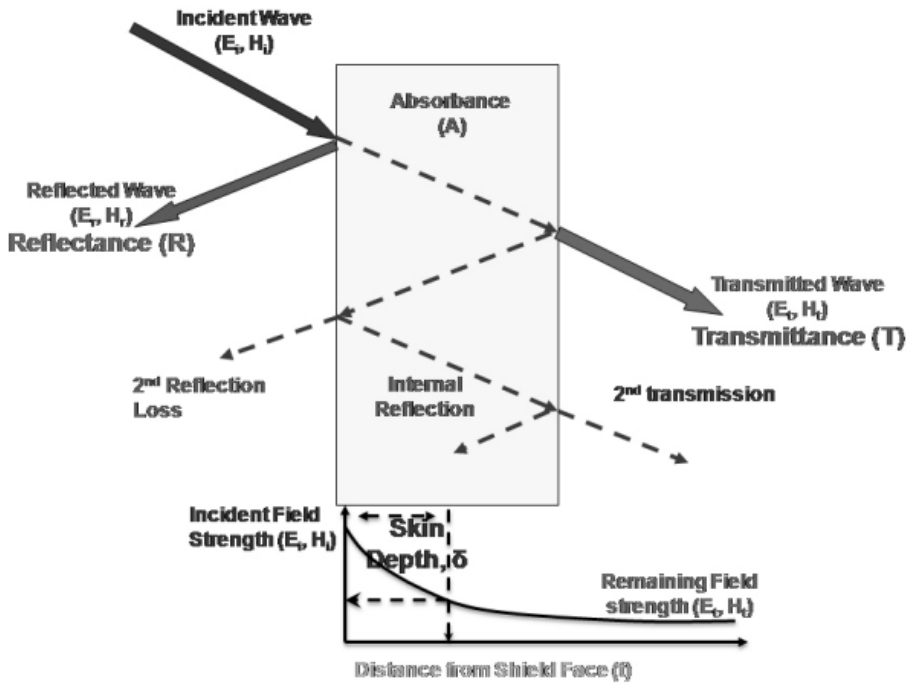

Figure 2.6. Schematic representation of EMI shielding mechanisms [31a].

The ability of any material to be used for EMI shielding applications is presented by shielding effectiveness (SE) of that material. The SE of any material increases as the electrical conductivity (σ) increases. Based on EMI shielding theory (far-field shielding), the EMI SE can be calculated using Eq. (2.5) [32-33],

$$\textbf{EMI SE} = 20 \log \left(1 + \frac{1}{2} \sigma . t . Z_0 \right) \qquad \textbf{(2.5)}$$

In above equation Z_0 is the impedance of free space, σ is the electrical conductivity and *t* is the thickness of the shield.

2.4 Polymer based composites for electronic applications

Polymer matrix composites or nanocomposites (PMCs/PNCs) have various advantages that make them potential candidates for advanced miniaturized electronics due to good flexibility, low density, easy processability at lower temperature and low cost. PMCs/PNCs with high dielectric constant are required in various embedded capacitor functions. For example, the dielectric constant in the range of 25-170 is required for advanced decoupling capacitors [34]. Such dielectrics are called high-k dielectrics and can be defined as the materials possessing higher dielectric constant as compared to SiO_2 which is used in semiconductor manufacturing processes [35]. PMCs/PNCs are also used in EMI shielding/ radio frequency interference (RFI) shielding, and electrostatic dissipation (ESD) [36-37]. Electrical properties of these composites can be tuned by varying the volume fraction of fillers in the matrix.

In recent years, there has been an increasing interest in high dielectric constant polymer composites composed of mixture of ferroelectric ceramic and polymer for high energy storage and embedded capacitor applications related to microelectronic packaging [38-54]. For instance, $BaTiO_3$ and PZT have been widely used as filler materials in polymer composites because of their high dielectric permittivity and low cost. Addition of ceramic particulates with high dielectric constant in polymer matrix, results in light weight polymer composite with improved dielectric constant with respect to polymer matrix. The dielectric constant increases with increasing volume concentration of ceramic particles. However, one can not increase the volume concentration of ceramic particles to any extent as above certain value, the composites tend to become brittle and porosity also increases.

Dielectric constant of polymer composites can also be increased by incorporating electrically conductive fillers (such as CNT, graphene, metal particles) in the polymer matrix such as epoxy, polyethylene, polyurethane, polyester, polyvinylidene fluoride etc. [55-67]. It has been reported that the addition of both conducting and dielectric filler in the polymer matrix increases the dielectric constant to a significant extent (up to 2 to 3 orders of magnitude) [68-72].

In couple of years, carbon nanotubes (CNTs) and graphene have been added in the ceramic/polymer composites in order to achieve high dielectric constant [58-64]. For a given volume percentage, the nano fillers provide better improvements in the

properties of the composite because of their high surface area to volume ratio. Nano material can be defined as "the material which sized in the range of 1-100 nanometre (nm) at least in one dimension" [73]. In case of nanocomposites the size of the filler is in the range of 1-100 nm. The composites mainly consist of filler, matrix and the interface. If the composite consists of only one type of filler then it is called as *two-phase* composite, whereas, if there are two types of filler in the matrix then the resultant composite is termed as *three-phase* composite

2.4.1 Ceramic-filled two phase PMCs/PNCs

Some ceramics are well known for high dielectric constant. Hence, filling the polymer matrix with such a high dielectric constant ceramic is the straightforward approach to combine the high dielectric constant of ceramic with the advantages of polymers. As the high dielectric constant ceramic materials are filled in the polymer matrices, the dielectric constant of the resultant composite increases with respect to polymer matrix. Ferroelectric ceramics such as $Pb(Mg_{1/3}Nb_{2/3})O_3–PbTiO_3$ (PMNPT), $Pb(Zr,Ti)O_3$ (PZT), $BaTiO_3$, and $CaCu_3Ti_4O_{12}$ (CCTO) are commonly used filler materials in two-phase PMCs. Das-Gupta and Doughty [74] incorporated PZT with an average grain size of 20 μm in PVDF matrix using rolling mill operation at about 160 °C. Prediction of the effective dielectric constant of the polymer-ceramic composite is very important from designing point of view. A number of theoretical models have been proposed in literature for predicting and calculating the dielectric constant of such two phase composites. Here, some frequently used theoretical models are discussed.

2.4.1.1 Theoretical Models for predicting dielectric constant

(a) Lichtenecker's general mixing rule

In a model capacitor, the effective dielectric constant of the composite dielectric consisting of two different homogeneous dielectrics in parallel or series combination is given by the Eq. (2.6), as suggested by Lichtenecker [75-77].

$$\in^{\alpha} = V_f . \in_f{}^{\alpha} + V_m . \in_m{}^{\alpha} \quad \textbf{(2.6)}$$

Equation (2.6) is known as Lichtenecker's general mixing rule. Where, $\in$ is the effective dielectric constant of the combination; $\in_f$ and $\in_m$ are the dielectric constants of first (filler) and second (matrix) dielectric, respectively; V_f and V_m are the volume fraction of filler and matrix dielectrics, respectively, α is the parameter which have the value 1 and -1 for parallel and series mixing rule respectively [76]. Parallel and series mixing rules provide upper and lower limits of the dielectric constant. For a true heterogeneous composite, Lichtenecker proposed an intermediate form with $\alpha \rightarrow 0$, which is called as Lichtenecker Logarithmic mixing law.

(b) Lichtenecker Logarithmic Law

Lichtenecker logarithmic law is represented by the Eq. (2.7) or by Eq. (2.8). This rule is valid if the dielectric constant of dielectric is nearly same. In case when one dielectric is filler and the second is matrix (in case of composites).

$$\log \in = V_f . \log \in_f + (1 - V_f). \log \in_m \quad \textbf{(2.7)}$$

or

$$\log \in = \log \in_m + V_f . \log \frac{\in_f}{\in_m} \quad \textbf{(2.8)}$$

Where $\in$, $\in_m$ and $\in_f$ are the dielectric constants of the resultant composite, matrix, and filler, respectively. V_f is the volume fraction of filler. The Lichtenecker rule does not consider the matrix-filler interaction [78].

(c) Modified Lichtenecker logarithmic law

Modified Lichtenecker logarithmic law includes a fitting constant, which presents the interaction between the filler and the matrix. It is expressed by the Eq. (2.9).

$$\log \in = \log \in_m + (1-k).V_f .\log(\frac{\in_f}{\in_m}) \qquad \textbf{(2.9)}$$

Where, k is an empirical fitting constant for the composites. Its value for most well-dispersed polymer/ceramic composites is found to be 0.3. For instance, the value of k reported by Goyal et al. [8] was 0.2 for the $BaTiO_3$/polyetheretherketone (PEEK) composites, while taking the dielectric constant value of 560. It was interesting to observe that when the dielectric constant value of $BaTiO_3$ was taken 1000, the k value changed to 0.3. Hence, the constant k, also depends on the dielectric constant of ceramic filler.

(d) Maxwell-Wagner Mixing Rule

Another mixing rule to calculate the dielectric constant of composites was proposed by Maxwell-Wagner and is expressed by Eq. (2.10), which is kwon as Maxwell-Wagner mixing rule. However, this rule is valid only when filler particles are of spherical shape, low in concentration and are uniformly distributed in the polymer matrix [79].

$$\in = \in_m . \left[\frac{2 \in_m + \in_f + 2V_f .(\in_f - \in_m)}{2 \in_m + \in_f - V_f .(\in_f - \in_m)} \right] \qquad \textbf{(2.10)}$$

(e) Jayasundere and Smith Equation

To predict the dielectric constant of 2-phase composites and considering the interaction between fillers, Jayasundere and Smith derived an expression given in Eq. (2.11) [79]. The interaction between filler will be significant when these are of fine size and in sufficient concentration.

$$\in = \frac{V_m \in_m + V_f \in_f \cdot \left[\frac{3\in_m}{\in_f + 2\in_m}\right]\left[1 + \frac{3V_f(\in_f - \in_m)}{\in_f + 2\in_m}\right]}{V_m + V_f \cdot \left[\frac{3\in_m}{\in_f + 2\in_m}\right]\left[1 + \frac{3V_f(\in_f - \in_m)}{\in_f + 2\in_m}\right]} \qquad \textbf{(2.11)}$$

Here V_m [i.e. $(1\text{-}V_f)$] is the volume fraction of matrix. Finer the size of filler larger is the surface area and more significant is the interaction in between filler particles. Based on this concept, nanosize filler as reinforcement/filler for polymer matrices has been gaining wide acceptance.

(f) Yamada Equation

Yamada and his co-workers proposed another model to explain dielectric as well as piezoelectric behaviour of the binary PZT/PVDF composite system using the properties of constituent materials [79]. They considered the shape of the ceramic particles ellipsoidal. Based on this, they derived an equation [Eq. (2.12)] expressed as.

$$\begin{aligned} \in &= \in_m \cdot \left[1 + \frac{\eta V_f \left(\in_f - \in_m\right)}{\eta \in_m + \left(\in_f - \in_m\right)\left(1 - V_f\right)}\right] \\ &= \in_m \cdot \left[1 + \frac{V_f \left(\in_f - \in_m\right)}{\in_m + n\left(\in_f - \in_m\right)\left(1 - V_f\right)}\right] \end{aligned} \qquad \textbf{(2.12)}$$

Where $n = 1/\eta$, which is the morphology factor depends on the shape of the ellipsoidal filler and their orientation in the composite

These above discussed models are very important to predict the dielectric constant of designed composite material, though; it is controversial which model should be used to predict the dielectric constant of composite. It is also difficult to predict the effective dielectric constant of the composite because of not availability of any direct method to measure the dielectric constant of ceramic powder. In such cases the dielectric constant of the bulk ceramic is used instead of the dielectric constant of ceramic powder, which is not proper. There are other factors due to which the effective dielectric constant is deviated from the predicted value for the composites, like: non uniform dispersion of dielectric filler, different particle size and shape of the filler, presence of impurity, presence of voids in the composite.

2.4.1.2 Dielectric behaviour

(a) Effect of ceramic filler content on dielectric behaviour of the composites

Olszowy [80] studied the dielectric behaviour of PZT/PVC and $BaTiO_3$/PVC composites prepared by hot pressing. The effect of ceramic powders content on the dielectric constant of the composite is depicted in Fig (2.7).

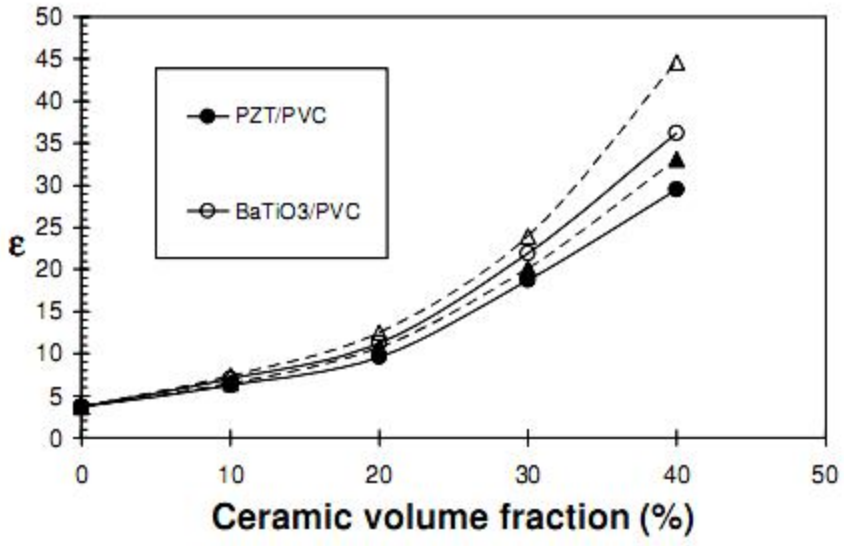

Figure 2.7. Variation in dielectric constant as a function of ceramic content at 1 kHz. The dashed curve with ▲ and △ are showing Lichtenecker mixing rule for filler PZT and $BaTiO_3$ respectively [80].

The maximum dielectric constant, measured at 1 kHz, for the PZT/PVC and $BaTiO_3$/PVC composites containing 40 vol % ceramic powders was 29.5 and 36.2, respectively. The experimental dielectric constant was found lower than the values predicted by the Lichtenecker rule. This discrepancy may be due to the presence of pores as visible in the SEM images in Figure 2.8.

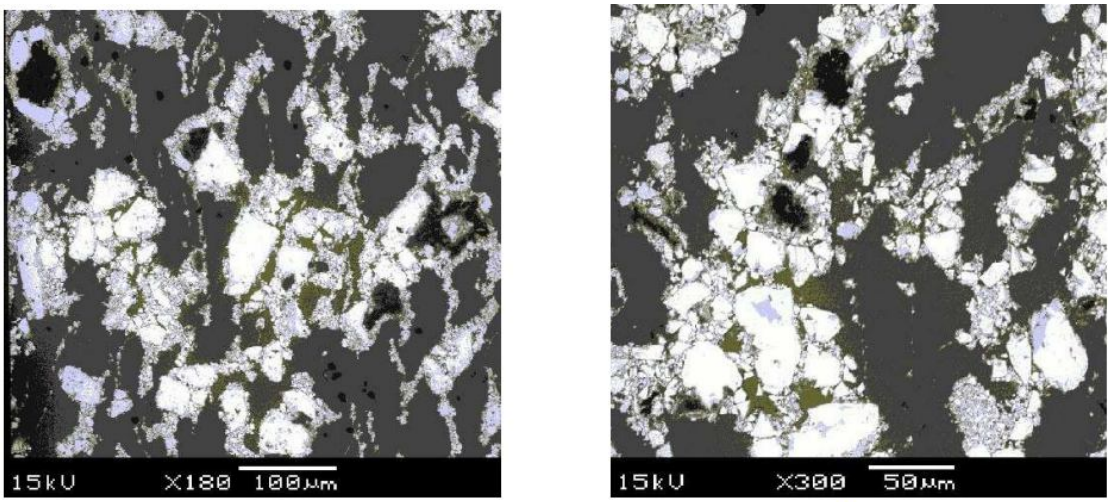

(a) (b)

Figure 2.8. SEM images of the microstructure of (a) PZT/PVC and (b) $BaTiO_3$/PVC composites. Both composites are having 30 vol % of filler [80].

Subodh et al. [81] studied the dielectric behaviour of $Sr_9Ce_2Ti_{12}O_{36}$ (SCT) filled high density polyethylene (HDPE) and epoxy resin. Figure 2.9 shows the trend for dielectric constant and dissipation factor with increasing SCT content. The dielectric constant for both the composites increased continuously and reached to the value of 12.1 and 14.1 for 40 vol % SCT content, respectively. In SCT/epoxy composites the dissipation factor first increased and then decreased. At higher loadings, as the ceramic content increases, the wetting between polymer and ceramic decreases which in turn increases porosity and hence the dissipation factor.

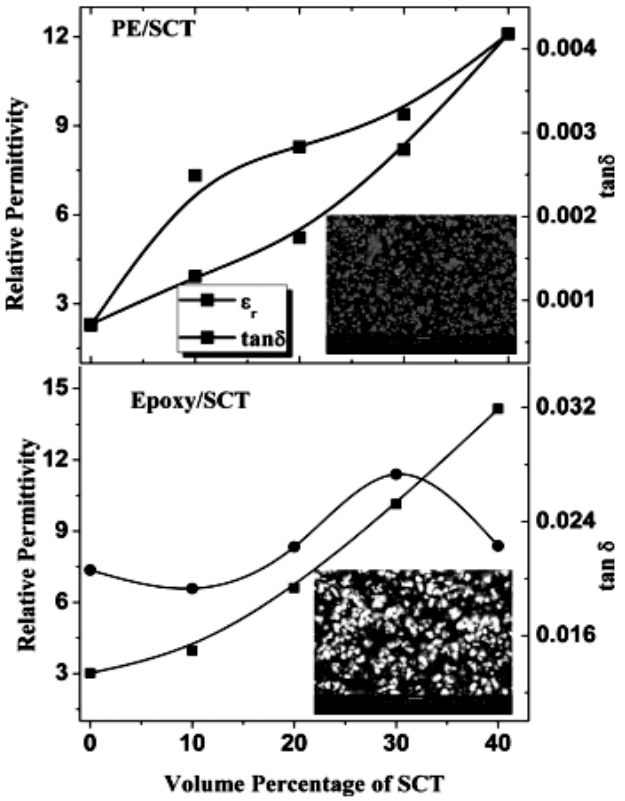

Figure 2.9. Variation of permittivity and dielectric loss with SCT volume for PE/SCT and epoxy/SCT composites at 8 GHz. The inset shows microstructures of 40vol % SCT loaded epoxy and polyethylene [81].

Vrejoiu et al. [82] studied dielectric behaviour of $BaTiO_3$/perfluorocylcobutene (PFCB) composite prepared by using spin-coating. Figure 2.10 shows the results for dielectric permittivity and dissipation factor with increasing vol % of $BaTiO_3$. The dielectric permittivity was increased with increasing ceramic content and reached at the maximum of 33 at 45 vol %. Further increase of ceramic content resulted in the decrease of permittivity which may be due to the formation of pores. The dissipation factor was below 0.06 for all the compositions.

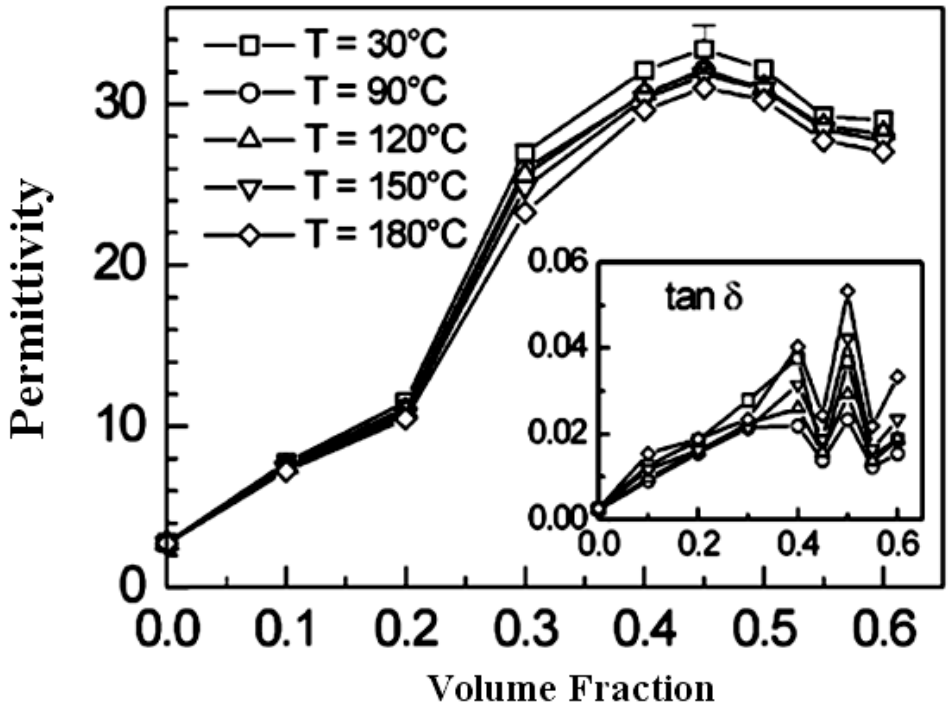

Figure 2.10. Dielectric permittivity of the $BaTiO_3$/PFCB composite layer as a function of $BaTiO_3$ volume fraction at different temperatures. The inset shows the variation in the dissipation factor with increasing ceramic volume fraction [82]

Previous studies showed that with increasing content of ceramic in polymer, in general, dielectric constant and dissipation factor increase but the behaviour may also be affected by polymer matrix, type of ceramic filler, preparation method and interfacial area between ceramic and polymer which ultimately affect the microstructure of the composite and hence the dielectric properties of the composite. Excess amount of ceramic particles may disturb the closely packed distribution of ceramics in the polymer due to formation of aggregates which may result in voids/pores in the composites. Hence, the trend with ceramic content generally varies at higher loadings.

(b) Effect of frequency on dielectric behaviour of the composites

The resultant dielectric constant of ceramic-filled PMCs/PNCs is due to the relatively high dielectric constant of ceramic component and the interfacial polarization due to ceramic and polymer [83]. Das-Gupta and Doughty [74] studied

the effect of frequency on the relative permittivity of PZT, PVDF and PZT/PVDF composite as shown in Figure 2.11. The result confirmed very weak dependence of relative permittivity on the frequency for PZT. However, the relative permittivity of PVDF and PZT/PVDF composite shows a dependence on the frequency within 10 to 10^5 Hz. Frequency dependence for ceramic-polymer composite should be attributed to the polymer and interfacial part in the composite.

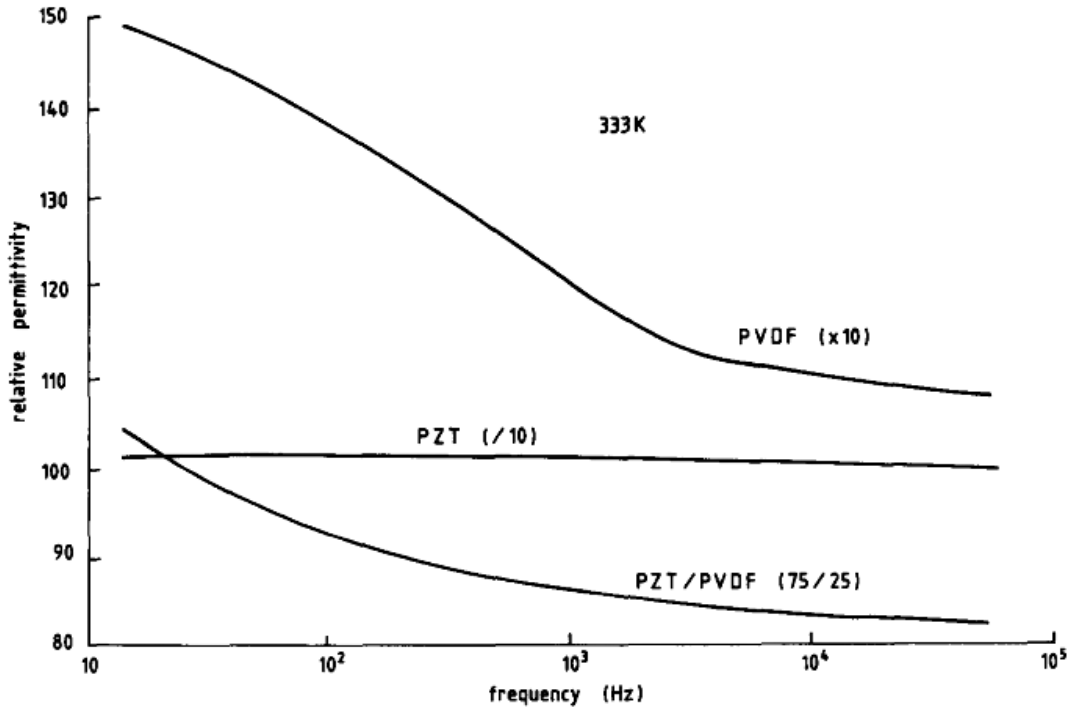

Figure 2.11. The dependency of relative permittivity (of PVDF, PZT and PZT/PVDF composite) on frequency at 333 K (60 °C) [74]

$BaTiO_3$/cyanoethylated cellulose polymer (CR-S) composite prepared by solution mixing was studied by Chiang and Popielarz [84]. The dielectric constant of the composite increased to 133 (from 21 for pure polymer) at 1 kHz. The dependency of dielectric constant of CR-S and its composites with $BaTiO_3$ is shown in Figure 2.12 and Figure 2.13, respectively. For pure CR-S, the dielectric constant starts to decrease significantly at about 10^5 Hz. The trend for dielectric loss factor was also consistent and having a peak at about 4 MHz. The dependency of dielectric constant of the composites has shown similar trend as for pure CR-S.

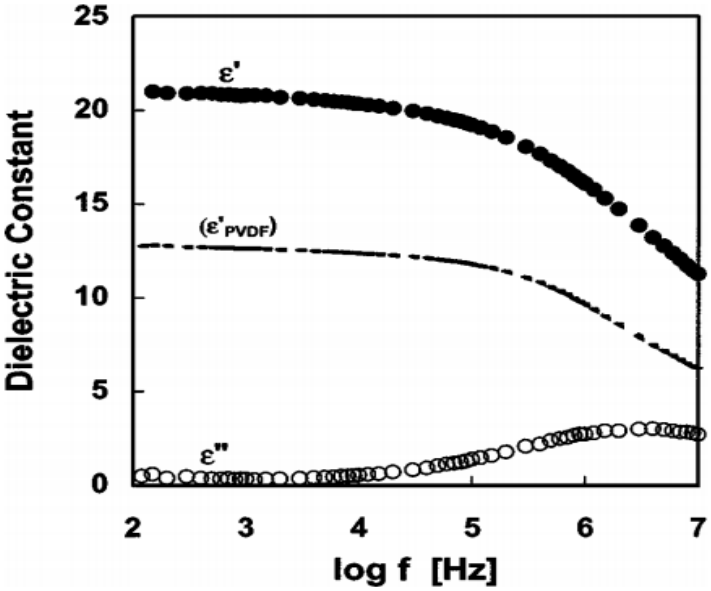

Figure 2.12. Frequency dependency of real and imaginary part of dielectric constant for pure CR-S at 25 ºC [84].

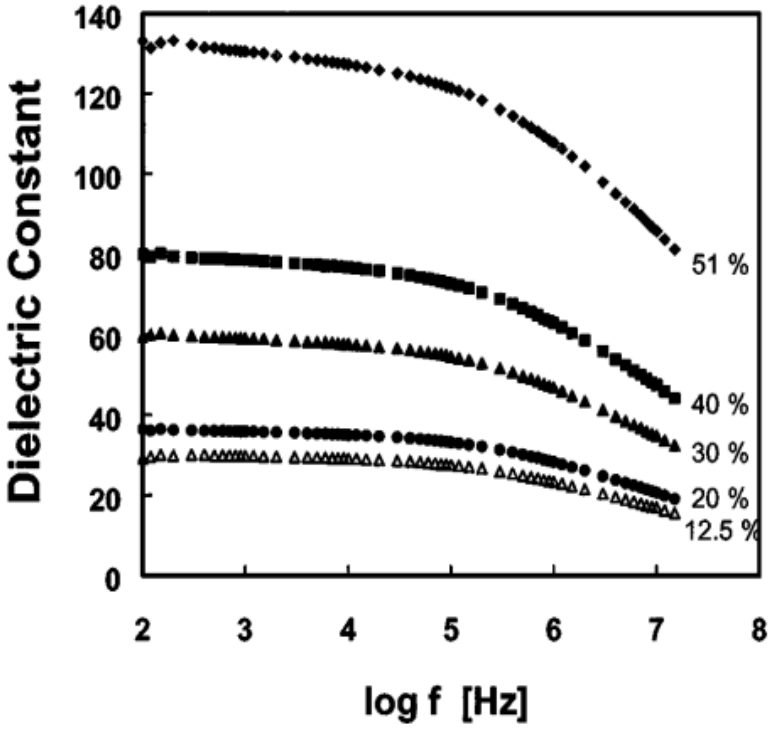

Figure 2.13. Frequency dependency of dielectric constant of $BaTiO_3$/CR-S composites with different volume fractions of $BaTiO_3$ [84].

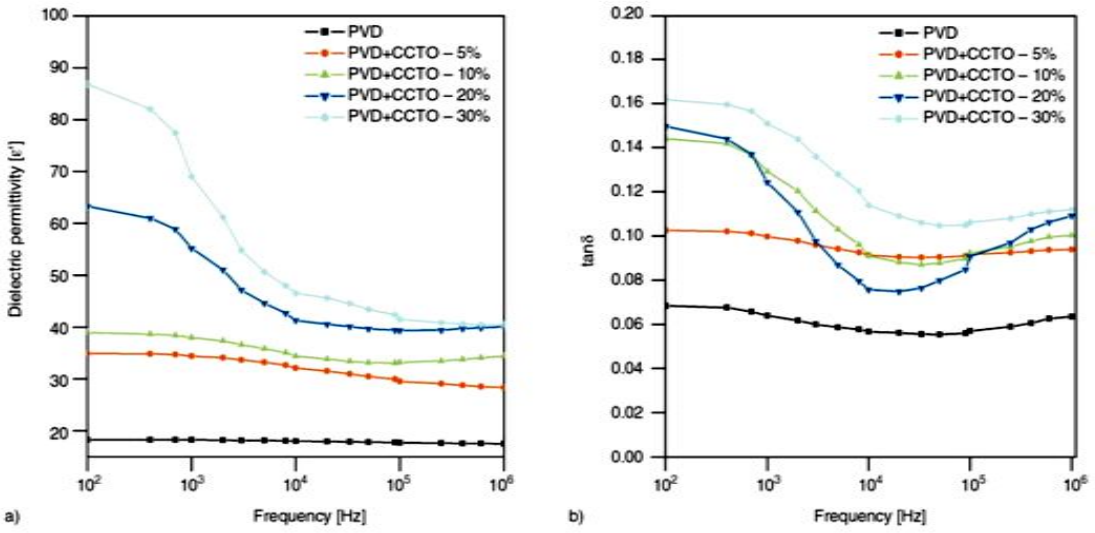

Figure 2.14. The frequency dependence of (a) dielectric permittivity and (b) dissipation factor in CCTO/PVDF composites [48].

Thomas et al. [48] reported remarkable frequency (10^2-10^6 Hz) dependent dielectric properties for $CaCu_3Ti_4O_{12}$ (CCTO)/PVDF composite prepared by solution method, as shown in Figure 2.14. Both dielectric permittivity and dissipation factor decease with increasing frequency in particular above 10^3 Hz. However, a slight increase was observed in dissipation factor beyond 10^5 Hz.

(c) Effect of temperature on dielectric behaviour of the composites

Three competitive mechanisms are responsible for temperature dependency of dielectric behaviour. Segmental mobility in the polymer increases with increasing temperature, which increases the dielectric constant. Secondly, due to higher CTE of polymer compared to ceramics, polymer matrix will expand more and hence will disturb the distribution of ceramic in the composite, which results in decrease in the dielectric constant (c) the crystal structure of ceramic particle could be changed with increasing temperature (e.g. near to Curie temperature) which could change the dielectric response of ceramic filler [85].

Chiang and Popielarz [84] explained the dependency of dielectric behaviour of polymer and composite on temperature. The temperature dependency of CR-S polymer and its composite with 30 Vol % $BaTiO_3$ is shown in Figure 2.15. From ambient temperature to 150 °C the dielectric constant of the composites exhibited slight increasing trend. Below ambient temperature the dielectric constant decreases with decreasing temperature which reflects the relaxation process in the polymer matrix. Dielectric loss factor for both polymer and composite shows a peak near about -11 °C, consistent with the decrease in dielectric constant.

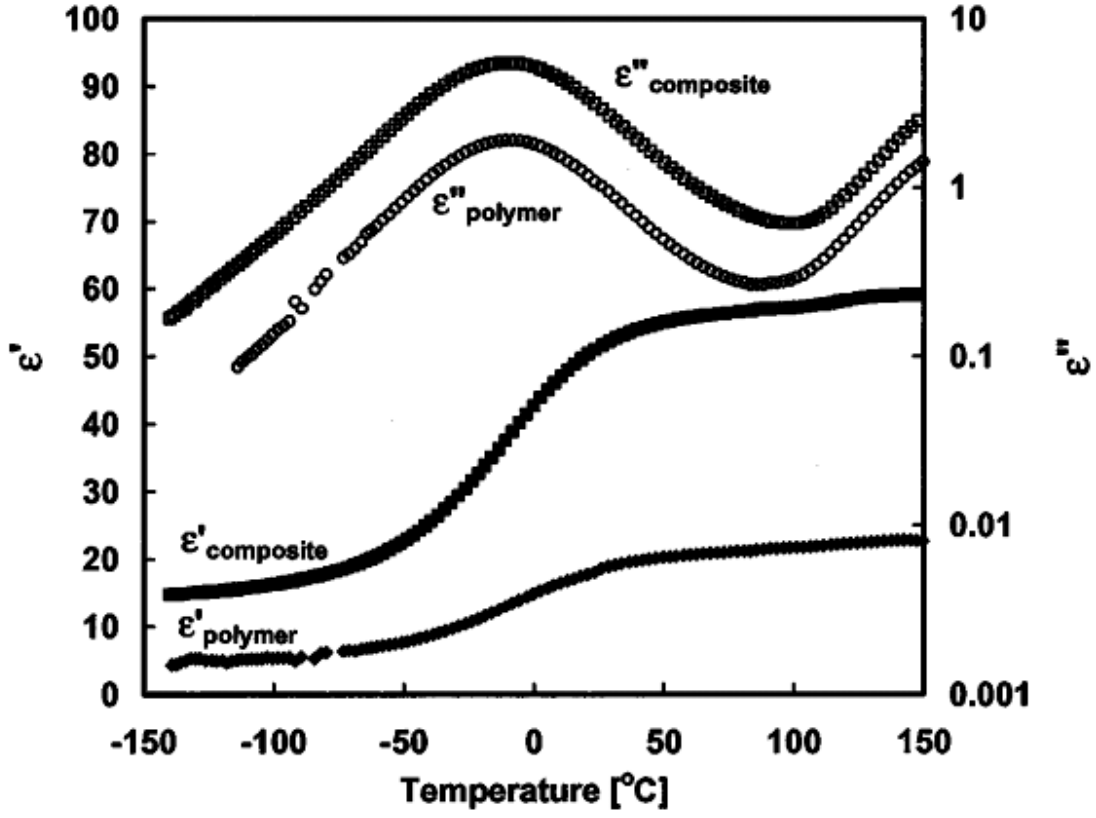

Figure 2.15. Temperature dependence of the dielectric constant and dielectric loss of pure polymer (CR-S) and its composite with 30 vol % $BaTiO_3$ [84].

In contrast to above, Subodh et al. [81] reported that there was not significant change in the dielectric constant (at 1 MHz) for SCT filled PE and epoxy based composites with increasing temperature, as shown in Figure 2.16. Since, SCT is an incipient ferroelectric material and hence its permittivity decreases with increasing temperature. In case of SCT/epoxy composites, the dielectric constant is increased

with increasing temperature. According to authors this may be because of the additional charge carriers due to ionization of impurities in epoxy and breaking of chemical bonds. This increased space charge density outplays the role of incipient ferroelectric nature of SCT and hence permittivity increases with increasing temperature.

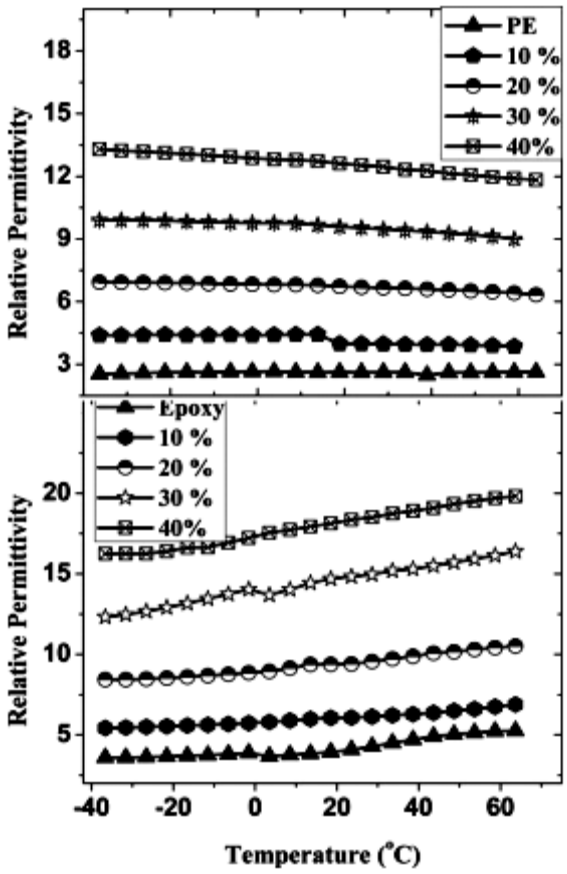

Figure 2.16. The variation in the permittivity with temperature for SCT/PE and SCT/epoxy composites at different Vol % [81].

Hyun et al. [86] also reported the temperature dependent dielectric properties of $BaTiO_3$/epoxy composite embedded capacitor films (ECFs), prepared by mixing and coating. With increasing temperature, the dielectric constant of the EFCs increased. The rate of increase in dielectric constant was higher at temperatures above the glass transition temperature (T_g). The effect of sample thickness between the electrodes, while measuring the capacitance, was also highlighted in the study. At 150 ^oC, the change in the dielectric constant and thickness for the composite containing 10 vol % $BaTiO_3$ was 57% and 5%, respectively.

(d) Effect of filler size on dielectric behaviour of the composites

In nano size domain, as the particle size of ferroelectric ceramic decreases, the Curie temperature shifts towards lower values [87] and their crystal structure changes. In addition to the inherent change in the dielectric constant with reduction in particle size, the surface area also changes for the same volume fraction in the polymer matrix. Therefore, the particle-particle and the particle-polymer interaction increases, this may alter the dielectric properties of the composite.

Yoon et al. [88] studied dielectric properties of $BaTiO_3$-epoxy composites containing 200, 300, 400 and 500 nm particle sizes of $BaTiO_3$ which were prepared by ball milling. The SEM image of these powders is shown in Figure (2.17). For a given vol %, the dielectric constant of the composite increases almost linearly as the particle size of $BaTiO_3$ decreases as shown in Figure 2.18. The finer particles have higher surface area which provides better particle-particle contact and hence increase the polarization due to dipole-dipole interactions.

In contrast to above study, Cho et al. [89] reported a different behaviour for $BaTiO_3$ (100 nm to 900 nm)-epoxy composites prepared by spin coating at 2000 rpm and 4000 rpm. As shown in Figure 2.19, the dielectric constant decreases with decreasing particle size. It is well reported [89] that the dielectric constant of $BaTiO_3$ changes with reduction in size and reaches to its maximum value of 5000 at 1000 nm and further it reduces drastically with reduction in size. With reducing particle size, the tetragonal structure of $BaTiO_3$, transits to cubic structure at a critical size of 120 nm [90]. Hence, the decrease in tetragonality of $BaTiO_3$ with reduction in size may be responsible for decrease in dielectric constant. In this case the inherent change in the dielectric constant of the ceramic particle with size is dominant over the increased surface area effect as was the case in the work of Yoon et al. [88].

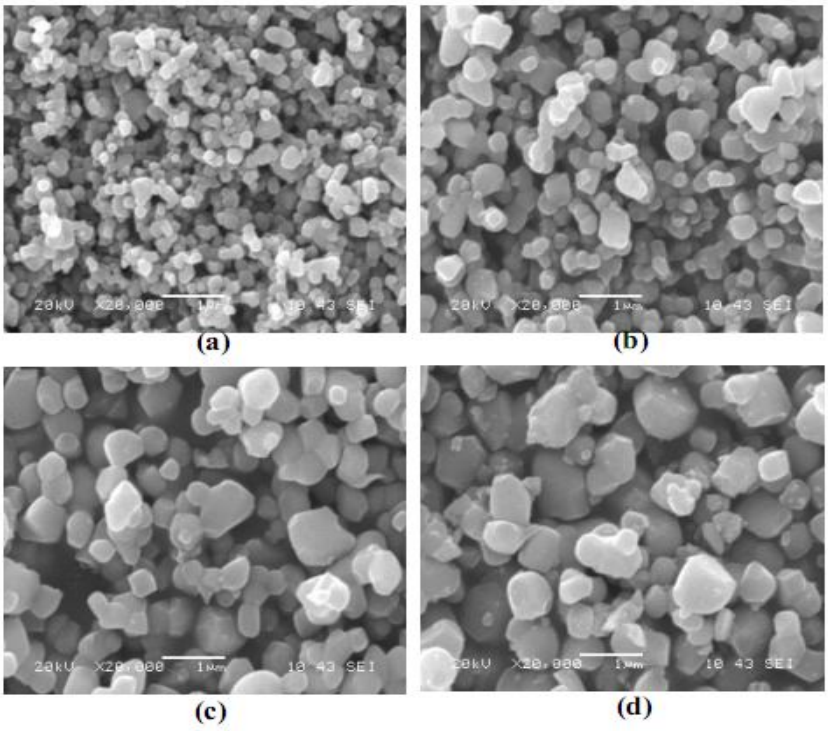

Figure 2.17. SEM images of $BaTiO_3$ powders with sizes of (a) 200 nm, (b) 300 nm, (c) 400 nm and (d) 500 nm [88]

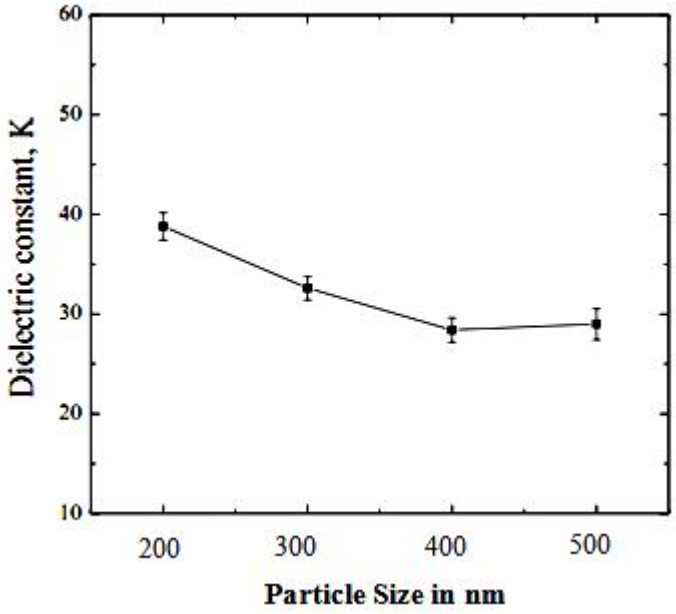

Figure 2.18. Dielectric constant of the $BaTiO_3$ (40 vol %)/epoxy composites as a function of the $BaTiO_3$ particle size [88].

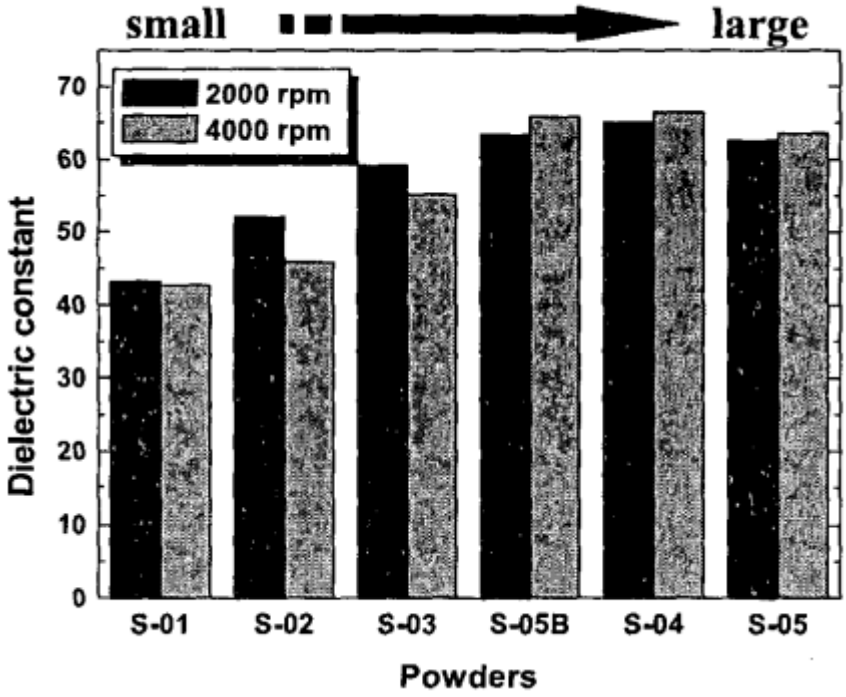

Figure 2.19. Variation in dielectric constant of $BaTiO_3$-epoxy composites with particle size of $BaTiO_3$ [89]. Where, S-01, S-02, S-03, S-04 and S-05/S-05B are in the order or increasing particles size (0.1 to 0.5 nm).

As discussed in the current section, the content of the ferroelectric ceramics should be as high as 45 vol% in the polymer matrix to significantly increase the dielectric constant of the resultant composite [83]. Such high volume fraction of the ceramics makes the composites brittle and difficult in processing [74]. There is challenge for the research society to increase the dielectric constant of polymer based composites without impairing their mechanical properties and processability. It is only possible when the filler content is small. Therefore, a different approach is required to improve the dielectric constant of composites.

2.4.2 Conductive filler-filled two phase PMCs/PNCs

The common conductive fillers are metallic particles/fibres, carbon black (CB), carbon nanotubes (CNTs), graphene etc. While filling the conducting filler in any polymer matrix, a phenomenon called percolation, occurs.

2.4.2.1 Theory of Percolation

Percolation is basically a mathematical model developed in 1950, and has been widely used since then as a simple model of statistical physics. Percolation theory is used to analyse the physical phenomena found above or below the onset of global connectivity in disordered systems [91]. The statistical percolation theory predicts the dependence of physical properties on the filler concentration as the percolation onsets, by the following scaling law given in Eq. (2.9)

$$\textbf{Properties} \propto (\Phi - \Phi_p)^{\pm e} \qquad \textbf{(2.9)}$$

Where, Φ is the volume fraction and Φ_c is the volume fraction at percolation threshold, and **e** is the critical exponent. According to the above equation (2.9) abrupt change occurs in the properties of composites near percolation especially when there is a large difference between the properties of matrix and filler.

In polymer composites, this theory is employed to study the behaviour of the composite system as a function of conducting filler. When the content of conductive filler increases in the polymer matrix, beyond certain filler loading, the conducting filler makes 3 dimensional inter-connections throughout the composite material. This critical amount of filler is called *percolation threshold* (Φ_p). The region where there is transition from non-conducting to conducting state is known as smearing region On further addition of conducting particles, after the end of smearing region, the composite shows saturation in electrical conductivity [92]. Thus, phenomenon of 3-dimensional (3D) connectivity in heterogeneous composite systems is called as

percolation phenomenon. The percolation phenomenon is schematically illustrated in the Figure 2.20.

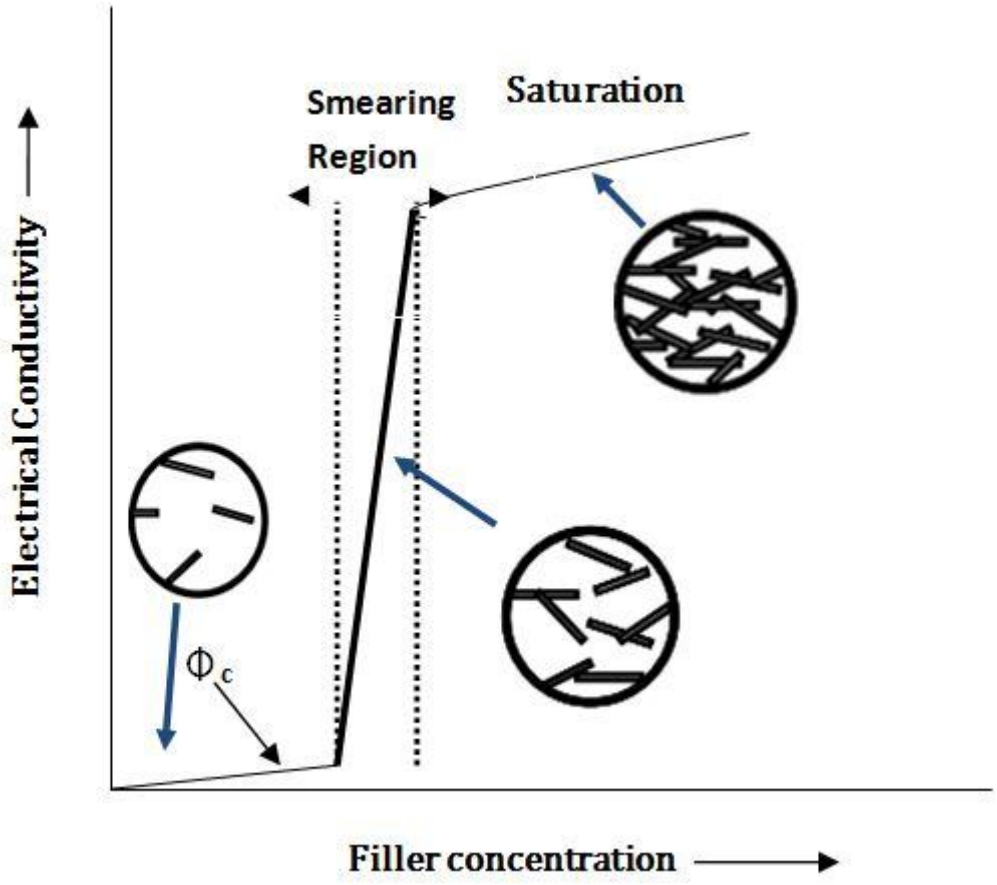

Figure 2.20. Schematic representation of percolation phenomenon in conducting filled polymer composites.

The nature of the composite whether it is conducting or dielectric is decided by the filler concentration. Close to the transition, the power law for electrical conductivity and dielectric constant can be expressed by Eq. (2.10) and Eq (2.11), respectively.

$$\sigma = (\Phi - \Phi_c)^t \qquad \textbf{(2.10)}$$

$$\varepsilon = (\Phi - \Phi_c)^{-s} \qquad \textbf{(2.11)}$$

Where, t and s are critical exponents for conductivity and dielectric constant respectively. For 3D systems, the universal values of t and s are t ~ 2 and s ~ 0.72 respectively [93].

2.4.2.2 Dielectric behaviour

The dielectric constant of polymer can be increased significantly by taking the advantage of their percolative behaviour. Before the percolation threshold the dielectric constant increases very slightly and beyond saturation the composite becomes conducting and hence the composite cannot be used as practical dielectric material. The smearing region is the possible region where the dielectric constant can be increased fairly. But such composites exhibits very narrow smearing region. In the vicinity of percolation (just before saturation) the dielectric constant increases abruptly.

(a) Effect of conductive filler content on dielectric behaviour of the composites

Kulthe et al. [94] studied Cu/PVC composite prepared by ball milling. Figure 2.21 clearly shows the increase in 3D networks of copper particles and increase in the thickness of the network in the PVC matrix with increasing Cu content in the composite. Deng et al. [95] reported a dielectric constant of 400 at 1 kHz for the Ag/PI composites (Figure 2.22), containing 12.5 vol % Ag (almost spherical and size-0.5 μm) and prepared by in-situ polymerization. The increase in the dielectric constants was attributed to the increasing number of Ag-PI-Ag type micro-capacitors in the composite. According to Qi et al. [96], the dielectric constant (1 kHz) of Ag/epoxy nanocomposite containing 22 vol % Ag increased to 308 at room temperature as shown in Figure 2.23(a). Beyond 22 vol %, the decrease in dielectric constant was observed due to porosity in the composite as revealed from the microstructure. As shown in Figure 2.23(b), the dissipation factor of Ag/epoxy composite varied from 0.008 to 0.05 with increasing Ag vol % in the composite for all frequencies. Similar trend for enhancement of dielectric constant was reported for Al/epoxy composites as shown in Figure 2.24 [97]

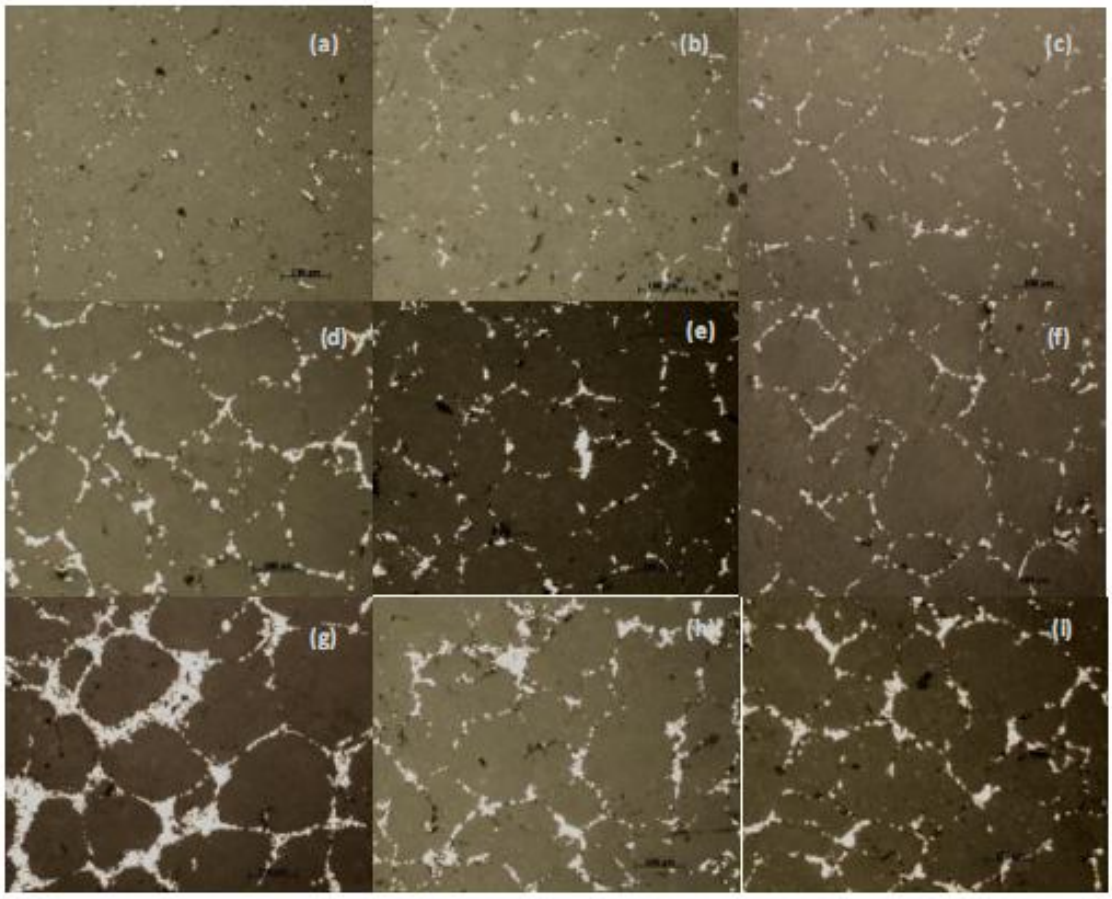

Figure 2.21. Optical microscopy images of composites containing (a-c) 20 wt % (d-f) 30 wt % and (g-i) 40 wt % after 12 hour (a, d & g), 24 hour (b, e & h) and 36 h (c, f & i) ball milling time [94].

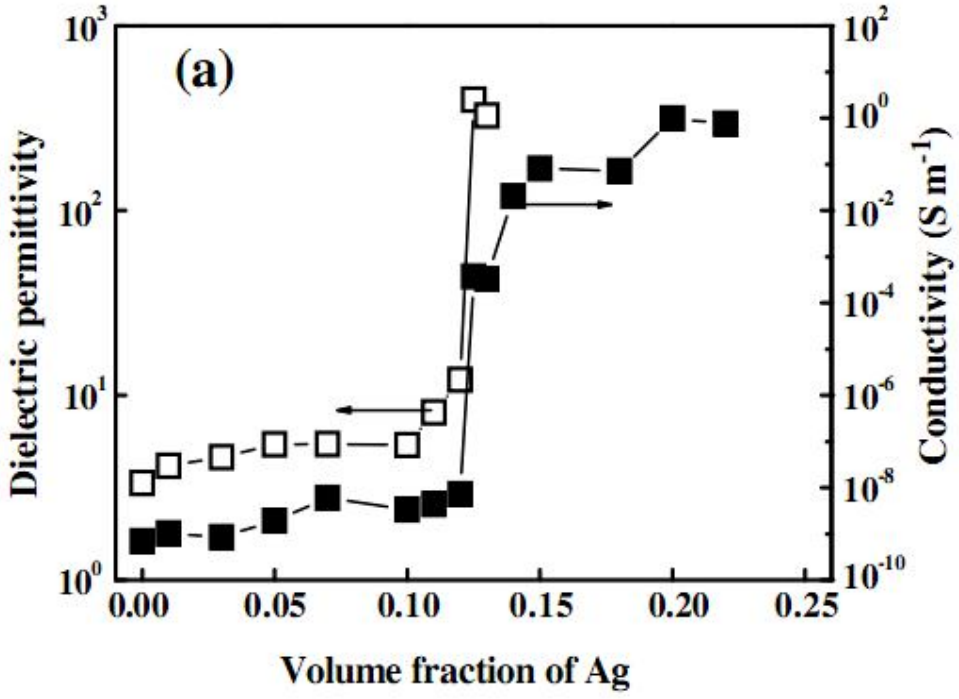

Figure 2.22. The variation in dielectric permittivity and conductivity of Ag/PI composite at 1 kHz, as a function of Ag volume fraction [95].

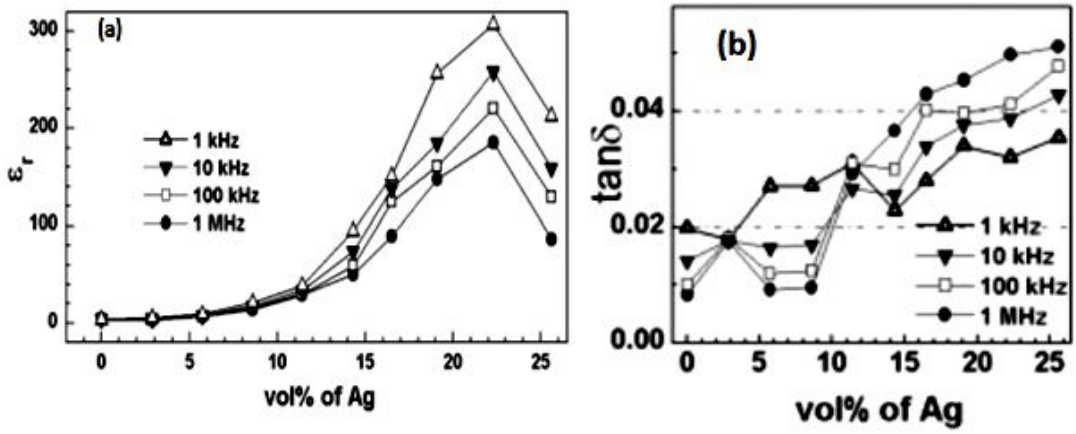

Figure 2.23. Variation in the (a) dielectric constant and (b) dissipation factor in Ag/epoxy composite with increasing vol % of Ag nanoparticles at different frequencies [96].

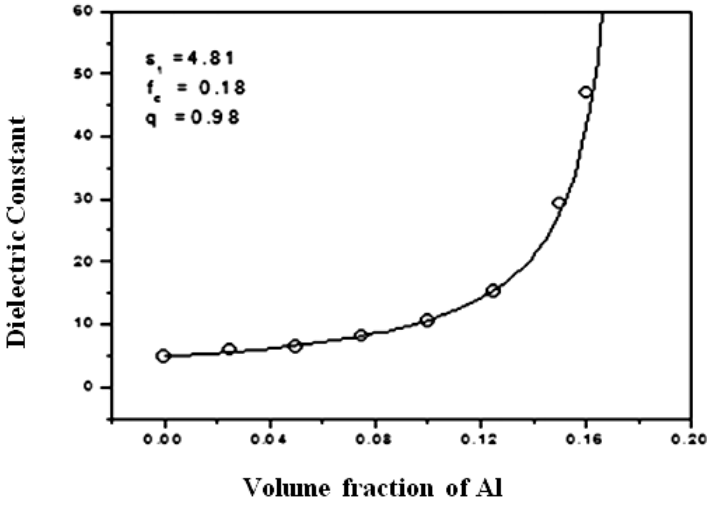

Figure 2.24. Variation in dielectric constant of Al/epoxy composite as a function of Al volume fraction, at room temperature and 10 kHz frequency [97].

It is found that metallic particle content in the matrix gives higher percolation threshold i.e. > 12 vol %. To reduce the filler concentration required for the percolation threshold, some authors have added carbon allotropes like carbon fibres, carbon nanofibres, carbon nanotubes, graphite, expanded graphite /graphene etc. [98-101] in the polymer matrices. For example Goyal and Kadam reported the electrical properties of the graphite flakes (EF) [36] and expanded graphite (EG) [102] filled polyphenylene sulphite (PPS) composites prepared by hot pressing. The percolation threshold obtained was about 5 wt % and less than 1 wt % respectively. The dielectric properties of EF/PPS and expended EG/PPS are shown in Figure 2.25, and Figure 2.26, respectively

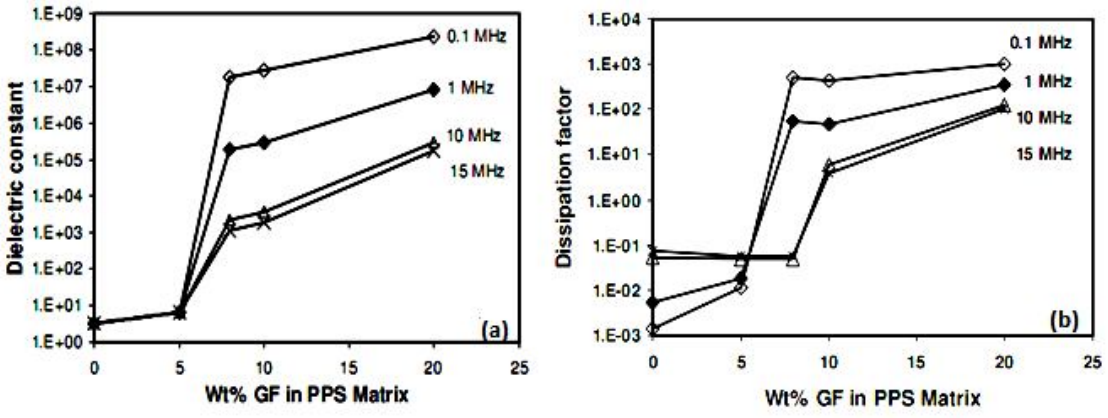

Figure 2.25. The variation in the (a) dielectric constant and in the (b) dissipation factor in GF/PPS composites as a function of GF wt %, at different frequencies [36].

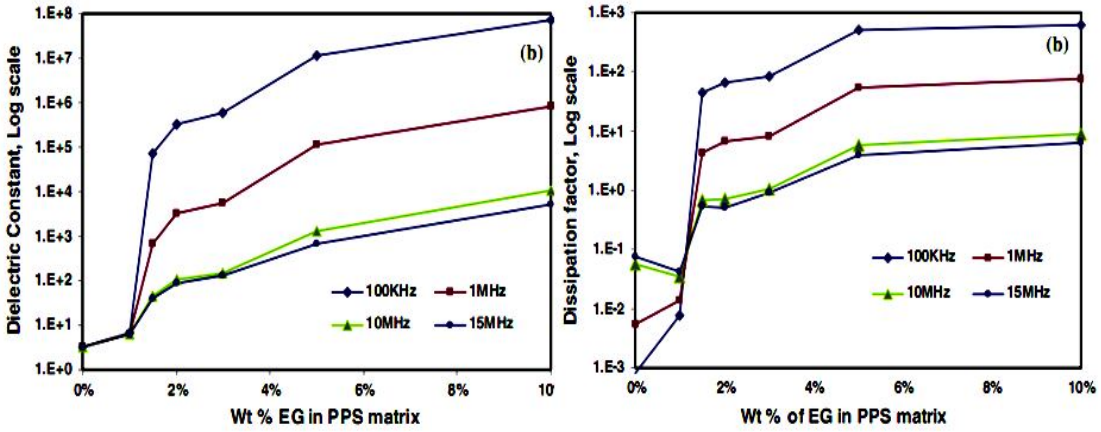

Figure 2.26. The variation in the (a) dielectric constant and in the (b) dissipation factor in EG/PPS composites as a function of EG wt %, at different frequencies [102].

The dielectric constant was increased from 3.3 for the pure PPS to 6.6 for PPS composite containing 5 wt % GF, at 1 MHz. Beyond 5 wt % GF, the dielectric constant and dissipation factor increased rapidly due to the formation of conducting paths. The dissipation factor for pure PPS was 0.005 and for 5 wt % it was below 0.1 for all the frequencies (100 kHz to 15 MHz). In case of 2 wt % EG filled PPS nanocomposites the dielectric constant (1 MHz) was increased by more than 100 times compared to pure PPS. This is due to the higher aspect ratio of the expended graphite sheets compared to graphite flakes; however, the dissipation factor was higher at higher frequencies [102].

As discussed in the above sections that as the filler concentration increases, initially the dielectric constant and dissipation factor increases gradually and at critical filler content i.e. at percolation threshold, their values start to increase abruptly. As the dielectric constant abruptly increases just in the vicinity of the percolation, hence a title change in the particle distribution could drastically change the dielectric properties of the composite. Therefore, such PMCs/PNCs may be very sensitive to changing frequency and temperature. Local charge transportation can extend their domain on increasing frequency and temperature.

(b)Effect of frequency on dielectric behaviour of the composites

Huang et al. [103] reported the frequency dependent dielectric behaviour of Al/ linear low density polyethylene (LLDPE) nanocomposites. The dielectric constant of the nanocomposites containing Al particles up to 12 wt %, showed weak frequency dependency and beyond 12 wt %, the dielectric constant significantly increased as shwon in Figure 2.27. Similarly, Li et al. [104] reported that the dielectric constant of stainless steel fiber (SSF)/PVDF composites containing more than 10 vol, % SSF drops with increasing frequency from 50 Hz to1 kHz, as shown in Figure 2.28(a). This was attributed to the large leakage current due to the high conducting nature of the composites. Beyond percolation, at lower frequency the dissipation factor showed a sharp hike, and decreased with increase in frequency, as shown in Figure 2.28(b). This sharp hike in dissipation factor was the consequence of raised conductivity of the composites. Below percolation the dissipation factor was below 0.3, almost irrespective of frequency. Similarly, the effect of the frequency on the dialectic constant of GF/PPS composite was reported [36] as shown in Figure 2.29.

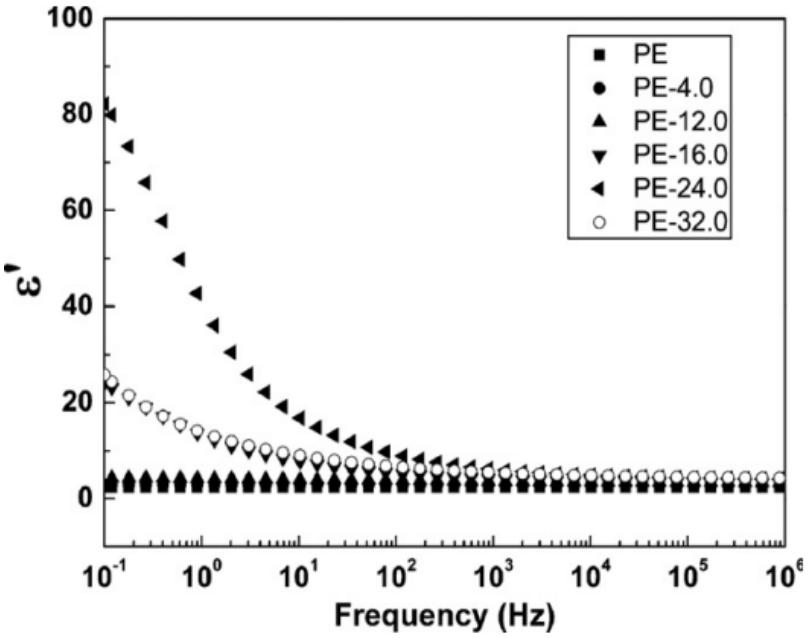

Figure 2.27: The frequency dependence of the real part of dielectric constant in Al/PE nanocomposites at different wt % of Al [103].

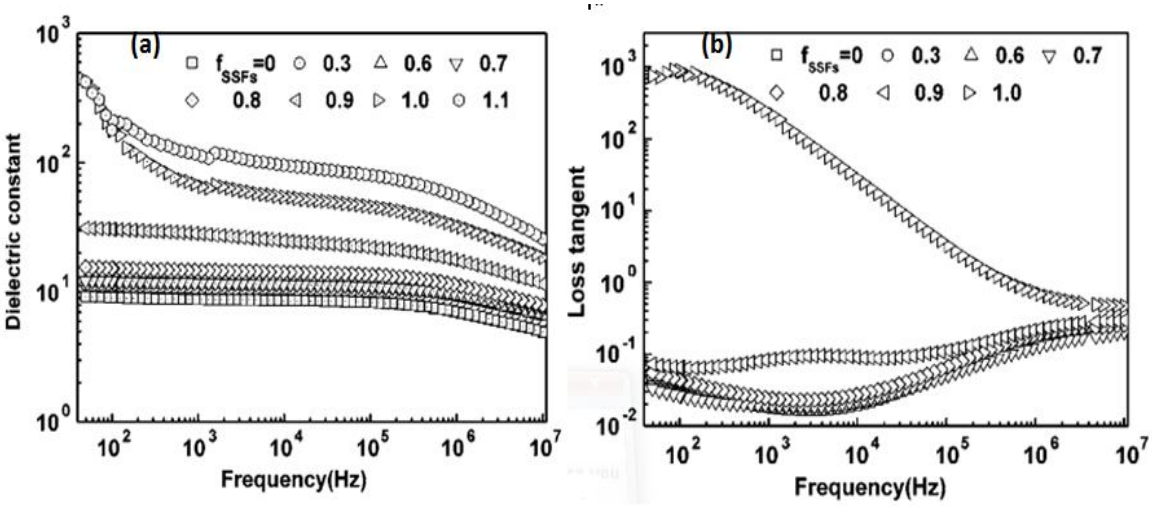

Figure 2.28. Frequency dependence of dielectric constant and dissipation factor on frequency in SSF/PVDF composites with different volume fractions [104].

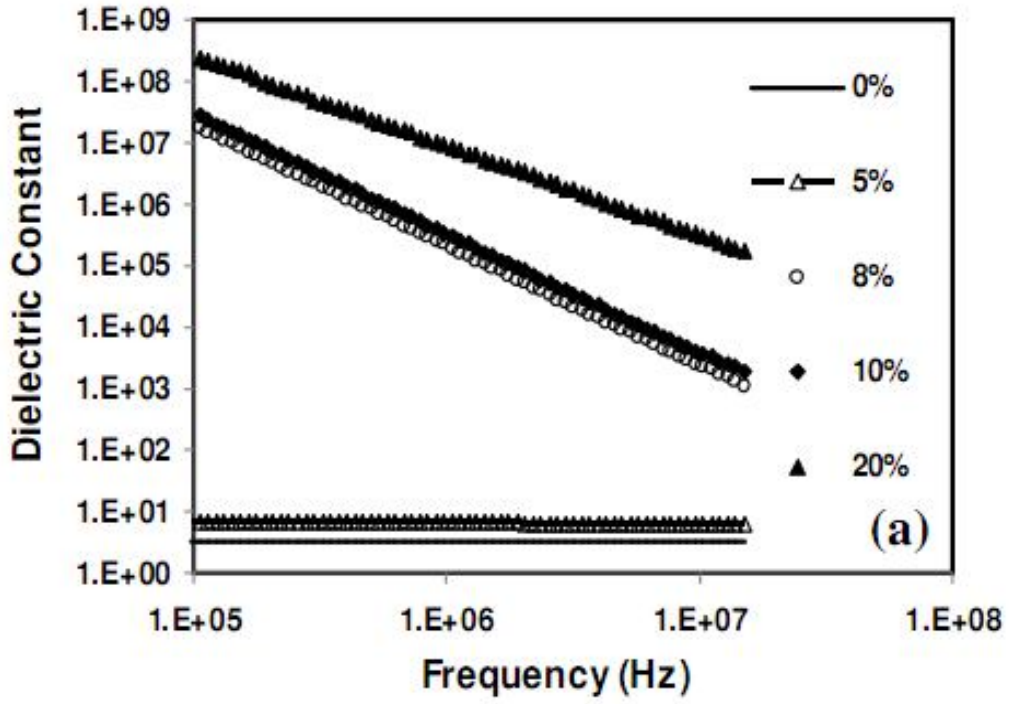

Figure 2.29. Frequency dependency of dielectric constant in GF/PPS composites having different vol % of GF [36].

(c)Effect of temperature on dielectric behaviour of composites

Dang et al. [95] reported weak temperature dependent dielectric constant for Ag (0.5 μm)/epoxy composites as depicted in Figure 2.30 which was attributed to the steady microstructure of the composites. Similarly Qi et al [96] reported weak temperature dependent dielectric constant for the mercaptosuccinic acid coated Ag (40 nm) particle filled epoxy nanocomposites as shown in Figure 2.31.

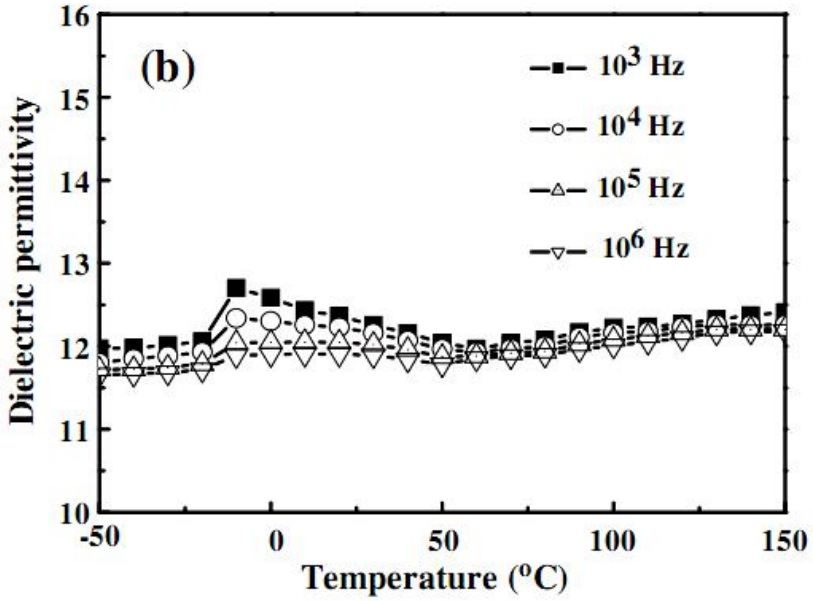

Figure 2.30. Temperature dependency of dielectric permittivity for Ag/epoxy composite film with12 vol %Ag, at different frequencies [95].

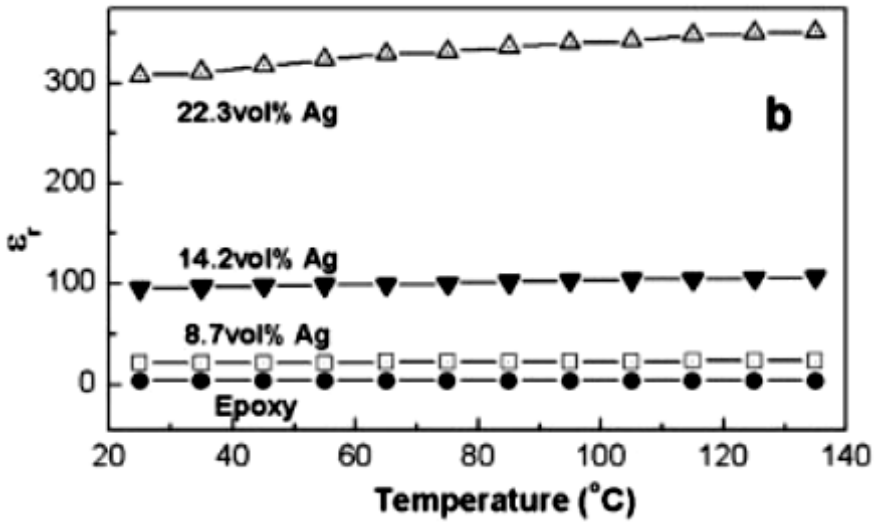

Figure 2.31. Variation in dielectric constant with temperature in Ag/epoxy nanocomposite at different vol % of Ag at 1 kHz [96].

(d) Effect of filler size on dielectric behaviour of composites

Boudenne et al. [105] reported the effect of Cu particle size on the percolation of Cu/polypropylene (PP) composites as depicted in Figure 2.32(a) and 2.32(b). The percolation threshold for the composites containing smaller size Cu particles occurred at 6.1 vol % whereas it was at 11.2 vol % Cu for the composite containing larger size Cu The low percolation threshold with lower size of particle is attributed due to higher probability to form 3D conducting chain in the composite than with the larger size particles. According to Luyt et al. [106] the percolation for the Cu filled low-density polyethylene (LDPE) and Cu linear low-density polyethylene (LLDPE) was about 19 vol % Cu as shown in Figure 2.33.

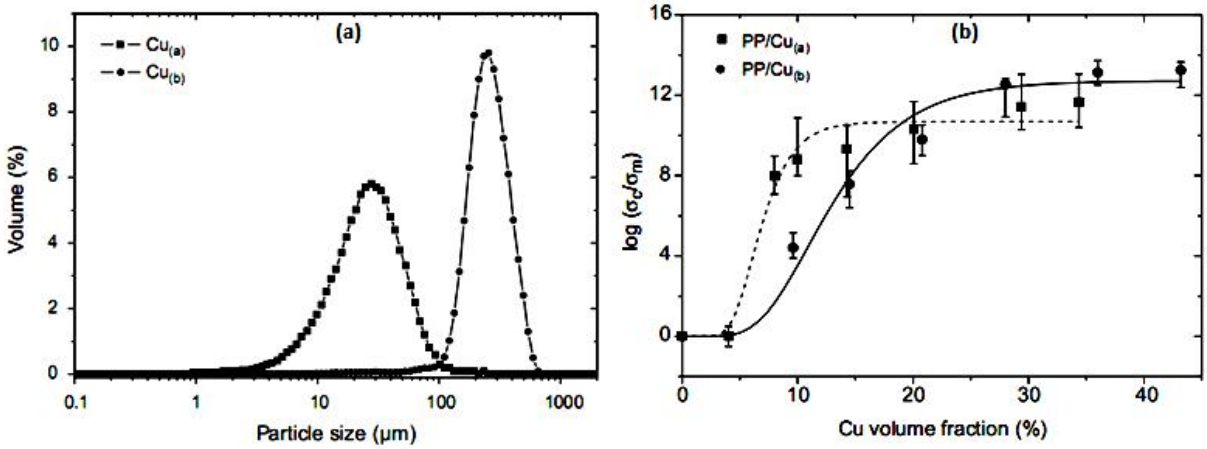

Figure 2.32. Presentation of (a) particle size distribution for $Cu_{(a)}$ and $Cu_{(b)}$ (b) percolations threshold in $Cu_{(a)}$/PP and $Cu_{(b)}$/PP composites [105].

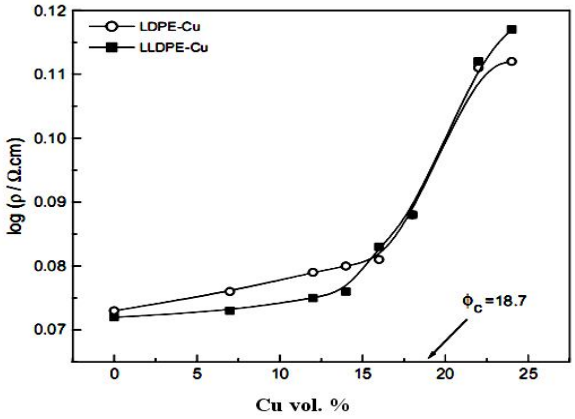

Figure 2.33. Electric conductivity of the Cu/LDPE and Cu/LLDPE composites with vol % of Cu, showing percolation at 18.7 vol % of copper in both composites [106].

Li et al. [104] reported percolation at 9.4 vol % for SSF (average aspect ratio-16)/PVDF composites as shown in Figure 2.34(c). The optical micrographs for SSF and SSF/PVDF are also shown in Figure 2.34(a) and 2.34(b). In contrast to this, Moreno et al. [107] found the percolation only at 0.04 wt % of silver nanowires (aspect ratio of 85)/ polycarbonate (PC) composites as shown if Figure 2.35.

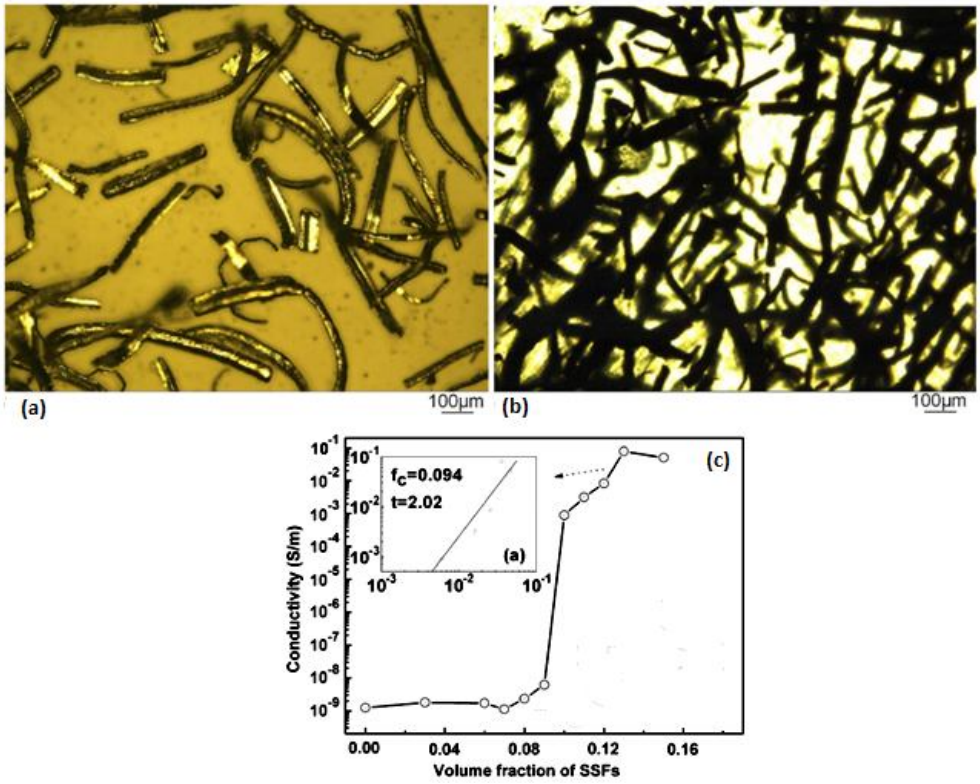

Figure 2.34. (a) Optical micrographs of (a) SSF, (b) SSF/PVDF composite (c) Effective dielectric constant of SSF/PVDF composite as a function of SSF volume fraction [104].

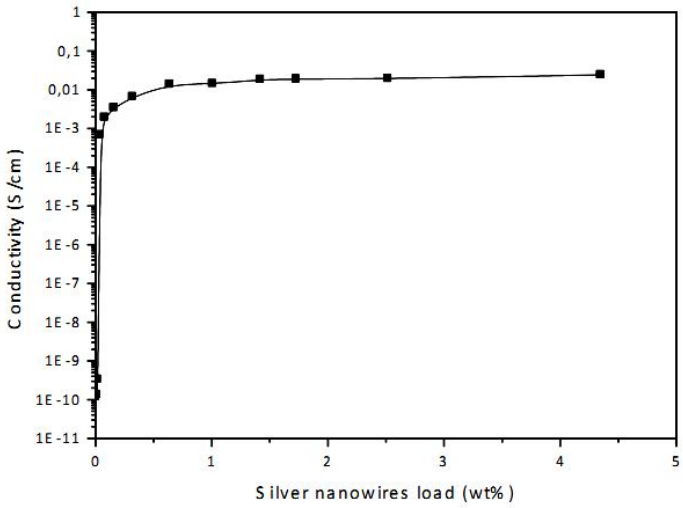

Figure 2.35. The conductivity of silver nanowire/PC composite with the wt % of silver nanowire [107].

In recent years the carbonaceous fibrous materials such as *carbon nanotubes* (CNTs), graphene, graphene oxide etc. [63-64,108-112], which possess aspect ratio greater than 1000, have been widely studied as filler in the polymer matrix. Pötschke et al. [108] reported percolation between 1 wt % and -1.5 wt % MWCNT Figure 2.36 for MWCNT/polycarbonate (PC) nanocomposites, prepared by melt mixing.

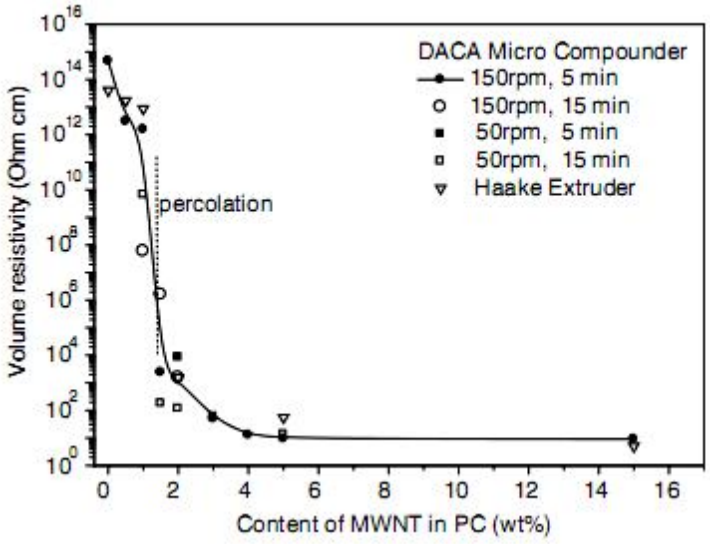

Figure 2.36. Volume resistivity as a function of wt % of MWCNT in PC matrix [108].

As discussed previously, the formation of large number of micro-capacitors/nano-capacitors by filler-polymer-filler combination is the probable reason of increase in dielectric constant. Hence filler with large surface area, such as graphene, will result in higher capacitance of nano-capacitors in the nanocomposites. Yousefi et al. [112] reported exceptionally high dielectric constant of over 14000 in reduced graphene-oxide (rGO)/epoxy nanocomposites at 1 kHz. The high dielectric constant of the composites was due to the network of numerous nano capacitors which offer a high charge storage capacity as illustrated schematically in Figure 2.37. The frequency and temperature dependency of the dielectric constant on temperature is shown in Figure 2.38. The reduction in the dielectric constant with increasing frequency was attributed to the dissipation of energy at the filler matrix interface into

heat. The temperature dependence shows a peak at about 70-80 °C and was attributed to the ordering of electric dipole corresponding to α-relaxation at T_g.

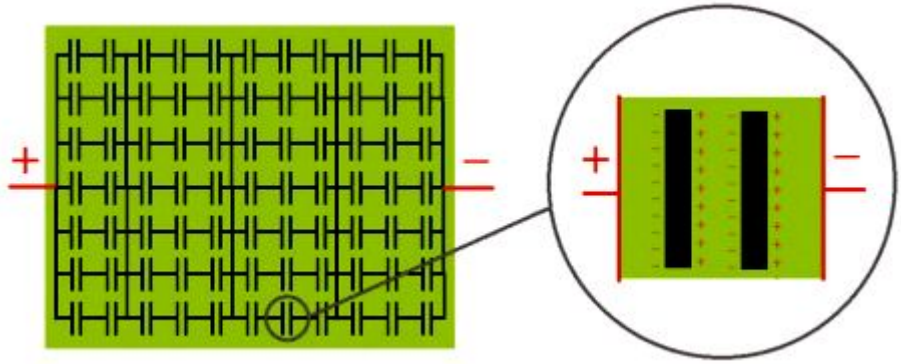

Figure 2.37. Schematic presentation of formation of nanocacacitors in nanocomposite [112].

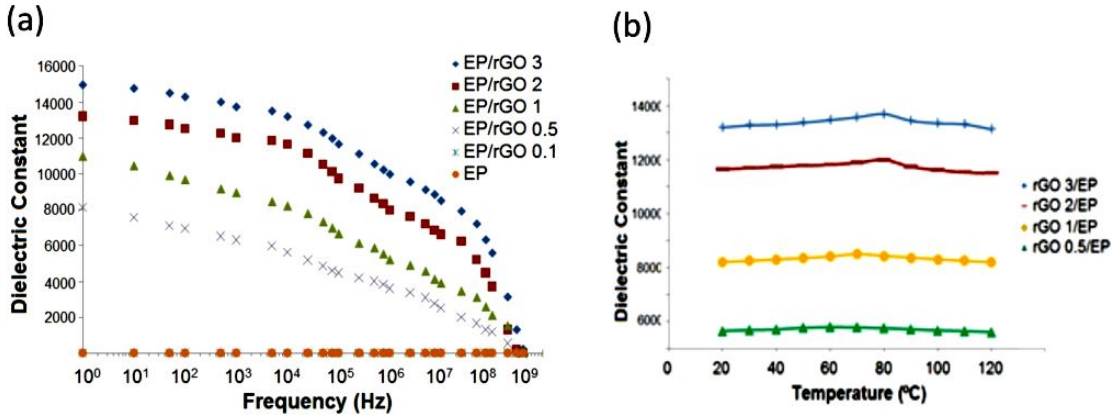

Figure 2.38. The effect of (a) frequency and (b) temperature on the dielectric constant of rGO/epoxy nanocomposites at different rGO content [112].

2.4.3 Dielectric and conductive filler filled three-phase PMCs/PNCs

As discussed in previous section about two-phase ceramic filled polymer composites, a ceramic filler content of more than 50 vol % is required to increase the dielectric constant significantly. At such higher level, the composites suffer from brittleness, low adhesion and pores/voids etc. The presence of pores or defects may also increase the dissipation factor. If a filler having high electrical conductivity is used the dielectric constant of the composites increases abruptly near the percolation. So it is very difficult to control the filler concentration near the percolation i.e. in smearing region. In addition, the dissipation factor is very high is such percolative two-phase systems. As discussed earlier, both types of filler (ceramic and conductive filler) have also been inserted in the polymer matrices for better dielectric properties. The presence of ceramic filler obstructs the early formation of 3D network among the conductive fillers in the composites thereby the smearing range extends. With extended searing range, the control of conductive filler concentration becomes somewhat easier.

Lim et al. [13] studied the three-phase Ni-$BaTiO_3$-PMMA composites. The variation in dielectric constant of the PMMA composites (two phase) containing $BaTiO_3$ and Ni particles is shown in Figure 2.39 (a) and Figure 2.39(b), respectively.

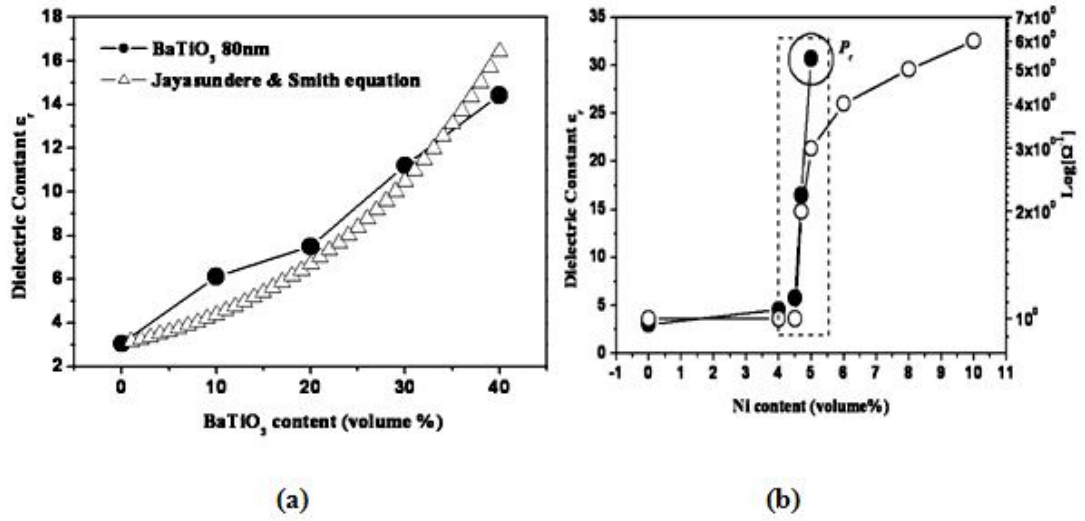

Figure 2.39. The variation in dielectric constant with increasing vol % of (a) $BaTiO_3$ in two phase $BaTiO_3$/PMMA composite, (b) Ni in two phase Ni/PMMA composite [13].

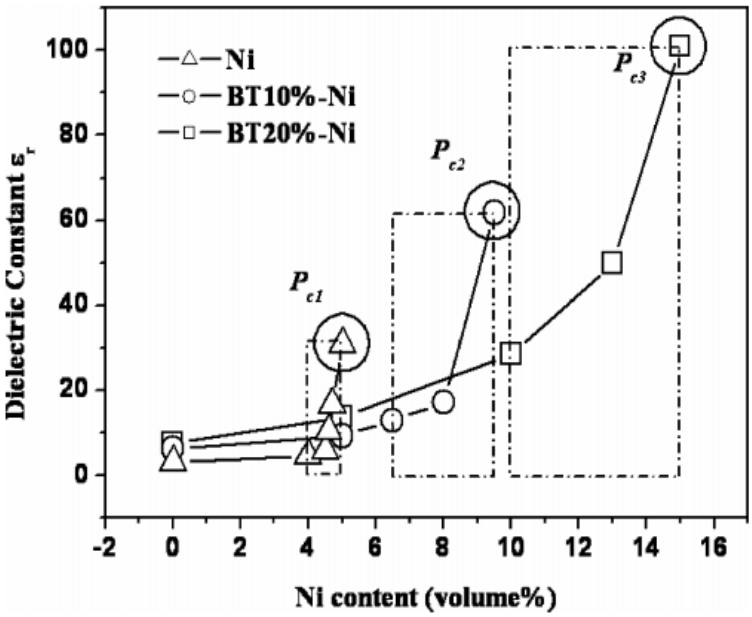

Figure 2.40. The dielectric behaviour of three-phase Ni-$BaTiO_3$-PMMA composites as a function of Ni vol % [13]

The maximum achieved dielectric constant for $BaTiO_3$-PMMA containing 40 vol % $BaTiO_3$ was 15. In contrast to this it was 31 for the Ni-PMMA composite containing 4.7 vol % Ni, but its dissipation factor was 11.3.The maximum achieved dielectric constant for the three phase Ni-$BaTiO_3$ (10 vol %)-PMMA and Ni-$BaTiO_3$ (20 vol %)-PMMA composites, containing 9.5 vol % and 15.0 vol % Ni particles was found 60 and 101, respectively. For a given vol % (10 vol%) of conducting Ni particles, the 10 vol % BT filled PMMA showed higher dielectric constant (i.e.~60) compared to the 20 vol % BT filled PMMA composites which has dielectric constant of 30. It could also be seen from the Figure 2.40 that the smearing region was extended with increasing dielectric filler content in the matrix.

Goyal and Kulkarni [12] studied expanded graphite/PZT/PVDF composites. In two-phase PZT/PVDF composites the dielectric constant was increased up to 57 with 80 wt % of PZT (C-80). At a given frequency, the dielectric constant was further increased for the C-80 composite containing 0.25, 0.50 and 0.75 wt % EG to 192, 237 and 842 respectively as shown in Figure 2.41 with concurrent increase of dissipation factor. According to the authors, the increase in the dissipation factor may be

attributed to the increased interfacial polarization, defects and induced space charge. It was also found that dielectric constant as well as dissipation factor of the composites decreased with increasing frequency. The frequency dependence was becoming more pronounced with increasing EG content as apparent in Figure 2.41 and Figure 2.42.

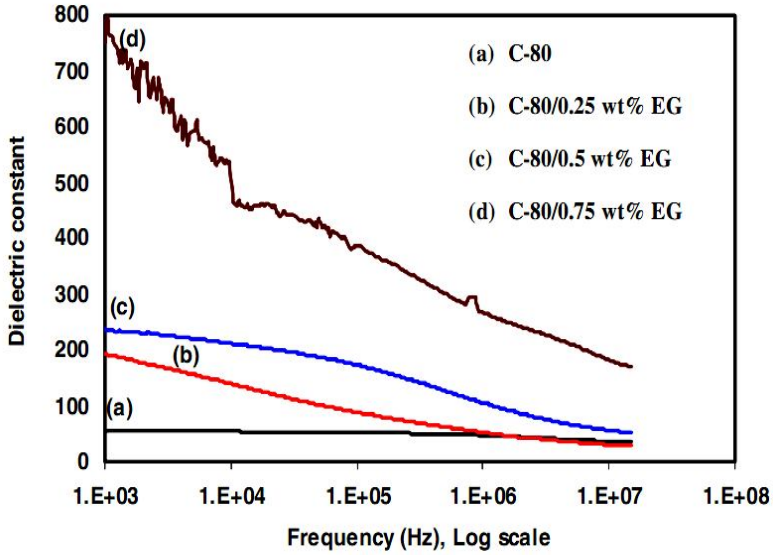

Figure 2.41. Variation of dielectric constant of three-phase EG-PZT-PVDF composite as a function of EG content and frequency [12].

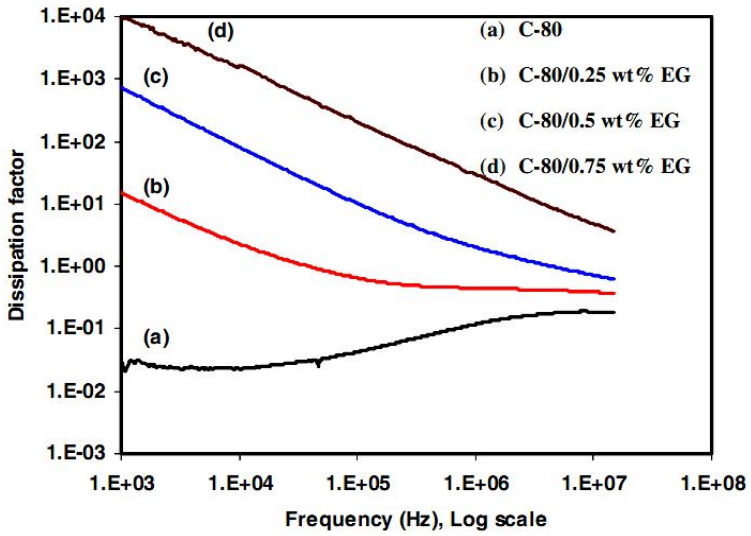

Figure 2.42. Variation in dissipation factor of three-phase EG-PZT-PVDF composite as a function of EG content and frequency [12].

Prakash and Verma [97] reported a maximum dielectric constant of about 700 (at 10 kHz) in a composite of CCTO-epoxy composites containing 25 vol % of Al, as shown in Figure 2.43. The required amount of Al for percolation was increased due to the presence of CCTO ceramic in the epoxy matrix which prevents the interconnectivity of Al particles. Similar to dielectric constant, the dissipation factor was also found to increase gradually with increasing Al vol % in the two-phase composite. The dissipation factor was increased from 0.009 for the Al free CCTO/epoxy composite to 0.237 for the 25% Al filled composite. As shown in Figure 2.43, as the Al content in the two-phase composite increased the frequency dependence of dielectric constant becomes more apparent.

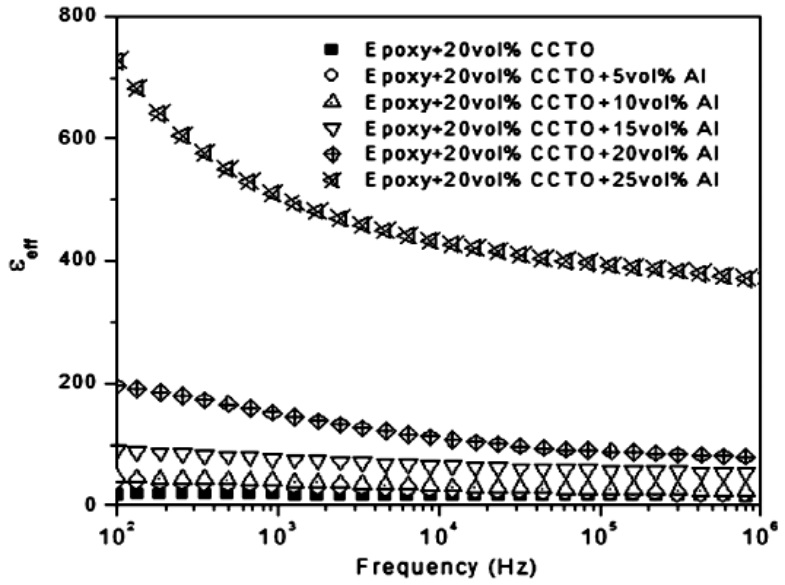

Figure 2.43. Frequency dependence of Al-CCTO-epoxy three-phase composite with different Al vol %, at 300 K [97].

The literature concludes that for embedded capacitor applications many types of polymer matrix composites/nanocomposits have been prepared and studied but many challenges are still there. In two-phase ceramic filled PMCs/PNCs, the dielectric constant increases due to the higher dielectric constant of ferroelectric ceramic. But the two-phase ceramic filled PMCs needed higher volume fraction of ceramic to significantly increase the dielectric constant. In two-phase conducting filler filled composites as the filler content increases below percolation threshold, the dielectric constant increases gradually due to the accumulation of charges at the filler/matrix interface which is also known as Maxwell-Wagner-Sillars polarization principle [36, 112]. Thereafter, beyond percolation threshold, a sharp increase in the dielectric constant was attributed to the formation of huge network of micro/nano-capacitors which possess high charge storing capacity.

The narrow smearing region is good for conducting PMCs/PNCs but not good for dielectric PMCs/PNCs. Such dielectric PMCs/PNCs could be practically used only before conducting transition, as beyond transition the dissipation factor also increases drastically. So, to increase the dielectric constant significantly with tolerable dissipation factor, it is a difficult task to control the vol % of conductive filler, if the smearing region is narrow. In view of these problems associated with two phase PMCs/PNCs; there has been focus in recent past to study the dielectric behaviour of three- phase composites containing both ferroelectric ceramic and conducting filler. These studies showed better results in three phase composites with respect to two-phase PMCs/PNCs due to the increased width of smearing region, but the filler concentration is still high, indeed. In order to maintain lower dissipation factor and stability with frequency and temperature, the control of the microstructure and interface between different phases is required.

CHAPTER 3

FORMULATION OF THE PROBLEM

3.1 The aim and importance of the chosen problem

As discussed in the literature review, polymers generally possess low dielectric constant (< 10) and very low conductivity, generally less than 10^{-12} S/m. Some inherent conducting polymers [polyaniline, polypyrrole, poly (p -phenylene), etc.] are available but cannot be used due to inadequate mechanical properties and difficulty in their processing [36]. The electrical properties could be improved by filling the insulating polymers with different dielectric or conductive fillers. In previous studies, polyvinyl chloride (PVC), polymethyl methacrylate (PMMA), polypropylene, polyethylene, poly(vinylidene fluoride), epoxy, etc. [55, 67, 104, 106] have been filled with different dielectric and conducting fillers and the resultant composites have been claimed as potential candidates for different electrical applications. As reported, in addition to the electrical properties, the resultant material should also possess a combination of mechanical and thermal properties as it matters for a good electrical performance at end use [33]. This restriction limits the concentration of filler in the composite as it harms the flexibility and thermal properties of the base polymer.

In the light of the above discussions, the present work is an attempt to prepare a light weight flexible polymer matrix composite by introducing a low concentration of dielectric ceramic and/or high conductive nanosize filler in a high performance polymer matrix.

Literature shows that polycarbonate (PC), an engineering thermoplastic is very tough material. It also has a great history of use as high quality capacitors for many years due to good combination of dielectric properties, namely low dissipation factor (0.001 at 1 kHz), high dielectric strength, and constancy of dielectric constant in the frequency range 1 Hz to 1 MHz. [113-115]. It exhibits good mechanical properties coupled with good heat resistance, not possible with the above mentioned commodity thermoplastics. PC maintains its rigidity as well as toughness up to 140 °C [115]. Very low water absorption makes it dimensionally stable. Hence, it is stable in terms of dimension and electrical behaviour over a wide range of temperature (-65°C to 125°C) [116].

As the nature, size and amount of the filler also affect the nature of the composite and hence, selecting the filler is also a crucial part here. The filler should provide required electrical properties and should not much affect the other aspect of the polymer's property.

As dielectric filler, various ferroelectric ceramics including barium titanate ($BaTiO_3$), lead zirconate titanate ($PbZrTiO_3$), barium strontium titanate ($BaSrTiO_3$), $CaCu_3Ti_4O_{12}$ (CCTO), etc. have been used by investigators. These ceramics have brittle nature and hence at higher loading the composite becomes brittle. The conducting fillers have also been used to increase the conductivity as well as the dielectric constant of the polymer-matrix composites. Most of the good conductive metals (except aluminum) have much higher densities and are prone to corrosion. A combination of both ferroelectric ceramic and conductive filler has also been used to increase the dielectric constant of such polymer matrix composites.

For last two decades, nano-carbonaceous filler materials namely, MWCNTs, SWCNTs, graphene have been used as conductive fillers. These carbonaceous nano-filler are light weight, having the density of about 2 to 3 g/cc, which fall close to the density of polymers, less prone to corrosion and exhibit intriguing electronic properties. Nano-sized fillers are advantageous over their bulk counterparts due to the large surface to volume ratio and hence produce more interfacial area at the same volume concentration, which is the crucial property deciding factor for the composites. The aspect ratio of filler determines the concentration required for percolation (3-dimenstional connectivity of filler in the insulating matrix). As the aspect ratio increases the required concentration decreases.

Now, it can be concluded that for a light weight and flexible polymer matrix composite (a) the conductivity should be tuned with conducting filler having high aspect ratio; (b) the dielectric constant should be tuned with dielectric/conducting filler having high surface area so that more interfacial polarization could be generated.

Carbonaceous filler materials MWCNTs, SWCNTs, and carbon fibers have very high aspect ratio (generally >1000). Graphene is the material which has both the qualities viz. good aspect ratio with large surface area. The improvement in the conductivity of the polycarbonate has been reported by filling such carbonaceous fillers [60, 63-64, 110-112, 117-121] but to the best of our knowledge, no literature

has been found in which the dielectric properties have been improved by filling such single carbonaceous filler in polycarbonate.

In view of above, it was decided to fill polycarbonate with carbonaceous fillers e.g. MWCNT, SWCNT and FLG (few-layer-graphene) and the feasibility study of the resultant composite to be used as dielectric and/or conducting material have been carried out. For a comparative study, the polycarbonate was also filled with ferroelectric ceramic PZT, nano-Cu power and a combination of dielectric and conductive filler.

The SWCNT, MWCNT and FLG are the light weight carbon allotropes. Based on the geometry, among these carbon allotropes the SWCNT is expected to have the highest aspect ratio as against the lowest expected aspect ratio of FLG. Therefore, the former is expected to give percolation at a lower concentration than the later when embedded in polymer

FLG is having large surface area (due to sheet shape morphology), hence the interfacial area between FLG and PC will be higher than with the other fillers. Due to large interfacial area, high interfacial polarization should be there at the interface. Just below the percolation there should be the formation of large number of micro-capacitors due to FLG-PC-FLG combinations. The large surface area is also expected to result in high capacitance of the micro-capacitor combinations in the nanocomposites. This ultimately should increase the dielectric constant of the composite. In addition to high dielectric constant, controlled dissipation factor will be taken care of. This should prove the FLG-PC nanocomposite a very good dielectric material and the best output of the thesis. As the FLG is having sufficiently high aspect ratio, at somewhat higher concentration, the FLG-PC nanocomposite might work as conducting nanocomposite.

The possible output of a versatile two-phase, light weight, flexible (low filler concentration ensures the flexibility) polycarbonate based dielectric and conducting nanocomposite, proves the importance of the chosen problem.

3.2 A brief introduction on the materials selected for the present research

3.2.1 Polymer Matrix: Polycarbonate

Polycarbonate (PC) was selected as polymer matrix to prepare the micro-/nanocomposites. Polycarbonate (Bisphenol A polycarbonate) is an engineering thermoplastic. The polycarbonate from bisphenol A (BPA) was first prepared in 1953 by chemists Daniel Fox and Herman Schnell while working independently at their respective companies. However, the first significant report for the synthesis of aromatic polycarbonate was given by Einhorn in 1898 [115]. Its chemical structure is shown in Figure 3.1.

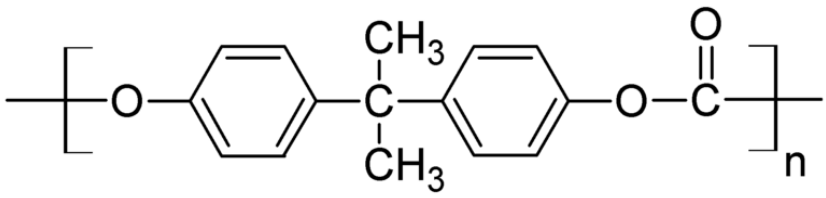

Figure 3.1. The chemical structure of Polycarbonate [115]

Polycarbonate is a transparent and stiff thermoplastic. The chemical structure of PC (Figure 3.1) consists of two phenyl rings in the backbone and two pendants - CH_3 groups introduce stiffness by steric hindrance and make polymer less crystalline and transparent. Some flexibility arises due to the O-C-O single bonds in the carbonate linkage along the backbone. This flexibility coupled with the para-linkage of phenyl rings provides excellent toughness to polycarbonate and hence in general, PCs are considered to be the toughest thermoplastic. Amorphous structure of PCs, gives rise low shrinkage during moulding. The rigid molecular backbone of the bis-phenol **A** polycarbonates leads to a high melting temperature *(T,* = 225-250°C) and glass transition temperature *(Tg*= 145°C).

PCs are stable in terms of dimension and electrical behaviour over a wide range of temperature (-65°C to 125°C) [116, 122]. PC is electrically resistant, resistant to oils and chemicals and negligible moisture absorber [115]. It has good tensile strength. The properties of PC are laid down in the Table 3.1.

Table 3.1: Thermal, mechanical and electrical properties of PC [115-116, 123-124].

Property	**Value/Range**
Density	1.30 g/cm crystallites density 1.20 g/cc macroscopic density
Electrical Properties	
Volume Resistivity	2.1×10^{18} ohm-m
Dielectric Constant	3.02 (at 1 kHz), 2.96 (at 1 MHz)
Dissipation Factor (Power factor)	~ 0.001 at kHz
Dielectric Strength 1/8 inch sample	157 kV/cm
Thermal Properties	
Glass Transition Temperature	~145°C
Melting Temperature	225-250°C
Thermal Conductivity	0.19 W/m.K
Coefficient of Thermal Expansion	7×10^{-5} /°C
Mechanical Properties	
Tensile Strength	~ 65 MPa
Impact Strength (Notched Izod)	600-800 J/m
Tensile Modulus	2.3 GPa
Flexural Modulus	2.5 GPa
Elongation at Break (%)	100
Hardness Rockwell	M70
Poisson's Ratio	0.37

PCs are the only material having a very good combination of properties e.g. toughness, rigidity, transparency, self-extinguishing characteristics, good electrical insulation characteristics and heat resistance [115] and at a reasonable cost. The application of polycarbonates, therefore, largely arise where at least two and usually three or more of the advantageous properties are required and where there is no cheaper alternative. The largest single field of application for moulded PCs is in electronics and electrical engineering.

Covers for time switches, batteries and relays, for example; utilize the good electrical insulation characteristics in conjunction with transparency, flame resistance and durability. The polymer is widely used in making coil formers. In this case the ability to winding the wire tightly without deformation of the former, the heat stability, the oxidation resistance and the good electrical insulation characteristics have proved invaluable. Polycarbonate mouldings have also been made for computers,

calculating machines and magnetic disc pack housing, terminals, contact strips, starter enclosures for fluorescent lamps, switch plates and a host of other miscellaneous electrical and electronic applications. Polycarbonate films are used in the manufacturing of capacitors [115, 123].

3.2.2 Filler Materials

Filler materials for making composites were selected so that the dielectric constant of the PC can be increased. As dielectric filler, Lead Zirconate Titanate (PZT) was selected. The filler with conducting nature can be used to increase the conductivity as well as to improve the dielectric constant of the polymer based composites. As conducting fillers, nano copper powder and nano sized carbonaceous fillers (CNTs and graphene) were used.

3.2.2.1 Dielectric filler: Lead Zirconate Titanate (PZT)

PZT is the solid solution of ferroelectric $PbTiO_3$ (Tc = 490 °C) and antiferroelectric $PbZrO_3$ (Tc = 230) [125-126]. PZT properties depend on the Zr/Ti ratio. It is generally represented by the formula $\mathbf{Pb[Zr_xTi_{1-x}]O_3\ (0 \leq x \leq 1).}$ With ABO_3 type formula PZT possesses perovskite structure where **O** stands for oxygen, **A** represents a cation with larger radius and **B** represents another cation with smaller ionic radius. Perovskite structures generally idealized as a cubical unit cell as shown in Figure 3.2 (a). On changing temperature the cations and anions may move slightly with respect to their equilibrium position in the cubic perovskite unit cell and may transform into other phases e.g. tetragonal, orthorhombic, and rhombohedral phases as shown in Figures 3.2 (b)-3.2(d) [127].

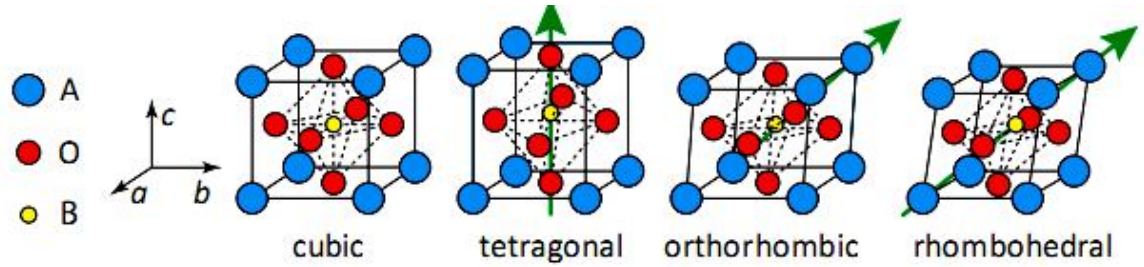

Figure 3.2. Perovskite structure of ABO_3 unit cell in (a) the cubic phase (b) tetragonal phase (c) orthorhombic phase and (d) rhombohedral phase [127].

Such perovskite type oxides exhibit high dielectric constant value with low dissipation due to the ferroelectric phases (tetragonal, orthorhombic, and rhombohedral phases). Above Curie temperature (T_c), the ferroelectric phase may change into the paraelectric phase (i.e. into cubical phase) and hence the dielectric properties may change considerably. The Curie temperature (Tc) for PZT is about 360 ^oC [125, 128] and therefore the properties are relatively stable over a wide temperature range than the other ferroelectric ceramics (e.g. the Curie temperature of $BaTiO_3$ is about 120 ^oC). The dielectric constant of the PZT may be found in the range of 100-3500 (at 1 kHz) depending upon the percentage of **x** in the above formula for PZT. The dissipation factor is found to be about 0.01 (at 1 kHz) [125,127].

3.2.2.2 Conducting fillers: Nano-Cu, SWCNT, MWCNT and FLG

As conducting fillers metallic (Cu) nanopowder and carbonaceous (SWCNT, MWCNT and FLG) fillers have been added into polymer/composites. The copper nanoparticles were almost of spherical in shape. Due to high surface to volume ratio, these nanoparticles are likely to get oxidized. The oxidised particles may be beneficial and detrimental depending on the applications. The oxide layer on the particle may become the obstacle in the occurrence of percolation while considering the quantum tunnelling or /micro-capacitor concept. The presence of oxide layer may results in lower dissipation factor of the nanocomposites compared to those of without oxide layer for a given volume fraction of conducting filler.

As carbonaceous fillers SWCNT, MWCNT and few layer graphene (FLG) have been used due to their excellent thermal, mechanical and electrical properties. In addition to this, they possess high aspect ratio (which is important for achieving percolation at lower filler loadings), high surface to volume ratio (which promotes larger interfacial interactions with matrix), and finally lower density comparable to most of polymers which is important to avoid settling of fillers in the matrix during processing and achieving light weight of final composite. Carbon nanotube (CNTs) can be considered as seamless 1-dimentional cylinders of one or more layers of graphene as can be seen in Figure 3.3 (a). Graphene is a 2-dimensional single-atom thick membrane of carbon atoms arranged in a honeycomb crystal (hexagonal structure) as shown in Figure 3.3 (b). It has sp^2 hybridization. These carbonaceous fillers are less prone to oxidation.

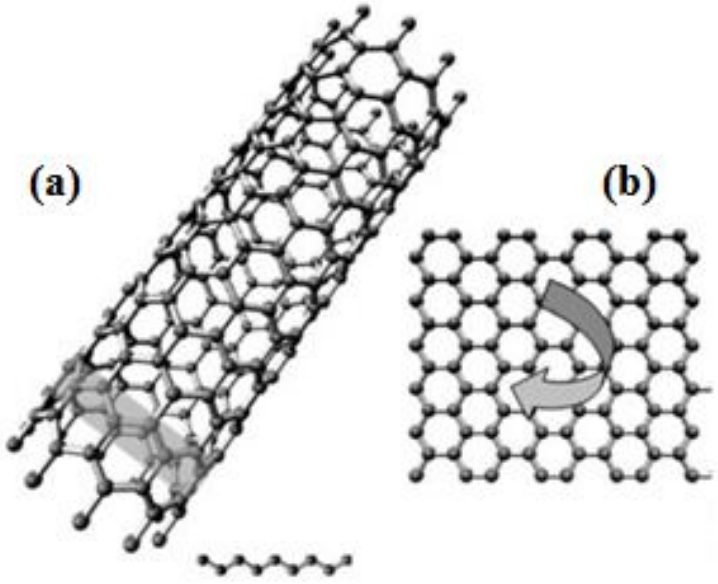

Figure 3.3. Schematic presentation of (a) SWCNT and (b) graphene sheet. The graphene sheet can be rolled in the form of SWCNT [129].

As discussed earlier, the conductivity of the PC has been improved by filling it with SWCNT and MWCNT. The previous findings are summarized in Table 3.2. The investigation reports on study of Cu-PC and graphene-PC micro-/nanocomposites have not been found, to the best of the knowledge of author. However, investigations have been carried out on commodity thermoplastic based and epoxy matrix composites containing graphene and Cu-fillers. The results are summarised in Tables 3.3 and 3.4, respectively.

Table 3.2: A brief summary of parameters and results obtained in previously reported works for SWCNT-PC and MWCNT-PC nanocomposites.

Filler	**Solution**	**Methods**	**Percolation threshold, wt %**	**Maximum achieved conductivity(S/cm)**	**Ref.**
SWCNT (HiPco),CarbonNanotech	$CHCl_3$	Shaken, sonicated	0.1	10^2 at 7wt %	[130]
SWCNT (HiPco), CarbonNanotech	-	Extruded	0.3	10^{-1} at 1wt %	[131]
SWCNT(Arc)	C_6H_8O	Sonicated	0.5	10^{1} at17wt %	[120]
SWCNT(HiPco)	C_6H_8O	Sonicated	0.5	10^1 at 1wt %	[120]
SWCNT(HiPco)		Extruded	0.5	10^{-1} at 2wt %	[120]
SWCNT(Arc)	$CHCl_3$	Sonicated	1.9	10^{-1} at 4wt %	[120]
SWCNT(Arc)	-	Extruded	1.9	10^{-1} at 10wt %	[120]
SWCNT(Arc)	-	Extruded	>5	10^{-1} at 7wt %	[131]
MWCNT (CVD)Hyperion Catalysis	-	Extruded AR ~1000	1	5E+0 at 3wt %	[118]
MWCNT (CVD)Hyperion Catalysis	-	Extruded AR >100	1.44	2E+0 at 5wt %	[60]
MWCNT (CVD)		Extruded	5	1E-4 at 15wt %	[119]
MWCNT (CVD)Hyperion Catalysis		Extruded	1-2	1E+1 at 15wt %	[121]

Table 3.3: A summary of parameters and results obtained in previously reported works for graphene based fillers-filled nanocomposites.

Filller	**Matrix**	**Methods**	**Percolation threshold, wt %**	**Maximum achieved conductivity (S/cm)**	**Ref.**
Thermally reduced functionalized Graphene Sheets	Epoxy resin	Ultraturrax and sonication	1.5 wt %	~ 10^{-8} at 1.5 wt%	[132]
Graphite oxide (prepared by ultrasonic exfoliation of graphite)	- Polystyrene	Solution dispersion	0.1 vol %	~ 10^{-3} at 1 vol %	[110]
Exfoliated graphene	PVC	Liquid phase blending	0.6 vol %	~ 10^{-2} at 6.5 vol %	[133]
Foliated graphite	Polystyrene	In situ polymerization	1.1 vol %	~ 10^{-2} at 3 vol%	[134]
Functionalized graphene sheets (FGS)	PVDF	Solution dispersion, sonication	2 wt %	10^{-2} at 14 wt%	[135]
Exfoliated graphite (EG)	PVDF	Solution dispersion, sonication	5 wt %	10^{-4} at 4 wt%	[135]
Graphene	PET	Melt compounding	0.47 vol %	10^{-2} at 3 vol%	[136]
Graphite nanosheets	PMMA		0.31 vol %	10^{-1} at 5 vol%	[137]
Reduced graphene oxide	Epoxy	Aqueous casting method	0.12 vol %	-	[112]

Table 3.4: Various polymer matrix composites with different size of Cu filler and the percolation threshold.

Matrix	Particle Size	Percolation Threshold	Method	Maximum achieved conductivity	Ref.
Polyvinyl Chloride (PVC)	~ 10-44 μm	~ 3.7 Vol %	Ball milling	~ 10^{-2} S/cm at 9.3 vol %	[94]
Low density polyethylene (LDPE)	< 38 μm	~18 Vol %	Mixing and melt press	~ 10^{1} S/cm at 24 vol %	[106]
Linear low density polyethylene (LLDPE)	< 38 μm	~18 Vol %	Mixing and melt press	~ 10^{1} S/cm at 24 vol %	[106]
Polypropylene (PP)	~ 10 μm	~ 6 Vol %	Mixing and compression molding	-	[105]
Polypropylene (PP)	~ 100 μm	~ 11 Vol %	Mixing and compression molding	-	[105]
Polyvinyl Chloride (PVC)	~ 100 μm	~5.0 Vol %	Mixing and hot pressing	~ 10^{1} S/cm at 30 vol %	[138]

In the above investigations, efforts have been made to increase the dielectric constant/conductivity of the commodity thermoplastics and epoxy resin by adding sophisticated high priced conducting fillers.

It would seem interesting to examine the effect of fillers on dielectric constant and electrical conductivity of engineering thermoplastics such as PC. Till date investigations on the dielectric behaviour of PC matrix micro-/nanocomposites are sparse. So, the present work is an attempt to study the effect of advanced dielectric and conducting fillers on the dielectric behaviour and electrical conductivity of PC by developing a micro-/nanocomposites. The prepared nanocompoistes would be potential materials for embedded capacitor and EMI/ESD applications.

CHAPTER 4 `

METHODOLOGY

This chapter is containing the discussion about the materials and methods adopted for composite preparation and characterization.

4.1 Materials

Polycarbonate (PC) was selected as polymer matrix. Lead Zirconate Titanate (PZT) was used as ceramic filler to prepare two-phase and three-phase PMC. Nanosize conducting filler of different forms (particle, sheet and tube) were used to prepare conducting particles filled two phase nano-composites. The conducting nano-size copper particles, few-layer-graphene (FLG) sheets, and CNTs (MWCNT and SWCNT) were used as conducting fillers. Three phase composites were prepared by adding CNT in two phase PC-PZT composite to examine its effect on dielectric behaviour.

Commercial grade of PC (in granule form) was obtained from local market. PZT powder (reported average particle size 0.85 μm and dielectric constant of 1105 in the polarisation state, density 7.56 g/cc) was donated by M/s Sparkler Ceramic Private Limited, Bhosari, Pune. Nano-copper powder (density 8.94), MWCNTs and SWCNTs (density 2.5 g/cc) were purchased from Nanoshel, India. According to manufacturer, the average particle size of Cu was 40 nm, the diameter and length of MWCNTs were (20-30 nm) and (3-8 μm) respectively. For SWCNTs the diameter and length were reported to be (0.7- 2 nm) and (3-8 μm). Few-layer-graphene (FLG) was prepared using dry ice method which was reported by A. Chakrabarti et al. [139]. The density of the prepared FLG was taken to be 2.1 g/cc.

4.2 Preparation of few layer graphene (FLG)

Magnesium ribbon of 99% purity, obtained from local market in Jaipur, was used to prepare graphene. A bowl was prepared from the dry ice (Solid carbon

dioxide). 3 gm of Mg ribbon was put in this bowl and ignited with the help of burner. The bowl was immediately covered with another dry ice bowl. The following reaction as given in Eq. (4.1) was involved during the combustion process.

$$2Mg\ (s) + CO_2\ (g) \longrightarrow 2MgO\ (s) + C\ (s) \qquad (4.1)$$

After the complete combustion of Mg, a black colour carbonaceous product was obtained and was collected in a beaker. The carbonaceous product was likely to contain MgO and unburned Mg as impurities. To remove these undesirable traces of impurities, the black product was stirred overnight in 100 ml of 1M hydrochloric acid. Both MgO and Mg form $MgCl_2$ when react with HCl. $MgCl_2$ is soluble in water. The mixture was filtered and washed several times with deionized water until the filtrate attained neutral pH. The final solid carbonaceous product was then dried in vacuum oven at 100°C for 18 hours. The carbonaceous product was analysed by a combination of XRD, Raman spectroscopy, TEM, electron diffraction (ED) pattern. The product was confirmed as few layer graphene (FLG).

4.3 Preparation of micro-/nano-composites

The micro- and nano-composites with varying content of filler materials (micron size PZT, nano size copper, SWCNTs, MWCNTs and FLG as the case may be) were prepared by solution mixing followed by hot pressing method. Initially, pre-calculated weight of filler was suspended in Tetrahydrofuran (THF) and subjected to sonication treatment. The timings of sonication were for 45 minutes for PZT, 60 minutes for nano copper, 90 minutes for FLG and CNTs to ensure the breaking of agglomerates and finally to achieve uniform dispersion of filler in the THF. Following this, weighed amount of PC granules was added slowly in the properly dispersed filler/THF suspension with concurrent stirring and heating at approximately 80 ^{0}C using hot plate cum magnetic stirrer. For making three-phase nanocomposites, the two-phase PZT-PC micro-composite having 14 vol % of PZT, has been considered as matrix and accordingly the weight was taken. Stirring and heating were continued till the viscous composite mass was obtained. The viscous nanocomposite mass was

poured on a glass plate and drawn in the form of thin film by rolling it by a glass rod; the thin film was air dried. Thereafter, the thin film was dried in a vacuum oven at 110 ºC for 15 h, crushed and then finally hot pressed in a laboratory press unit (15 ton manual hot and cold press, Kimaya Engineers Pvt Ltd, Pune) using a tool steel die. The dried and crushed composite film was filled in a three piece die cavity having diameter of 13 mm. A mould release agent was applied on the die surface to avoid sticking of PC when it flows during hot pressing. The filled-in die-assembly placed in the hot press and subjected to heating with an average heating rate of 7ºC/min under a pressure of 45 MPa to a maximum temperature of 240 ºC (the maximum temperature was 230ºC in cases of CNT and FLG filled composites). After a soaking period of 20 minutes under the constant pressure of 45 MPa, the sample was naturally cooled down to a temperature of approximately 50ºC. Finally the composite sample was ejected out from the die. The composite pellet so produced was having a diameter of 13 mm and thickness of 2±0.2 mm. Nanocomposite samples containing varying amount of filler materials were prepared in the same way. To prepare a nanocomposite with desired volume/weight percent of filler, the required weight percent/volume percent of filler particles was determined from the relation given as in Eq. (4.2)/Eq. (4.3) [36];

$$W_f = V_f * (\rho_f/\rho_m) / [1 - V_f + V_f * (\rho_f/\rho_m)] \quad (4.2)$$

$$V_f = W_f / [\, W_f + (1 - W_f) * (\rho_f/\rho_m)] \quad (4.3)$$

Where, W_f is weight fraction of filler, V_f is the desired volume fraction of filler, ρ_f is the density of the filler and ρ_m is the density of the matrix (PC). All the micro-/nanocomposites were prepared in THF solution and hence for comparison study the reference polycarbonate was also treated with THF solution. This treated PC has been designated as *control PC* and all the properties of the micro-/nano-composites were studied with respect to control PC (i.e. used as reference material). The density of the control PC was measured experimentally and found to be 1.23 g/cc. The same value was used for all compositions of composite samples.

4.4 Characterizations

Various characterization methods were employed to analyse matrix, filler component and various micro-composites/nanocomposites for phase identifications. The methods are discussed in subsequent paragraphs.

4.4.1 Density

The theoretical density (ρ_{th}) of the composites was calculated using the rule of mixtures (ROM) given by Eq. (4.4) [36]. The experimental density (ρ_{exp}) of the filled micro- and nano-composite samples was measured by Archimedes's Principle. The weight of the sample was measured in air and the medium and density was determined using Eq. (4.5).

$$\rho_{th} = \rho_m . (1-V_f) + \rho_f . V_f \quad (4.4)$$

$$\rho_{exp.} = [W_{air}/(W_{air} - W_{medium})]^* \rho_{medium} \quad (4.5)$$

Where, ρ_m and ρ_f are the densities of matrix and filler, respectively. W_{air} and W_{medium} are the weight of the sample in air and medium (ethanol is taken as medium), respectively. The ρ_{medium} is the density of the medium. In this work, ethanol was used as medium for density measurement which had the density equal to 0.789 g/cc. The composite pellets were precisely weighed using a precision electronic balance (CAX 200) having the accuracy of 0.1 mg.

4.4.2 X-ray Diffractometry (XRD)

X-ray diffraction Instrument X'Pert PRO PANalytical was used to characterise PC, fillers and composites at the scan rate of 0.1°/s in the 2 theta range of 10 to 90° (in some case it was varied). XRD of PC was carried out before and after solution treatment for any structural change. XRD of fillers was done to identify the presence of phases and impurity (if any) in them. The samples of micro- and nano-composites

were also characterised by XRD to reveal any phase change that might have occurred during their fabrication.

4.4.3 Raman Spectroscopy

Raman spectroscopy was employed to characterize FLG and CNTs so as to ascertain the formation of graphene in FLG and to ensure the identity of CNTs (SWCNT and MWCNT). Raman spectrometer (STR300, Laser: 532 nm) was used for this purpose. The filler materials were characterised in as prepared/received form.

4.4.4 Scanning electron microscopy (SEM)

Samples of PZT powder and the micro-composites/nanocomposite were characterized by SEM (JEOL: JSM 6010 (filament based) and FEI: NovaNano SEM-450 attached with EDS). The sample of PZT powder was prepared by dispersing the powder on carbon tap in order to make it conducting and analyzed under SEM. The samples of micro/nano composites were prepared by breaking the disc samples and preparing the flat surface of the cut section by grinding on a series of bonded abrasive paper (SiC) up to 1200 grit size. One of the fractured samples was examined in as-such condition. For good quality SEM images the sample should be electrically conductive and hence the polymer composites samples were made conductive by applying a thin coating of platinum using sputter coater. In addition to microstructural information, chemical information (of Cu-PZT-PC sample) was obtained from energy dispersive X-ray spectroscopy (EDS) detector attached with SEM instrument.

4.4.5 Transmission Electron Microscopy (TEM)

It is an important technique for providing structural information of nano size materials. The TEM instrument FEI: TECNAI G^2 operated at 200 kV was used to investigate nanostructural features of Cu, CNTs and FLG and the micro- and nano-composites. For TEM study of composite samples, each of the samples was dissolved in the THF and sonicated for 30 minutes for the sake of good dispersion of the filler

particles in the solution. Thereafter, one drop of the well dispersed sample was put on the carbon coated copper grid with the help of micro pipette. The copper grid was then dried for 2 hours and then used under TEM. The High resolution mode of TEM (HRTEM) was used to investigate the characteristic features of carbon nanotubes. Electron diffraction (ED) patterns were also taken for determination of crystal structure of the sample under consideration. The ED pattern has been indexed by (i) measuring the distances of reflection spots from the centre spot and (ii) by the cosine θ relationship using miller indices of two intersecting planes as given in Eq. (4.6) [140].

$$\cos\theta = (h_1h_2 + k_1k_2 + l_1l_2)/\{(h_1^2 + k_1^2 + l_1^2)(h_2^2 + k_2^2 + l_2^2)\}^{1/2} \quad (4.6)$$

4.4.6 Differential scanning calorimetry (DSC)

The DSC instrument (NETZSCH: DSC 204F1 Phoenix) was used in this study. The DSC analysis was carried out for PC and micro-/nanocomposites in the temperature range of 28 °C (room temperature) to 300 °C with 15 °C/min. heating rate, in nitrogen atmosphere.

4.4.7 Electrical properties

Electrical characterizations were carried out using a Wayne Kerr Electronics precision impedance analyzer (6515B, UK). Both sides of the composite pallets were coated with thin layer of silver paste for good electrical contacts with the electrodes of sample fixture. The capacitance, dissipation factor and electrical resistivity/impedance were measured in the frequency range of 10^2 Hz to 10^6 Hz. The capacitance and dissipation factor were also measured with varying temperature from ambient to 200 °C.

The dielectric constant and electrical conductivity of the composite samples were calculated using the relations given in Eq. (4.7) and Eq. (4.8) [36, 94], respectively.

$$\varepsilon = C.t/\varepsilon_0.S \quad (4.7)$$

$$\sigma = 1/ [Z. S/t] \quad (4.8)$$

Where, **ε** is the permittivity of the sample, **C** is the capacitance, **σ** is the conductivity, ε_o **(**8.854 x 10^{-12} F/m) is the permittivity of free space, **Z** is the impedance**, t** is the thickness and **S** is the cross sectional area of the sample. The measurements were taken for two samples of each composition and the average values were plotted.

The methodology adopted in the research work has been summarized in the flow diagram in Figure 4.1.

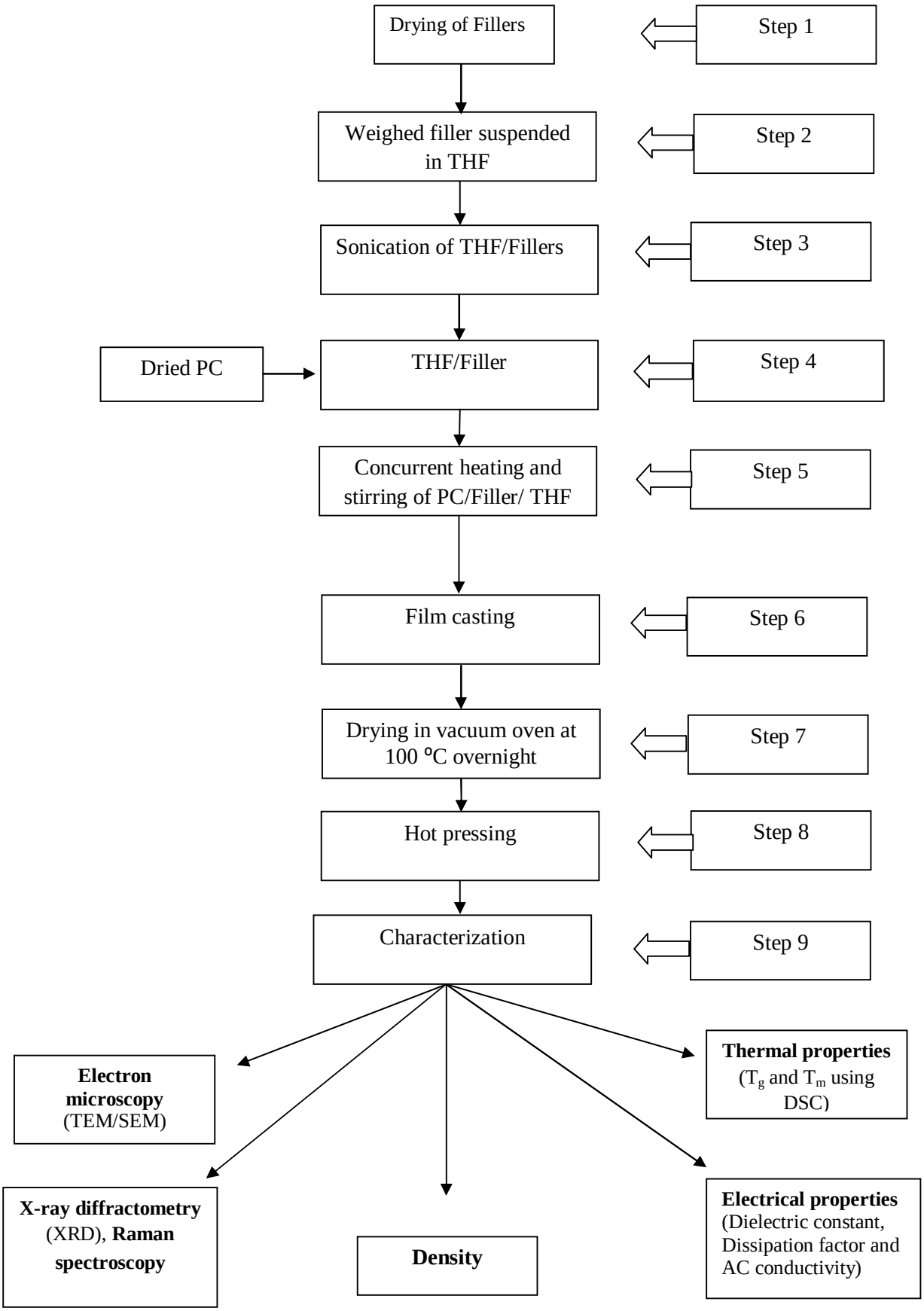

Figure 4.1. Flow diagram showing methodology for micro-/nanocomposite preparation and characterizations.

CHAPTER 5

RESULTS AND DISCUSSIONS
(Two-Phase Composites)

5.1 PZT-PC Composites

Two phase PZT-PC composites were prepared with different PZT content as given in Table 5.1. The prepared composites were characterized using XRD, SEM, DSC techniques. AC electrical conductivity, dielectric constant and dissipation factor were also measured. The effect of frequency and temperatures on the dielectric properties of composites was also studied.

Table 5.1: The concentration of the PZT in the PC matrix, by weight percent and volume percent.

PZT (density= 7.56 g/cc) content by	
wt %	**vol %**
0	0
10	1.77
20	3.91
30	6.52
50	13.99
60	19.61
70	27.51

5.1.1 Density

The density of the pure polycarbonate pellet, prepared by using as-received granules (or as-received) of polycarbonate, was 1.194 g/cc and density of control PC pellet, prepared by solution (in THF) method followed by hot pressing, was 1.23 g/cc. The difference in the density of as-received and control PC is probably due to increased crystallinity while solution treating [141]. Due to increased crystallinity, the ordered structure increases which reduces the free volume available in polymer structure. The experimental and theoretical densities of the PZT-PC composites are

shown in Fig. (5.1). Experimental densities are in well agreement with the theoretical densities, indicating the porosity free composites. The density of the composite was increased with increasing vol % of the PZT which is due to the higher density of the PZT (7.56 g/cc).

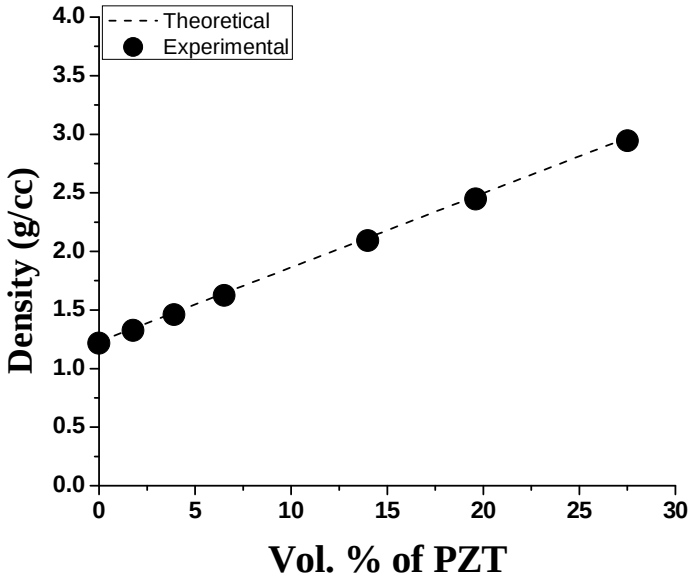

Figure 5.1. Theoretical and experimental densities of the PC-PZT composites.

5.1.2 X-ray diffractometry

The XRD pattern for as received PC shows a broad halo at about 17° as-shown in Figure 5.2(a). It was found that the halo-reflection was somewhat sharper and narrower in control PC than it was in case of as-received PC. In control PC, due to crystallization, the polymer chains were more orderly attached than that in as-received PC. In solution the polymer chains are separated with negligible interaction in between them. As the THF (solvent) starts to evaporate the concentration increases and chains start to interact with each other favouring the crystallization to some extent. Works by Schorn et al. [141] and Lehmann [142] strongly favour the crystallization from solution. Hence, in control PC, due to increased crystallized domains, the polymer chains were more orderly attached than attached in as-received PC, resulted in the narrower and sharper peak. A peak near about 73° was present in all the XRD traces and was due to the instrumental error (may be due to the impurity

in X-ray tube, as suggested by operator) as shown in inset of Figure 5.2 (a), and hence this peak has been neglected in all the cases. In the XRD of PZT, the reflections were found at 2θ = 21.8°, 31.1°, 38.3°, 44.2°, 50.2°, 55.3°, 64.9°, 69.1°, 73.6°, etc as shown in Figure 5.2 (b). The XRD reflections show that PZT has rhombohedral [Ref. PDF # 732022 for $Pb(Zr_{0.58}Ti_{0.42})O_3$] unit cell in perovskite structure. In this unit cell all the cations and anions move slightly with respect to their equilibrium position in the cubic unit cell and possesses a permanent dipole moment in the [111] direction.

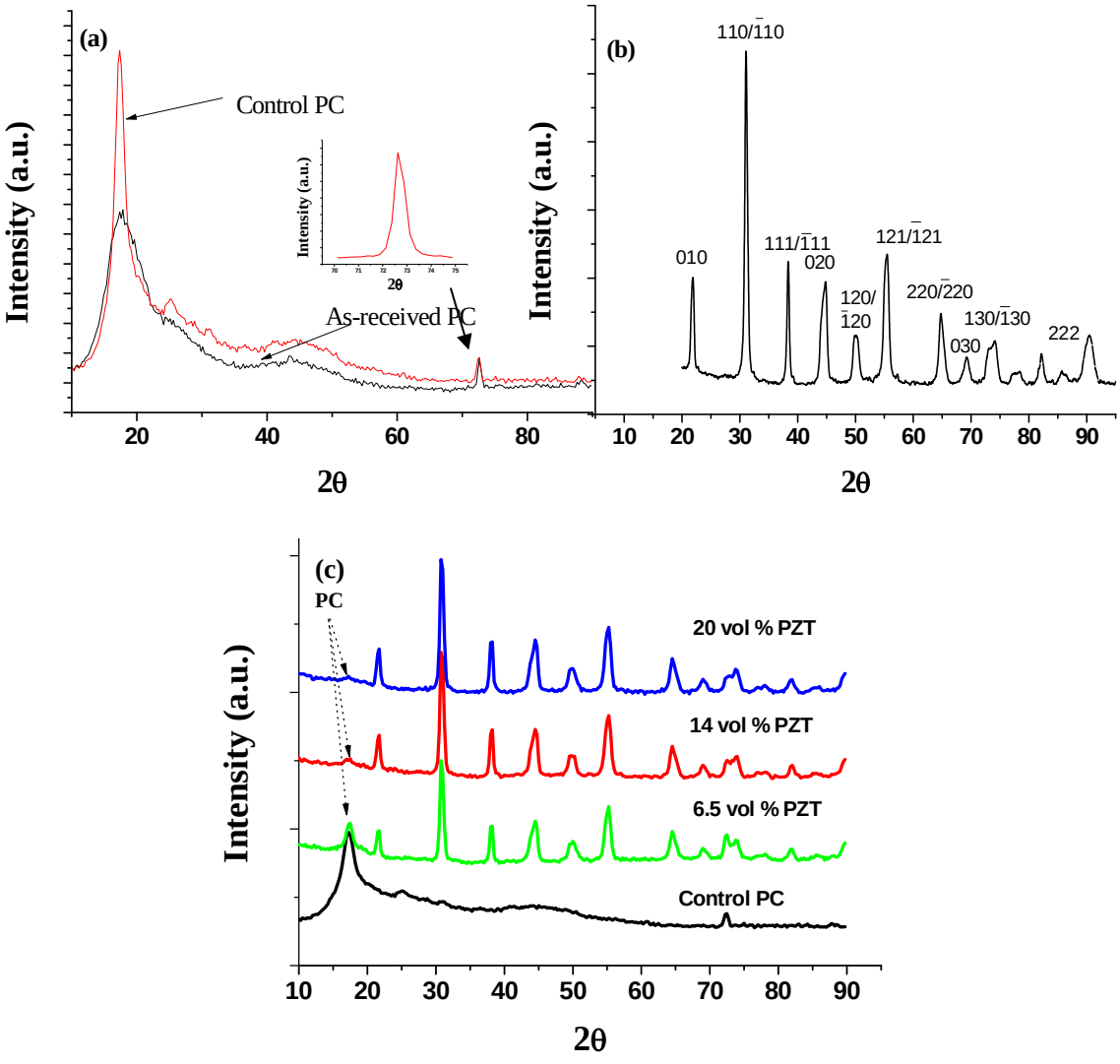

Figure 5.2. XRD patterns of (a) as-received and control PC, (b) as-received PZT powder (c) control PC and its composites containing ~6.5 vol %, ~14 vol % and ~ 20 vol % of PZT.

The XRD traces for PC-PZT composites are shown in Figure 5.2 (c). In comparison to control PC and PZT, the PZT-PC composites have not shown any

obvious difference; however, the intensity of PC halo is suppressed with increasing amount of PZT which is due to the decreased Vol % of PC with increasing PZT content.

5.1.3 Scanning electron microscopy

The SEM images for PZT powder and PZT-PC composites are shown in Figure 5.3 (a) and (b-c), respectively. It is clear from Figure 5.3 (a) that the particle of the PZT powder is below 1μm, confirming the average particle size (0.85 μm), reported by the supplier. PZT particles are of polygonal shape.

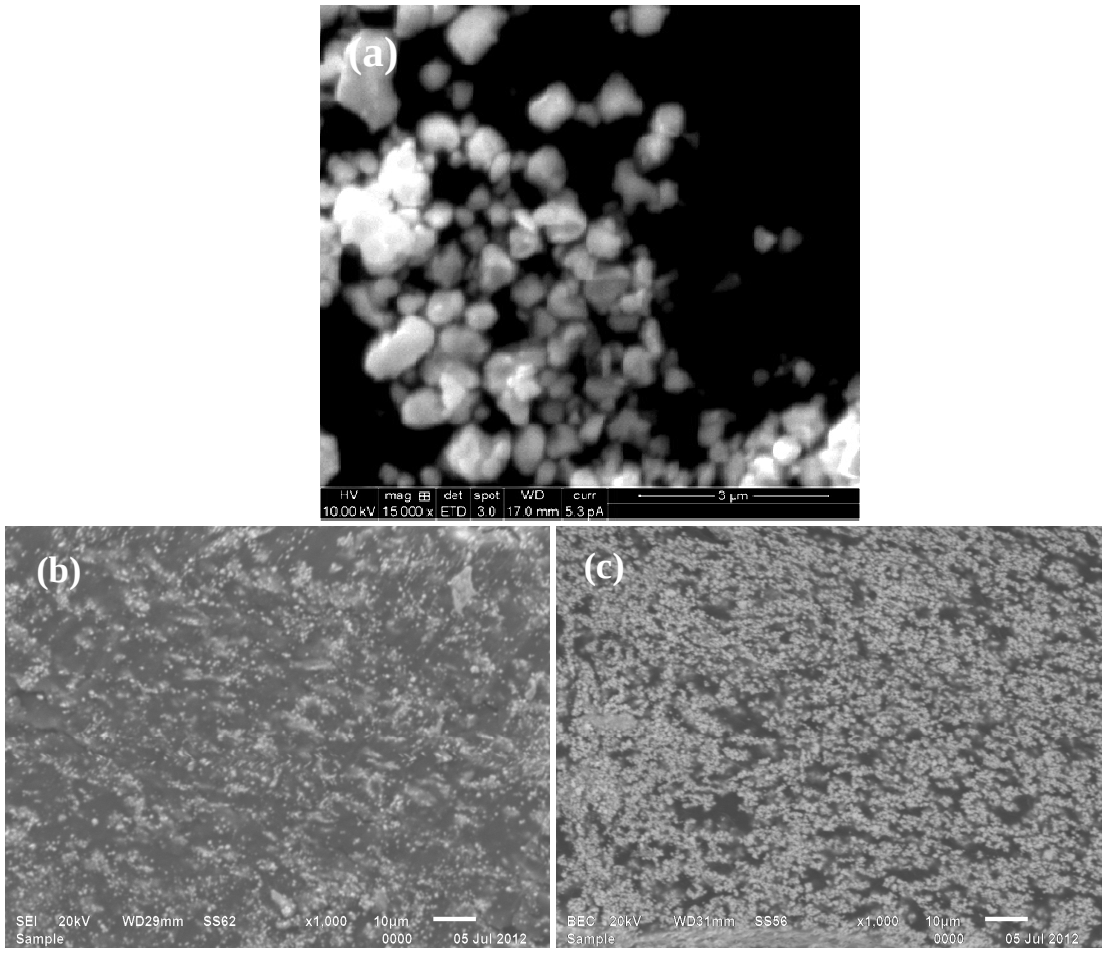

Figure 5.3. SEM images of (a) PZT powder, (b) PZT (6.5 vol %)-PC composite and (c) PZT (27.5 vol %)-PC composite.

Figures 5.3(b) and 5.3(c) show the SEM images of composites containing 6.5 vol % and 27.5 vol % PZT, respectively. Pores were not seen in both the images which indicate that the composites were almost porosity free. This was also confirmed by density measurement. These images also show a good dispersion of PZT particles in the PC matrix.

5.1.4 Differential scanning calorimetry

The DSC traces for as-received, control PC and composite with 6.5 vol % PZT are shown in Figure 5.4. The DSC trace for as received PC showed a sharp step change at about 149 ^{0}C whereas no such sharp step change is observable in control PC and PZT-PC composite. DSC trace for as received PC does not show any endothermic peak suggesting that the as received PC is having amorphous nature. On the other hand, control PC and PZT-PC composite show a sharp endothermic peak which indicates the crystallinity induced during solution treatment. The step change at 149.02 ^{0}C indicates the glass transition temperature which is a characteristic of amorphous polymer.

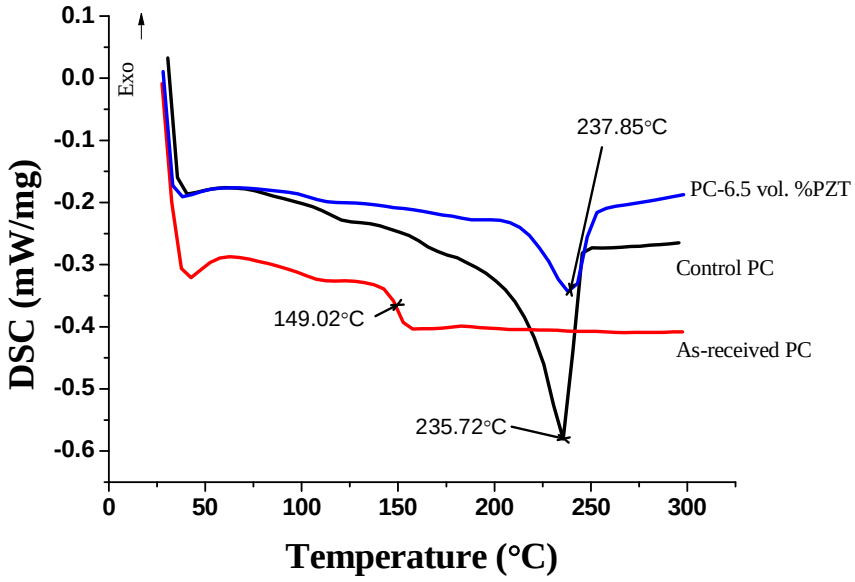

Figure 5.4. DSC traces of as-received, control PC and PZT (30 wt %)-PC composite.

Due to amorphous nature of as-received PC, beyond T_g, the segmental mobility of polymer chains starts and it goes from rigid solid state to rubbery state and does not show any sharp melting indication. The observations are in support of previous study [124]. In control PC, the crystalline structure was introduced as confirmed by density and XRD study. Hence, due to semi-crystalline nature, the control PC showed a sharp endothermic peak at 235.72 °C which is probably due to the melting of ordered crystallites of the PC. In case of PZT-PC composite, the melting point was slightly increased to higher temperature which might be attributed to the strong interfacial bonding between PZT and PC which may be correlated to the polar nature of PZT and PC. The reduced enthalpy of composite compared to controlled-PC might be due to the reduced vol % of PC.

5.1.5 Electrical Properties

In this section results of AC electrical conductivity, dielectric constant and dissipation factor of the composites have been discussed. The variations in dielectric constant and dissipation factor with the frequency and temperature were also examined.

5.1.5.1 AC electrical conductivity

Figure 5.5 shows the AC electrical conductivity of the PZT-PC composites as a function of vol % of PZT in PC matrix. As the vol % of PZT increased in the composite, slight increase in the conductivity was observed. However, the maximum achieved conductivity for the composites with 27.5 vol % was $7x10^{-9}$ S/cm which indicates that the composites are insulating. The slight increase in conductivity of the composites may be attributed to higher conductivity of PZT than that of PC [12, 143]

5.1.5.2 Dielectric constant and dissipation factor

As shown in Figure 5.6, the dielectric constant and the dissipation factor of PC are found to be 3.37 and 0.005, respectively. The dielectric constant of the composite increased with increasing PZT content which is attributed to the higher dielectric

constant of PZT as compared to PC matrix. The increment in the dielectric constant was about 8.7 (increased from 3.3 to about 12), for the composite containing 27.5 Vol % PZT. The increment in the dielectric constant was approximately 3.5 times than that of PC.

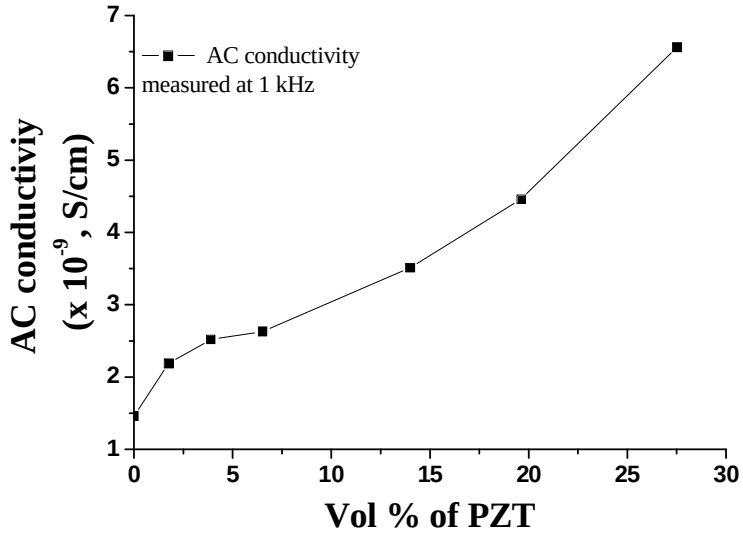

Figure 5.5. AC electrical conductivity of the PZT-PC microcomposite.

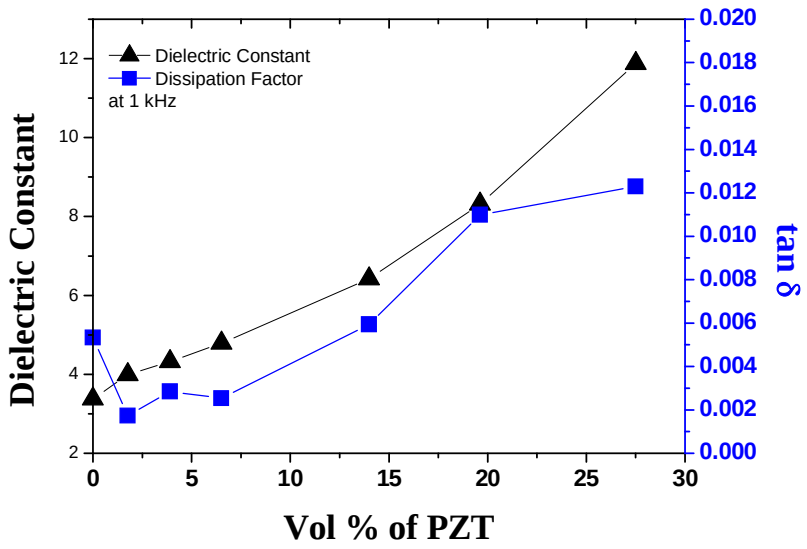

Figure 5.6. The behaviour of dielectric constant and dissipation factor (tan δ) for PZT-PC microcomposite with increasing volume fraction of PZT.

This increment was in agreement with the result for PZT/PVDF composites, reported by Goyal et al. [12]. In present work of PZT-PC for a given volume fraction, the highest dissipation factor is about 0.012 which is much lower than reported for PZT/PVDF composites. Compared to PC, it is decreased for the composites containing up to 6.5 vol % PZT. However, on further addition of PZT, the dissipation factor increased slightly with increasing PZT content. This may be attributed to the increasing interfacial polarization which increases ionic/space charge contribution in polarization mechanism. The formation of aggregates of PZT [Figure 5.3 (c)] at higher loading may be the probable reason for increase in the dissipation with increasing filler concentration [8]. The experimental dielectric constant of the composites is correlated with the values predicted from the various existing theoretical models as shown in Figure 5.7.

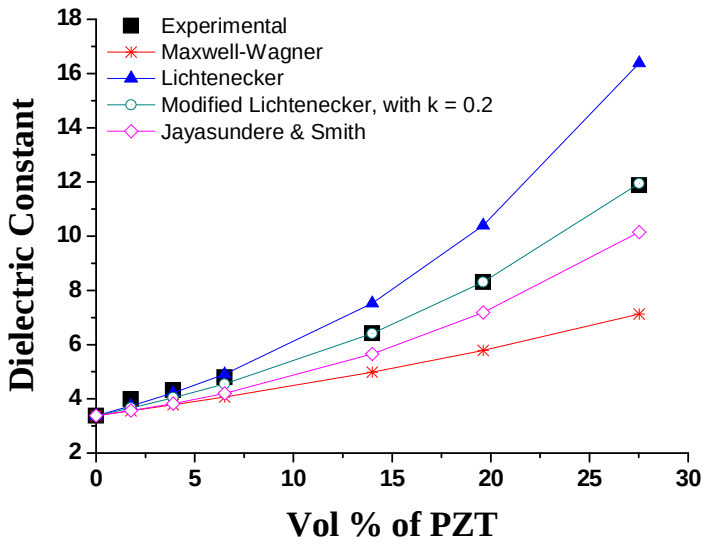

Figure 5.7. The correlation of experimental data with various existing theoretical models for dielectric constant of two-phase composites.

The experimental data were well fitted with the Lichtenecker Eq. (2.8), up to the PZT concentration of 6.5 Vol %. Beyond this concentration, the experimental data were found to be less than the predicted value from Lichtenecker Equation. This variation may be attributed to the presence of aggregates at higher filler loading; in

addition, the shape of the PZT particles is not perfectly spherical. It was interesting to observe that, the modified Lichtenecker equation (Eq. 2.9), with k = 0.2, correlated nicely the experimental data over complete range of PZT content. The value of k = 0.2 indicates the deviation from the uniform dispersion of the filler in the matrix; the aggregates of PZT particles can be observed in the composites [Figure 5.3 (b) and (c)]. These morphological factors might be responsible why the Jayasundere-Smith and Maxwell-Wagner equations have also underestimated the experimental data.

5.1.5.3 Effect of frequency on the dielectric constant and dissipation factor

The variation in the dielectric constant and the dissipation factor with increasing frequency (1 kHz to 1 MHz) is shown in Figure 5.8 (a) and Figure 5.8 (b), respectively. The composite is a heterogeneous system which shows anomalous dielectric constant behaviour due to a number of different physical mechanisms [144]. Various types of polarization mechanisms which contribute to the dielectric constant are interfacial polarization, dipole orientation polarization, atomic polarization and electronic polarization. In the given sequence, these polarization mechanisms become less dominant with increasing frequencies.

Polycarbonate and its composites with PZT showed good stability in the frequency range, however, a very slight decreasing trend was observed. The decreasing trend may be attributed to the fact that as the frequency increases the effect of particular polarization mechanism becomes less dominant. Das-Gupta and Doughty [74] explained the frequency independent behaviour of PZT within frequency range of 10 Hz to 10^5 Hz. PZT has permanent dipole moment, and hence polarization due to dipole orientation should be the dominant mechanism. In PC, the carbonyl group is the polar group in its chemical structure [145]. With increasing frequency, the contribution of dipole orientation polarization in the dielectric constant becomes lesser and lesser because the associated dielectric-relaxation fails to follow the rapid change in the direction of electric field. At higher frequencies, as the associated dielectric- relaxation fails to follow the in-phase field, the absorbed energy converts in to the heat, and hence the dissipation factor increases. However, the dissipation factor was found to be below 0.02 in the full studied frequency range.

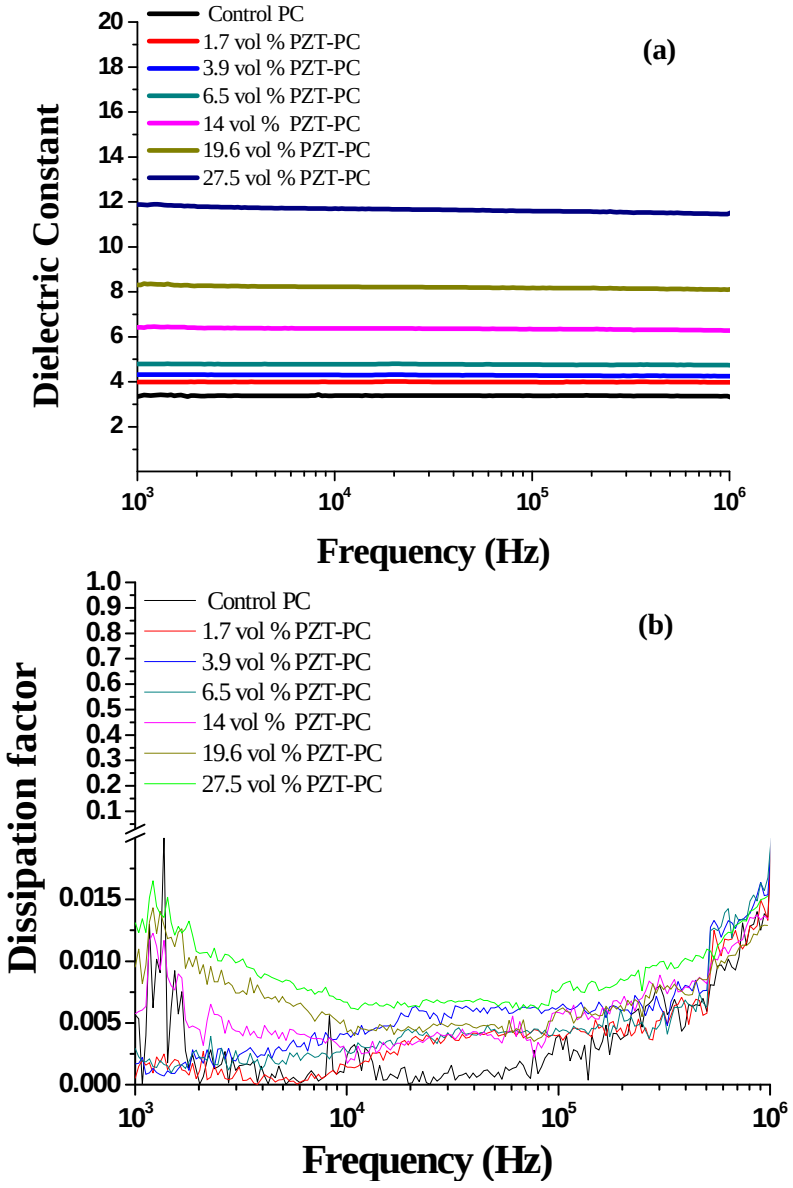

Figure 5.8. The effect of frequency on the (a) dielectric constant and (b) dissipation factor of PZT-PC composites.

5.1.5.4 Effect of temperature on the dielectric constant and dissipation factor

The temperature dependency of dielectric constant and dissipation factor were examined from room temperature to 200 °C. With increasing temperature three types of relaxation can be found in polymer dielectrics; (a) γ-relaxation, associated with liberation of phenyl ring and limited C-H segmental movement, (b) β-relaxation, associated with rotation of polar group about C-C bond, and (c) α-relaxation, associated with the micro-Brownian motion of the whole chain and related to glass transition [146]. As reported in previous studies [113,146] the γ-relaxation occurs below room temperature due to involvement of small entities of phenyl ring and C-H units. The β- and/or α- relaxation could be observed in the experimental frequency and temperature window.

The effect of temperature on dielectric constant and dissipation factor of as-received and control PC is shown in Figures 5.9 (a) and (b), respectively. The dielectric constant of as-received PC is almost constant up to 125 ^{0}C and above this it increased rapidly up to 165 ^{0}C. With further increase of temperature it remained almost constant up to 180 ^{0}C and then increased again and finally showed a rapid decrease. In contrast to this, the dielectric constant of the control PC is almost constant.

In as-received PC, as the temperature increases beyond T_g, the intermolecular forces between the chains are weaken and hence the dipoles are free to orient with the electric field. In other words, the relaxation time associated with the polarization mechanism is reduced with increasing temperatures and hence the dielectric constant increases. Liu et al. [147] also reported the similar dielectric behaviour of PC with increasing temperature. At temperatures much higher than T_g (>180 °C), the dielectric constant decreases which can be attributed to the strong thermal agitation which disturbs the orientation of dipoles.

In case of control PC, the polymer chains are closely associated in the crystallites which resulted in the restricted motion of dipoles due to increase in temperature. Hence, insignificant change in dielectric constant of the control PC was observed with increasing temperatures.

Figure 5.9 clearly shows three peaks of the dissipation factor for both PCs. The peak at about 80/90 °C may be associated with the β-relaxation in PC [148]. The second peak at about 150 °C might be associated with glass transition in PC [145, 113]. The third peak can be correlated to the thermal agitation in the polymer chains and thereby in the electric dipoles.

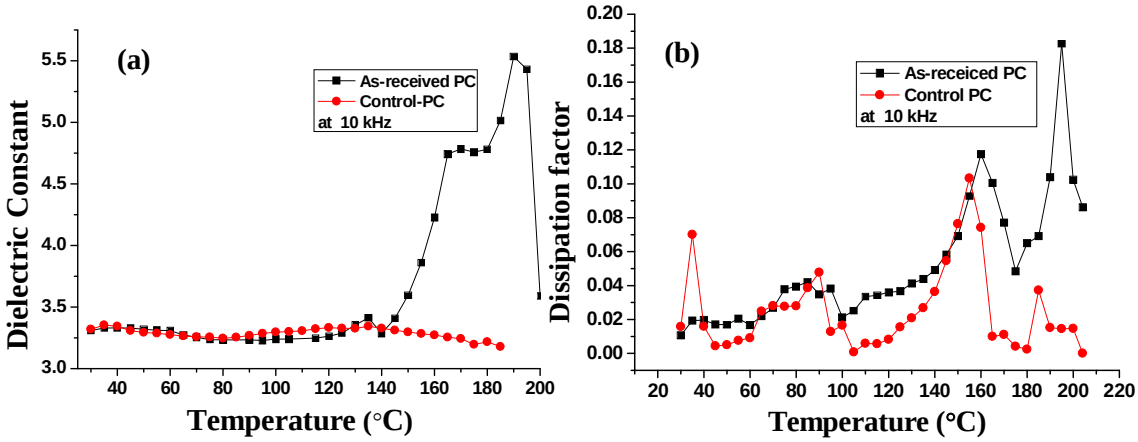

Figure 5.9. The variation in (a) dielectric constant and (b) dissipation factor with temperature for as-received and control PC.

In case of composites two competitive mechanisms involve with increasing temperature. The dipoles become freer as the temperature increases, which increases the dielectric constant. Due to different coefficient of thermal expansion the polymer matrix expands more than the filler and hence the distribution of filler in the matrix is disturbed. In case of composite containing 14 vol % of PZT, the dielectric constant and dissipation factor did not show any remarkable variation with temperature, however, above 170 °C, the composite, having 27.5 vol % of PZT, shows a drop in dielectric constant and corresponding hike in dissipation factor as shown in Figure 5.10 (a) and (b). In case of former, the both competitive mechanisms are comparable hence they balance each other (presence of crystallites also the strong reason for temperature independent behaviour, as was the case with control PC). However, in later case, above 170 °C, the decrease in dielectric constant, which might be due to disturbance of PZT clusters in the PC matrix, probably dominate over the increase in dielectric constant due to easy facilitation in dipole orientation and hence, net decrease in dielectric constant occurs. In addition, PZT particles are having permanent dipoles

which on increasing temperature disturb, hence, the dielectric constant of the composite may decrease with increase in temperature. The temperature dependency of dielectric constant of such polymer matrix composites have also been studied by different researchers. Chanmal and Jog [149] also reported the similar dielectric behaviour with temperature in PVDF/$BaTiO_3$ nanocomposites, at the studied frequency.

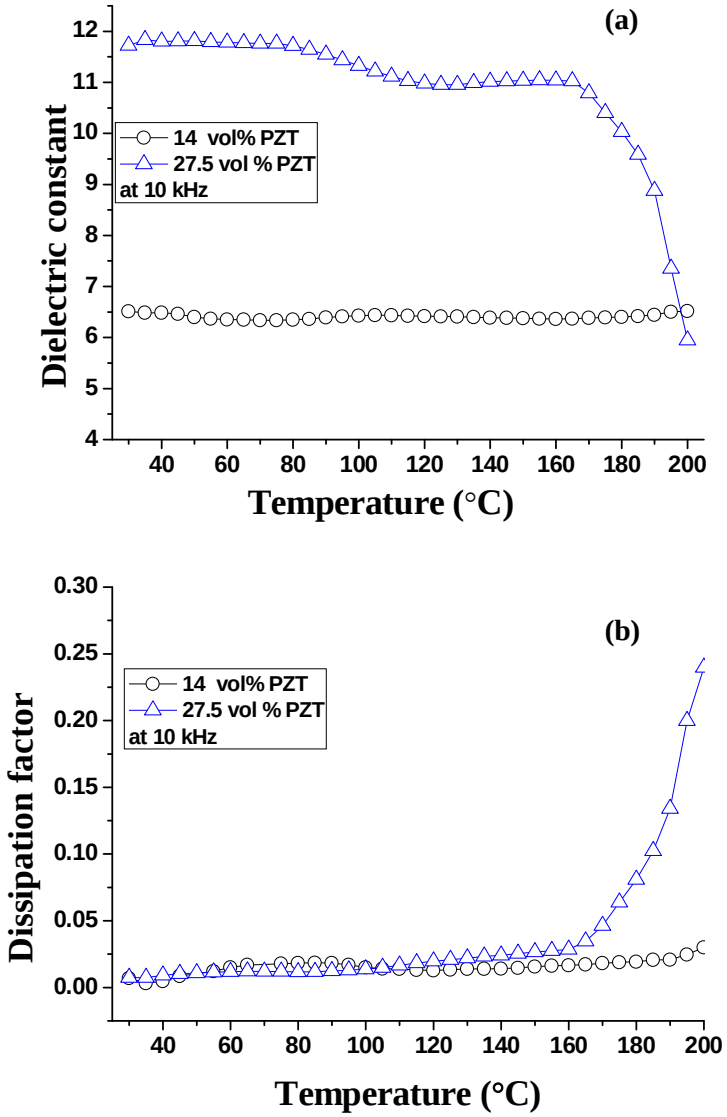

Figure 5.10. The variation in (a) dielectric constant and (d) dissipation factor with increasing temperature (at 10 kHz) for PZT-PC composites.

Dang et al. [34] also studied the effect of temperature on dielectric constant and dissipation factor in $BaTiO_3$/epoxy composites and reported [at 1 kHz] that with small size of filler (0.1 μm) the dielectric constant was almost constant up to 150 °C whereas with larger size particle (0.7 μm) the dielectric constant increased beyond 60 °C. However, the dissipation factor increased with increasing temperature for both cases.

Subodh et al. [81] reported almost constant relative permittivity (at 1 MHz), with increasing temperature (up to 60 °C) for SCT ($Sr_9Ce_2Ti_{12}O_{36}$)/PE composites.

It can be concluded that the dielectric behaviour of such composites varies differently with temperature depending up on filler, matrix, size and distribution of filler in the polymer matrix. For the studied PZT-PC composite, the maximum achieved value of dielectric constant was about 12 and the value of dissipation factor was below 0.015. These values were almost constant up to the temperature of 100 °C.

5.2 Conductive fillers (Nano-Cu, MWCNT, SWCNT and FLG) filled two-phase nanocomposites

Two-phase conductive filler filled composites were prepared with different content of Cu, MWCNT, SWCNT and FLG as shown in Table 5.2. All the prepared nanocomposites were characterized and their electrical behaviour was studied. The percolation threshold and smearing region for all the composites were determined. The feasibility study for the composites to use as dielectric materials was done.

Table 5.2: The concentration of the different conductive fillers in the different nanocomposites, by weight percent and volume percent.

Cu (density= 8.94 g/cc) content by		**SWCNT (density=2.5 g/cc) content by**		**MWCNT (density= 2.5 g/cc) content by**		**FLG (density=2.1 g/cc) content by**	
wt %	**vol %**	**wt %**	**vol %**	**wt %**	**vol %**	**wt %**	**vol %**
0	0	0	0	0	0	0	0
27.65	5	1	0.58	2	1	1	0.58
44.65	10	1.75	1.0	5.9	3	2	1.18
56.18	15	2.5	1.5	7.8	4	3.5	2.08
64.5	20	4	2.38	9.6	5	5	3
--	--	5	3	18.42	10	6	3.60
--	--	--	--	--	--	7	4.22

5.2.1 Density

The densities of the Cu-PC, MWCNT-PC, SWCNT-PC, and the FLG-PC are plotted in the Figure 5.11 to 5.13, respectively. The experimental densities of all the nanocomposites (except in the case of Cu-PC) were found almost close to their theoretical densities, indicating that the composites were almost pore free. A little difference may be due to filler's aggregates which may hinder the infiltration of polymer during hot pressing and air might be entrapped. In case of MWCNT-PC nanocomposite, the density is having slightly increasing trend in contrast to SWCNT-PC nanocomposite which might be due to the presence of higher impurity content in the MWCNT sample than that in SWCNT sample. The experimental density of the Cu-PC composites was found significantly less than the theoretical density, and the difference became more pronounced as the Cu content increased. The investigation revealed that the main factor for reduced experimental density was due to the presence of Cu-oxide (Cu_2O) in the nano-Cu filler. Cu_2O has the density of about 6 g/cc, which is much less than that of pure Cu (8.94 g/cc). The presence of Cu_2O was also confirmed by XRD analysis, as discussed in next section.

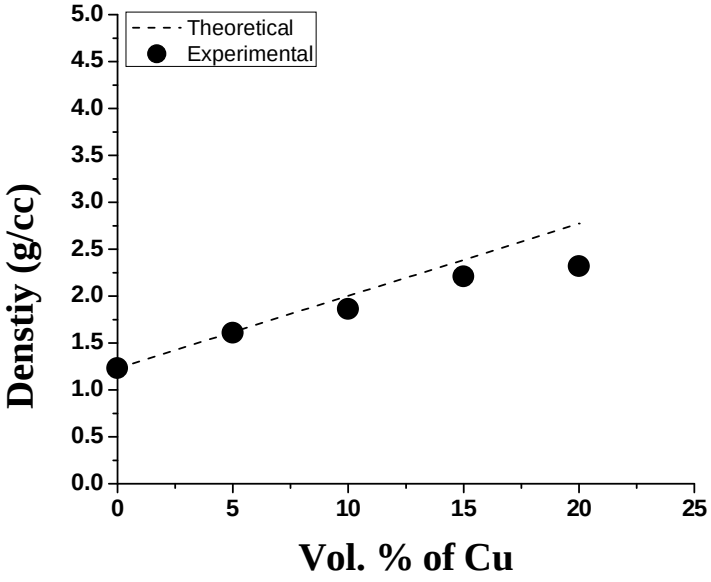

Figure 5.11. Theoretical and experimental densities of the Cu-PC nanocomposites.

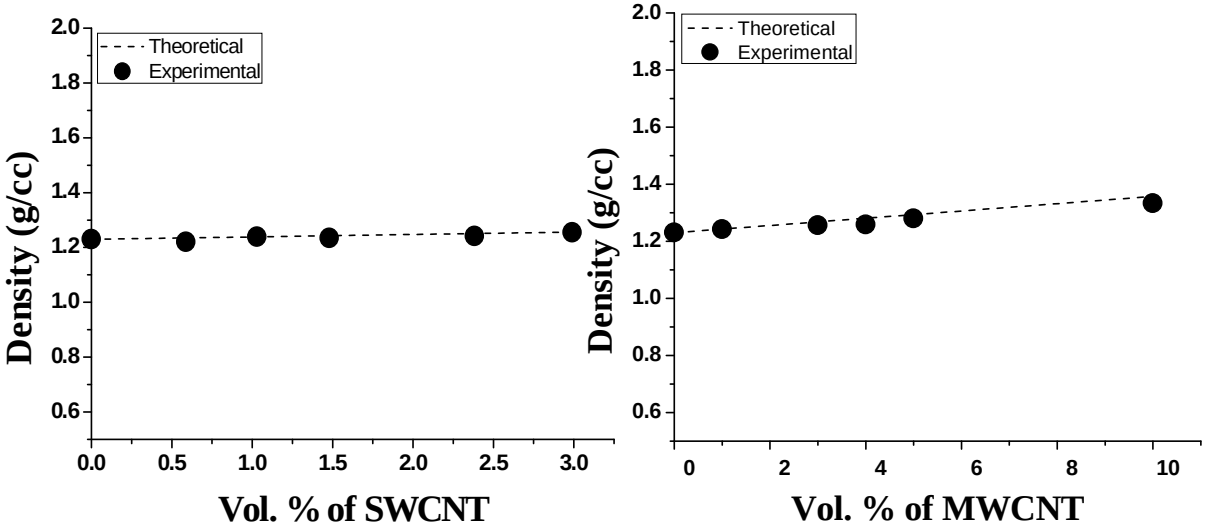

Figure 5.12. Theoretical and experimental densities of (a) SWCNT-PC and (b) MWCNT-PC nanocomposites.

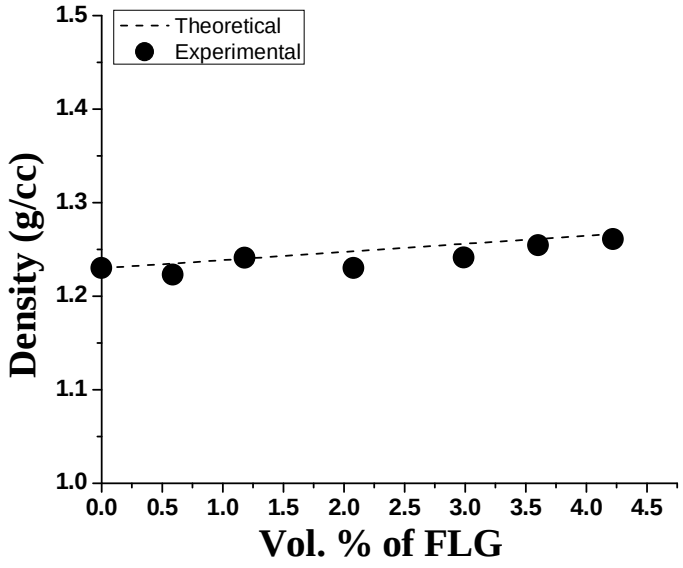

Figure 5.13. Theoretical and experimental densities of the FLG-PC nanocomposites.

5.2.2 X-ray diffractometry and Raman spectroscopy

Copper powder showed peaks [Figure 5.14] at 43.46° and 50.6° which corresponds to (111) and (200) planes, respectively, according to JCPDS (00-003-1005). In addition to the peak of Cu, the peaks at 29.5°, 36.5° and 42.5° were also found which were corresponding to plans (110), (111) and (200), respectively; of Cu_2O according to JCPDS file (01-077-0199). The study indicates that the Cu nano particles were covered with a thin layer of oxide. Due to large surface to volume ratio, the nano-copper particles were sensitive to the oxidation. In comparison to nano Cu and PC, the XRD pattern of Cu-PC nanocomposites did not show any obvious difference, except the suppression in the intensity due to PC which was due to the reduction in the percentage of PC in the composite. The peak from PC also seems to be somewhat narrower in Cu-PC nanocomposite which may be indicative of increased ordered structure in PC due to the presence of nano- sized Cu.

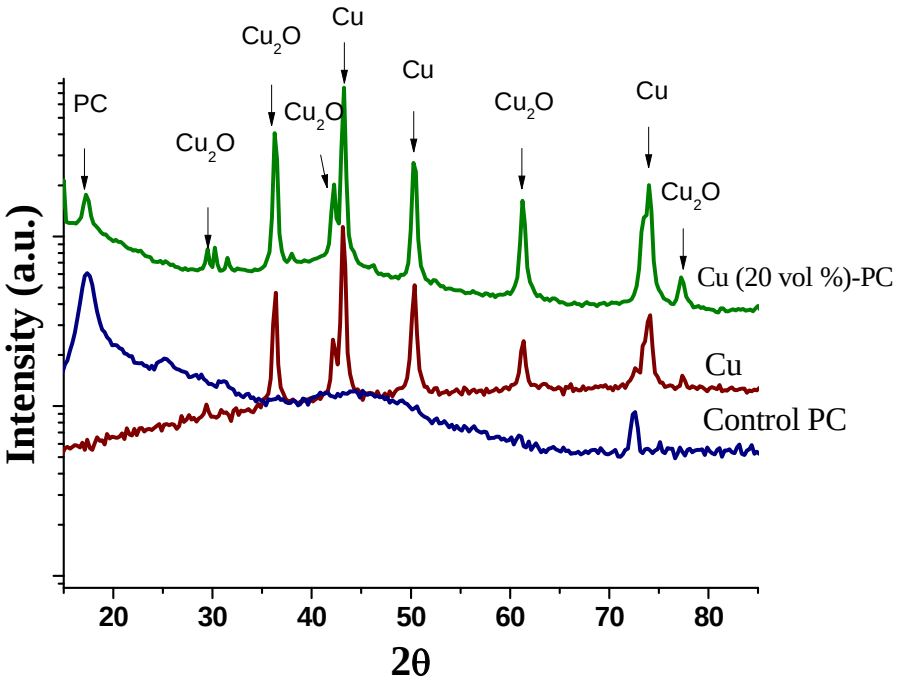

Figure 5.14. The XRD patterns of Cu powder, Cu-PC nanocomposite and control PC.

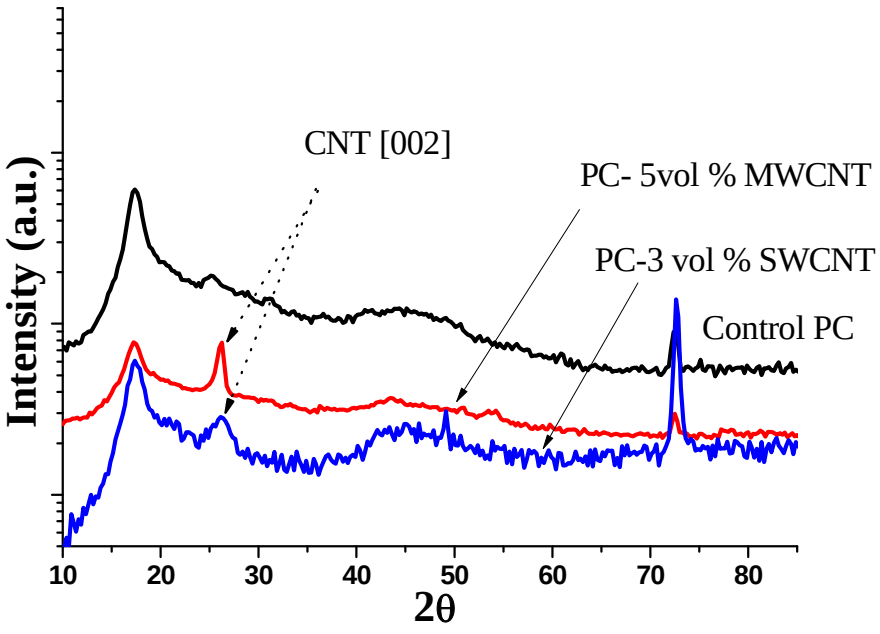

Figure 5.15. The XRD patterns of MWCNT-PC, SWCNT-PC nanocomposites and control PC.

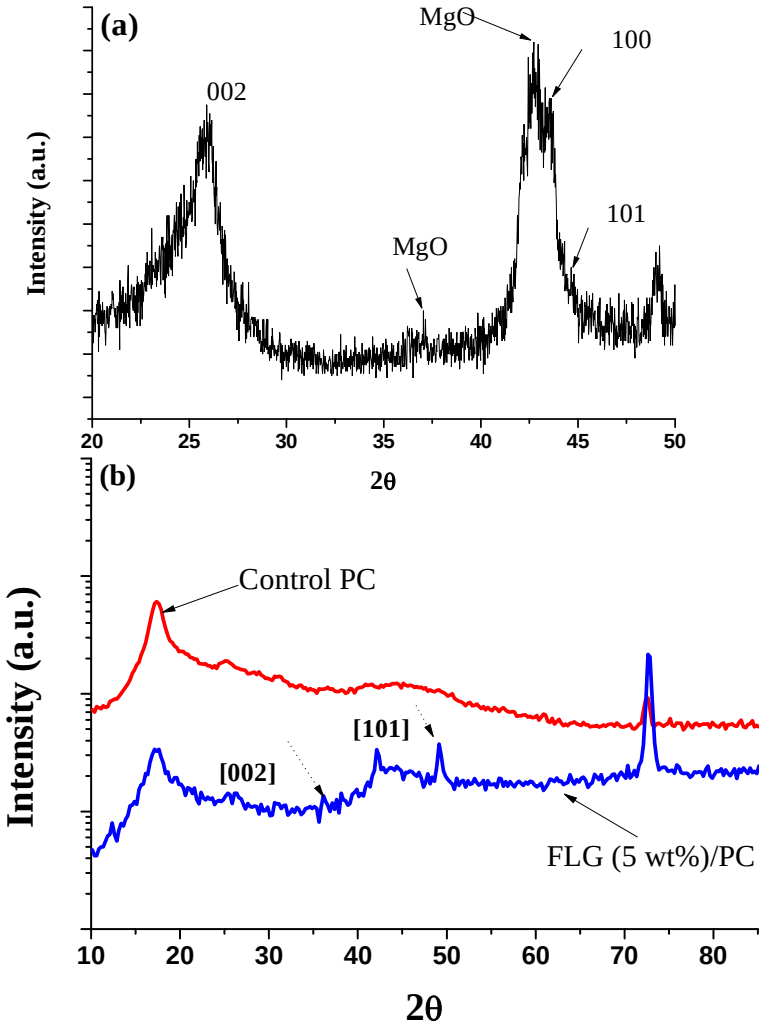

Figure 5.16. The XRD patterns of (a) FLG sample (b) FLG-PC nanocomposite with control PC.

Figure 5.15 confirms the presence of MWCNT and SWCNT in the respective nanocomposites with the peak at about 26° corresponding to (200) plane with interlayer spacing of 0.34 nm. CNTs also show another peak around 43° but in present case this peak is not appearing due to probably low concentration of CNTs. The XRD results for MWCNT/SWCNT-PC nanocomposites are also in support with the previous findings [150-151]. Figure 5.16(a) shows XRD pattern for FLG prepared by dry ice method. The presence of MgO as impurity is apparent from the peaks in XRD trace. The prominent broad peak which is the reflection from (002) plane of graphene, at 26.2 degree, is observed along with the reflection from (101) plane at 44.6 degree.

The other characteristic peak (100) for graphene structure is located at about 43.3 degree. Figure 5.16 (b) confirms the presence of FLG as well as some impurities (may be of Mg/MgO, indicated by dotted arrows) in the nanocomposite. The XRD pattern of FLG is in support with the findings of A. Chakrabarti et al. [139].

The Raman spectroscopy is very important tool for the characterization of carbonaceous materials. Therefore Raman analysis for the SWCNT, MWCNT and FLG has been carried out and the results are shown in Figure 5.17.

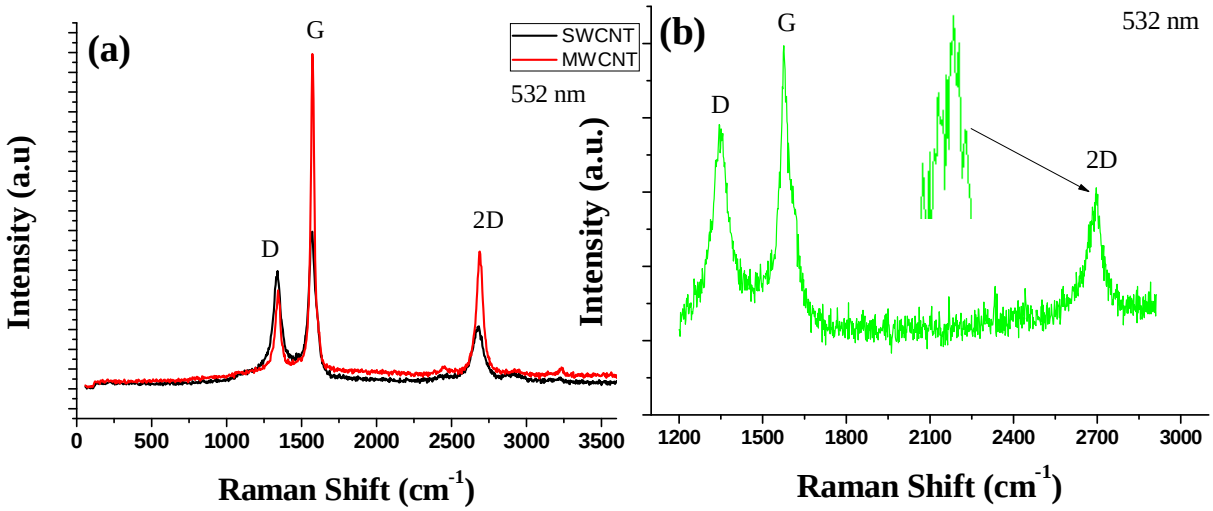

Figure 5.17. The Raman spectra of (a) SWCNT, MWCNT and (b) FLG samples.

Figure 5.17 is indicating that the SWCNT, MWCNT, and FLG are having similar bands at around 1340 cm^{-1}, 1575 cm^{-1} and 2690 cm^{-1}. These bands are designated as D, G, and 2D band, respectively. However, these bands having different intensities for different case. Presence of similar bands is obvious because the SWCNT and MWCNT are the rolled single layer and few layer graphene sheets. The D band originates due to the defects created in during the processing of these carbonaceous materials. The G band occurs due to the in-plane vibration mode involving the sp^2 hybridized carbon atoms. The ratio of the intensity of D and G band (i.e. I_D/I_G) can be correlated to the amount of defects present in the graphene/CNTs. The 2D band comes due to the stacking order and is used to confirm the layers present in the graphene/few-layer graphene. The sharp 2D band of few layer or multi layer

graphene comprises of multiple layer due to the splitting of electronic band structure of multi-layers.

As can be observed in Figure 5.17 (a) the 2D for MWCNT band is slightly shifted towards higher frequency side in comparison to the 2D band of SWCNT which may be correlated to the larger numbers of layers in MWCNT [152, 153]. The Raman spectrum of FLG is shown in Figure 5.17 (b) confirms the presence of sharp 2D band at 2700 cm^{-1} which in turn provides strong evidence in favour of graphene. The splitting of 2D band peak confirms the graphene to be few layered. The presence of D band at about 1350 cm^{-1} is confirming the highly disordered few layer graphene. As reported [152], the intensity of D band increases as the number of layer decreases which suggest that the defects can be easily introduced in the thinner graphene. The above characterization data for FLG are also in support with the finding of A. Chakrabarti et al. [139].

5.2.3 Transmission electron microscopy

Figures 5.18 (a) and (b) are the TEM images of the nano-Cu showing the shape and size distribution of particles and confirmed that the particles sizes were below 50 nm which is in close agreement with the particle size reported by supplier (average particle size of 40 nm). Figure 5.18 (c) is the electron diffraction (ED) pattern taken on a single Cu particle, confirming the FCC structure. The ED pattern was indexed by calculating the distance of diffraction spots from the centre spot. The calculation revealed that the lattice planes spacing were ~ 2 Å and ~ 1.8 Å, shown by arrows in Figure 5.18 (c), which are the crystal plane distances of Cu corresponding to (111) and (200). The diffused ring patterns along with the spot pattern were also observed and might be due to the coating of amorphous carbon on the copper grid. Figure 5.19 (a) shows good distribution of Cu particles in the PC matrix. However, some aggregates of filler were also observed in the nanocomposites as shown in Figure 5.19 (b).

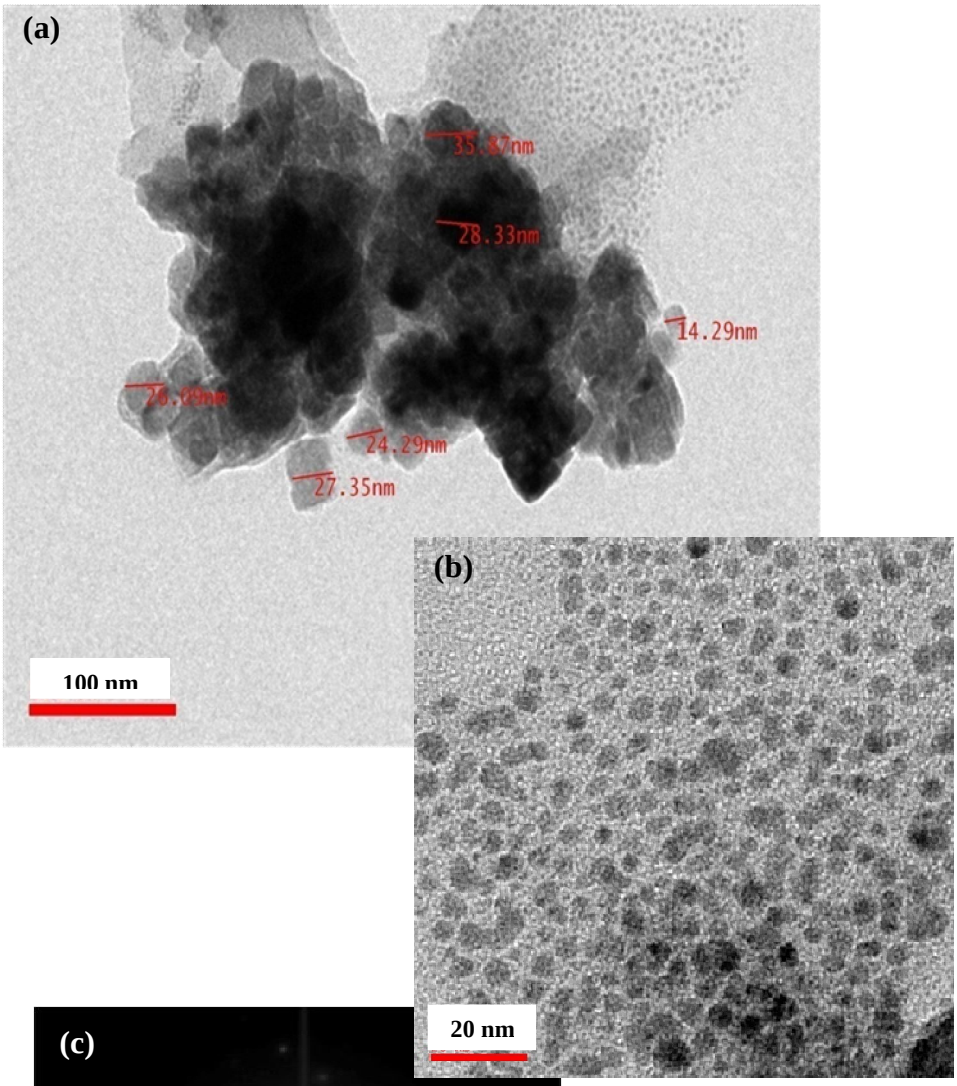

Figure 5.18. The TEM analysis of Cu filler (a) showing the particle size range between 15 nm to 50 nm (b) showing the particle size range below 15 nm (c) the electron diffraction pattern taken on an individual Cu particle.

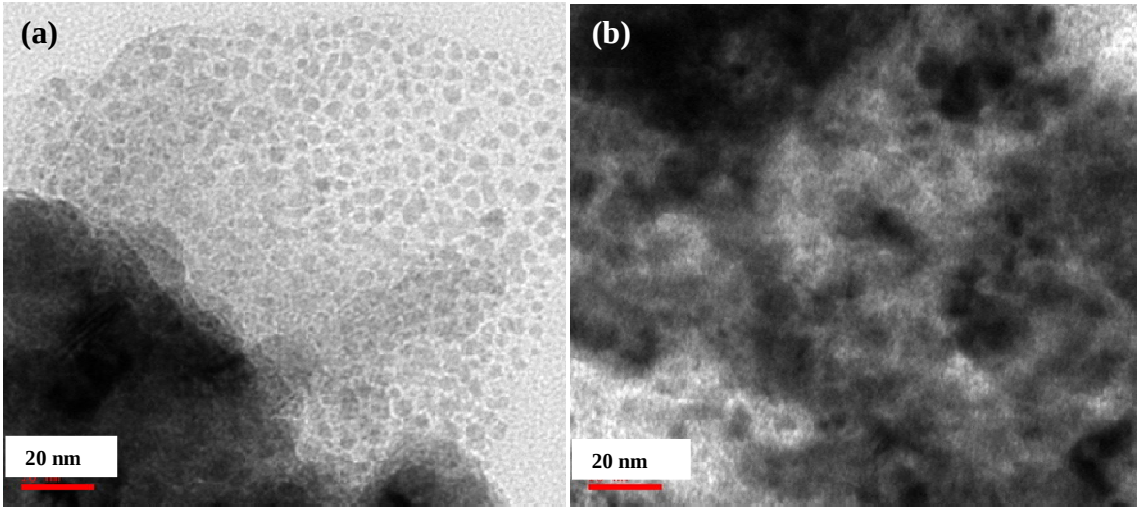

Figure 5.19. The TEM images of Cu (5 vol %)-PC nanocomposite (a) dispersion of Cu particles in a section of PC matrix; showing very good dispersion (b) dispersion of Cu particles in another location of PC matrix; showing aggregates of Cu filler.

Figure 5.20 (a) shows the TEM images of MWCNT sample; also showing some impurities in the sample. Figure 5.20 (b) shows the high resolution transmission electron microscopy (HRTEM) image of a MWCNT. Figure 5.21 (a) represents the TEM images of SWNCT sample; the impurities were rare in the SWCNT in comparison to MWCNT sample. Figure 5.21 (b) shows the HRTEM images of particular SWCNTs. The HRTEM images of both CNTs show their characteristic features; same type of HRTEM were also reported in literature [154-156]. Figure 5.22 shows the distribution of MWCNT [Figure 5.22 (a)] and SWCNT [Figure 5.22 (b)] in the PC matrix. In MWCNT-PC the impurities could be observed, whereas, in SWCNT-PC nanocomposite the impurity free distribution was observed. Figure 5.23 (a) shows TEM image of FLG sample. It can be seen that FLG has sheet like morphology. Presence of some impurities is also evident in the image. Figure 5.23 (b) is the electron diffraction (ED) pattern taken on an individual graphene layer. The ED pattern is favouring the reflection from hexagonal crystal structure of graphene. The relatively sharp rings should be indicative of amorphous carbon layer on the copper grid, because the electron beam might penetrate the thin graphene sheet.

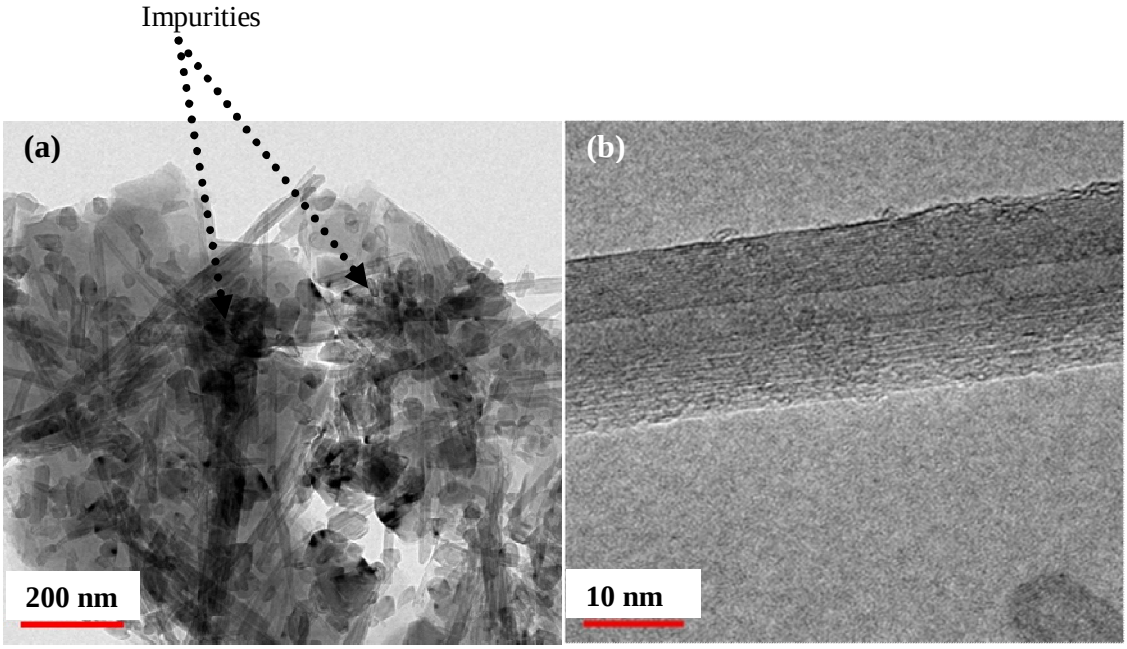

Figure 5.20. The TEM images of (a) a sample of MWCNT (b) HRTEM image of a particular MWCNT tube.

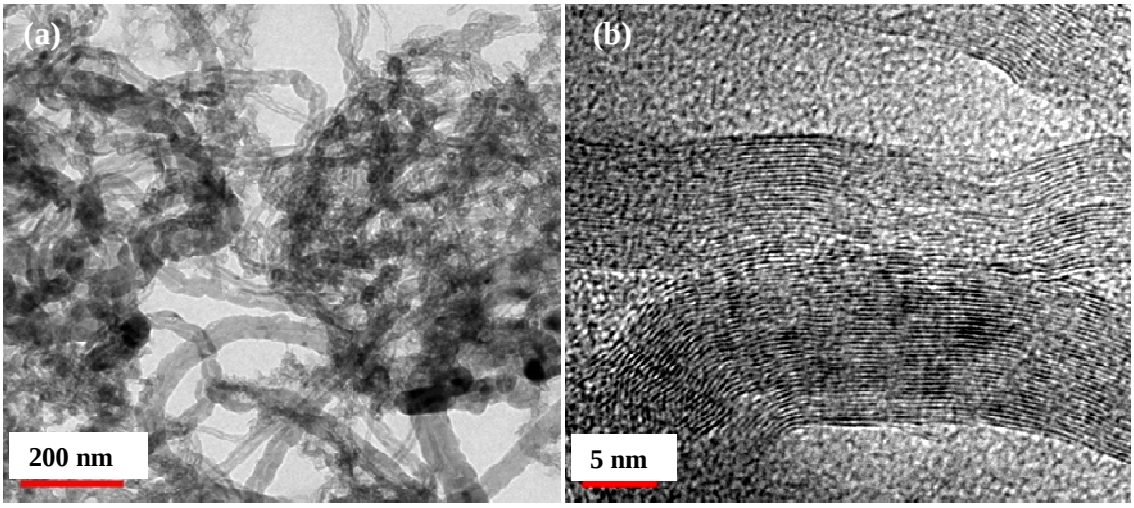

Figure 5.21. The TEM images of (a) a sample of SWCNT (b) HRTEM image of SWCNT; showing bundle of tube.

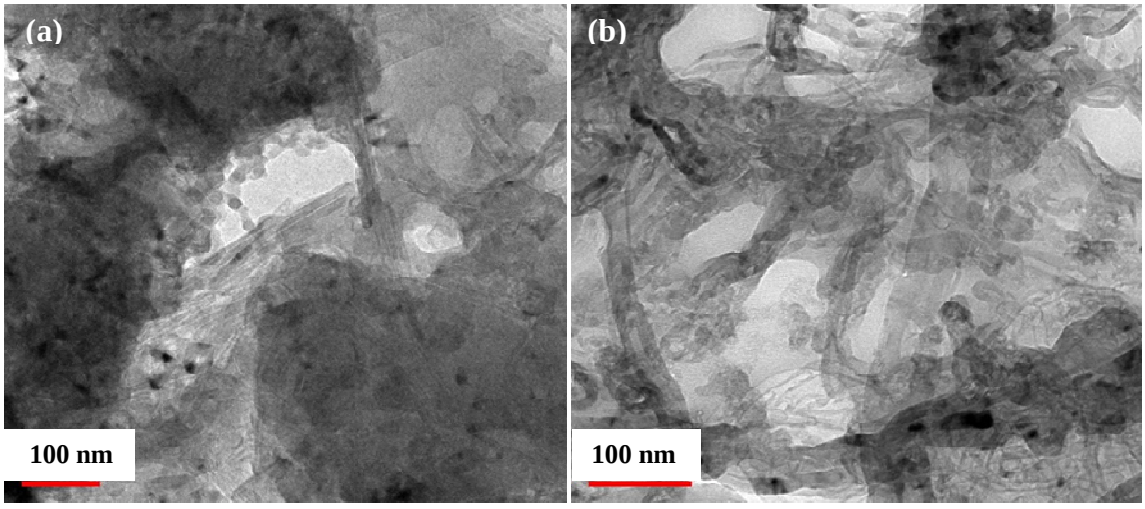

Figure 5.22. The TEM images of (a) MWCNT (1 vol %) -PC nanocomposite (b) SWCNT (1 vol %) nanocomposite.

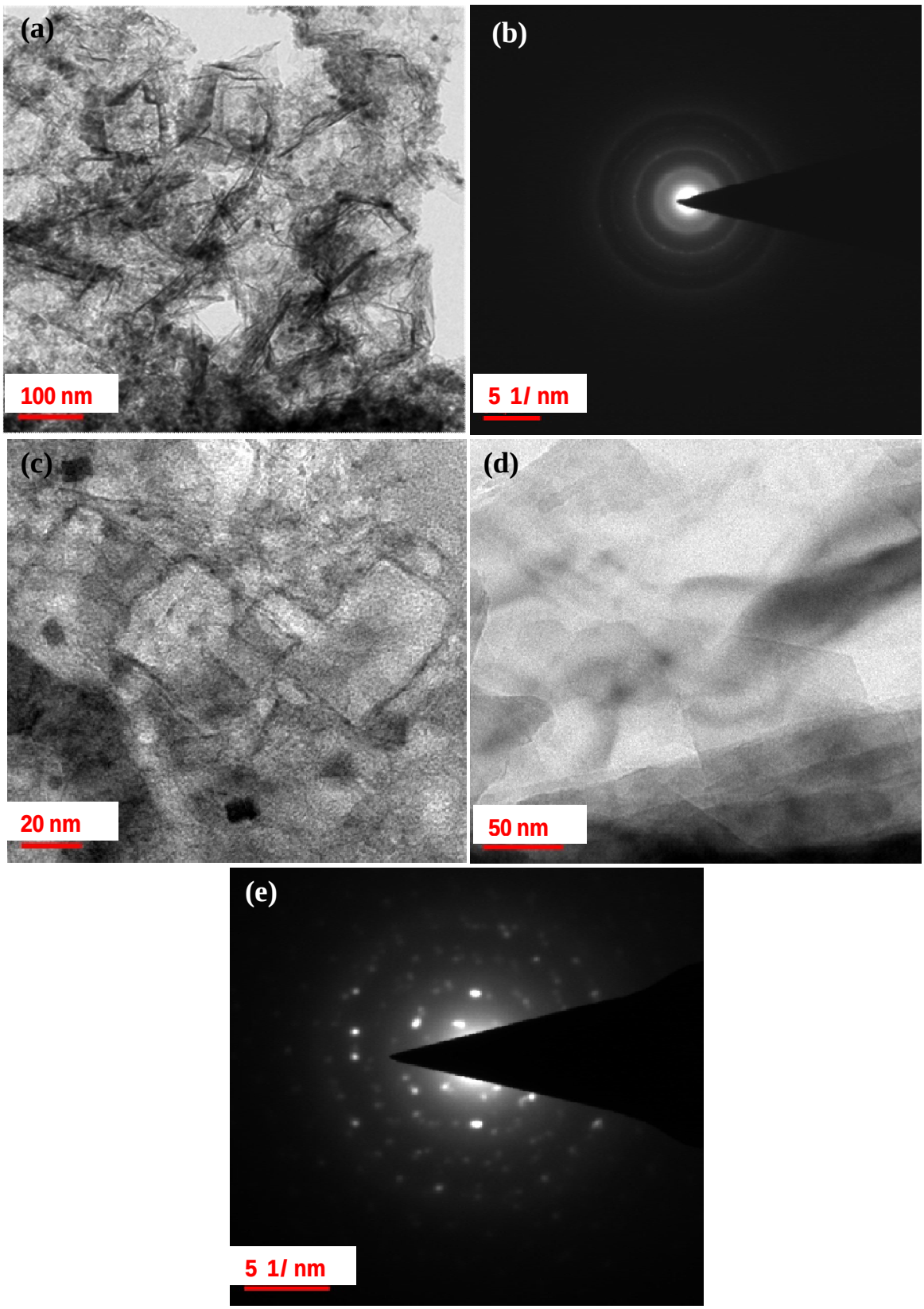

Figure 5.23. TEM analysis of FLG and FLG (3 vol %)-PC nanocomposite (a) The TEM image of FLG sample (b) The electron diffraction pattern taken on a FLG sheet (c) FLG (3 vol %) -PC nanocomposite (d) PC-FLG at thinner section; showing good dispersion of FLG in PC matrix, (e) ED pattern taken from FLG sheet embedded in PC matrix.

Figures 5.23 (c) and 5.23 (d) show the TEM images of a FLG (3 vol %)-PC nanocomposite at different locations and magnifications. Figure 5.23 (e) is the ED pattern taken on an FLG sheet embedded in PC matrix. The ED pattern is favouring the reflections from hexagonal crystal structure of FLG, but the reflection is coming from the different layers having different crystal orientation. Such type of ED pattern for graphene-filled polymer composite has also been reported in a previous work of Stankovich et al. [110].

5.2.4 Scanning electron microscopy

Figure 5.24 (a) and 5.24 (b) show the morphology of SWCNT in the SWCNT (3 vol %)-PC nanocomposite with polished and fractured surface, respectively. The SWCNTs are well distributed and making the connections among them. Figure 5.25 (a) and 5.25 (b) shows the distribution of MWCNT (5 vol %) in the PC matrix with polished and fractured surface conditions, respectively, showing well distribution of MWCNT. Both the SWCNT and MWCNT in the nanocomposites were having tubular morphology. As obvious, the diameter of the MWCNT in the nanocomposite is higher than that of SWCNT. Moreover, the impurity content was higher in the case of MWCNT filled nanocomposites as confirmed by the TEM image of the CNTs. Figure 5.26 (a) and 5.26 (b) are the SEM images of polished and fractured surfaces, respectively of FLG (3 vol %)-PC nanocomposite. The FLGs were having sheet like morphology in the nanocomposite. Due to sheet morphology they are having large surface area and hence the interface area between FLG and PC was high. These FLG sheets were well distributed in the PC matrix and making connections with each others throughout the nanocomposite. Some pores were also observed in the SEM images of the nanocomposites were indicated by arrows in the images.

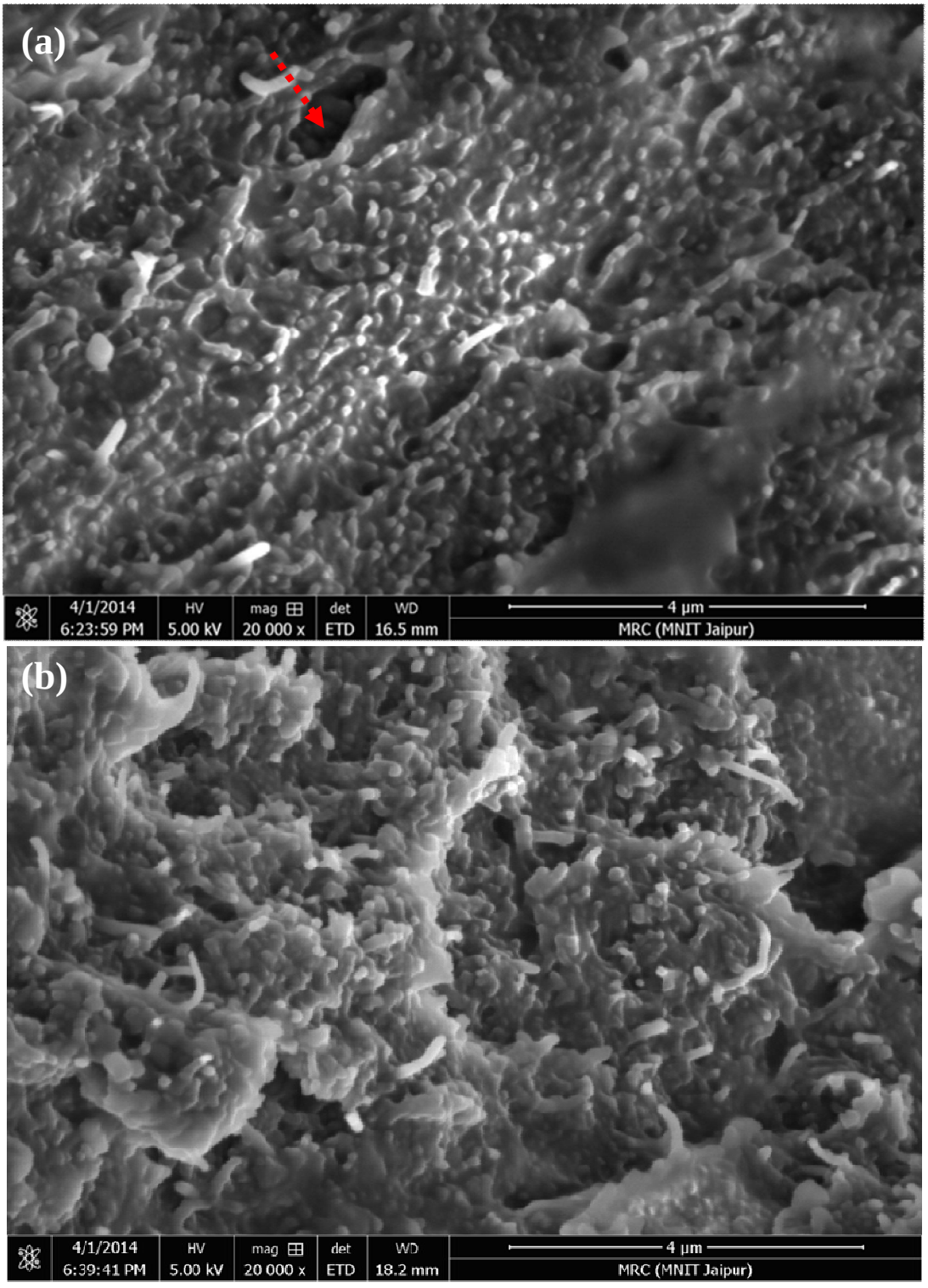

Figure 5.24. The SEM images of (a) polished surface (b) fractured surface of the SWCNT (3 vol %)-PC nanocomposite.

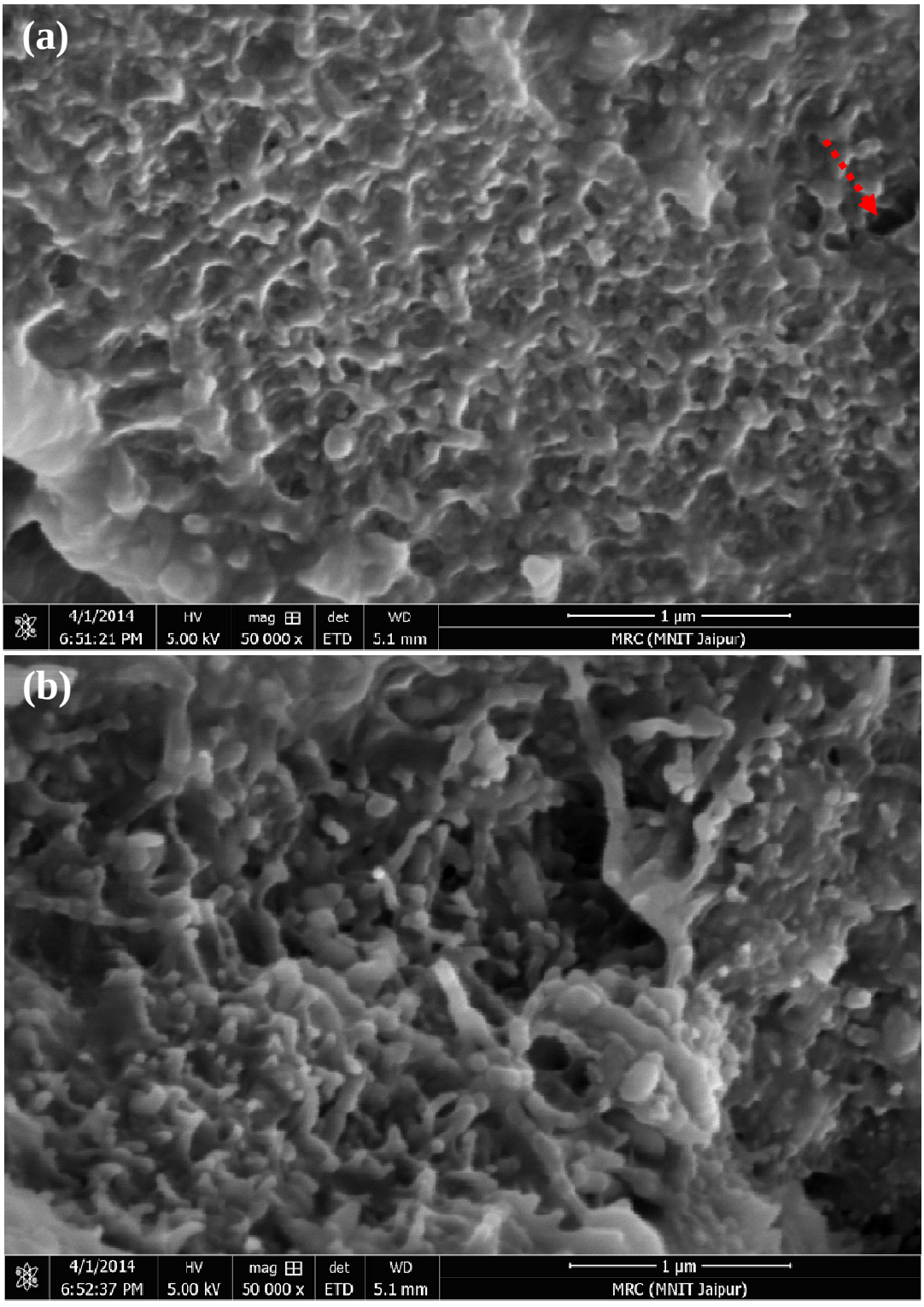

Figure 5.25. The SEM images of (a) polished surface (b) fractured surface of the MWCNT (5 vol %)-PC nanocomposite.

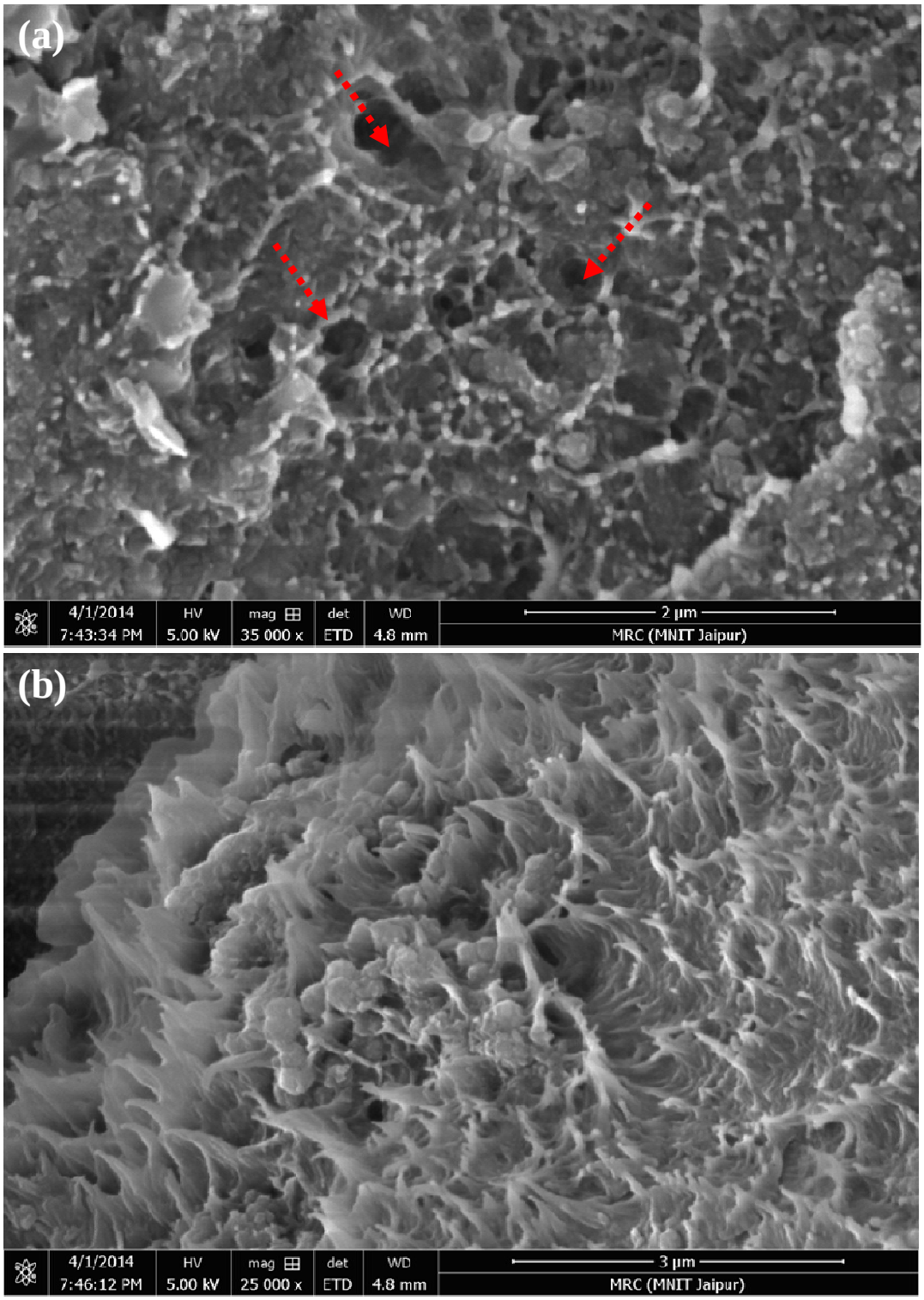

Figure 5.26. The SEM images of (a) polished surface (b) fractured surface of the FLG (3 vol %)-PC nanocomposite.

5.2.5 Differential scanning calorimetry

The DSC traces show the effect of nanofillers on the thermal behaviour of the nanocomposites. Figures 5.27 (a) to 5.27 (c) show the DSC traces of Cu (5 vol %)-PC, MWCNT (5 vol %)-PC and FLG (3 vol %)-PC nanocomposites, respectively. The fillers have considerable impact on the thermal behaviour of PC. The melting peak for Cu (5 vol %)-PC, MWCNT (5 vol %)-PC and FLG (3 vol %)-PC nanocomposites was at 228.58 °C, 225.99 °C and 228.57 °C, respectively, which indicates that the melting point of the nanocomposites decreased by 8-10 °C compared to control PC.

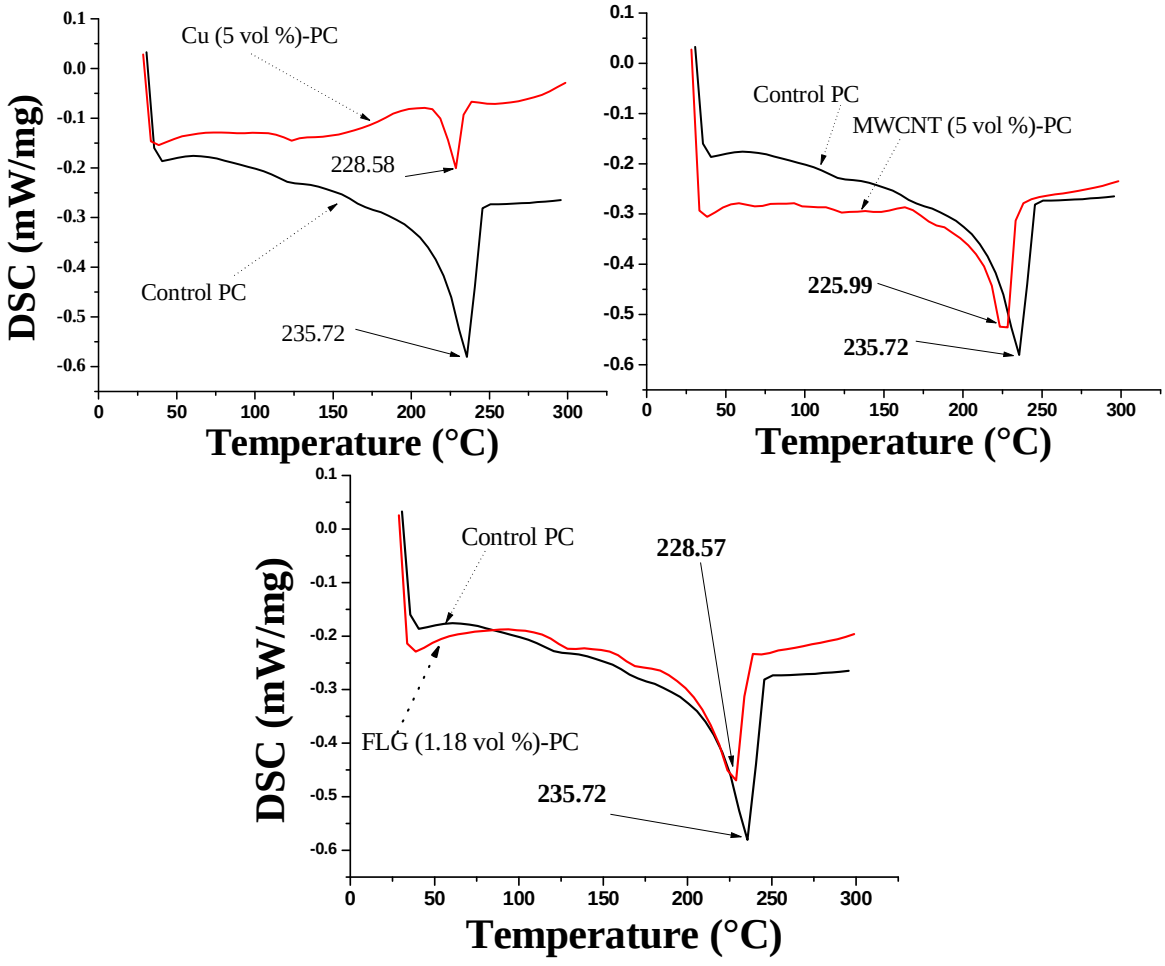

Figure 5.27. The DSC traces of (a) Cu (5 vol %)-PC (b) MWCNT (5 vol %)-PC and FLG (3 vol %)-PC nanocomposites.

The effect of filler on the melting point may be understood by the following possibilities (1) it is very likely that, during solvent evaporation, the polymer chains orient themselves in the vicinity of the filler which creates a larger number of ordered domains (crystallites) surrounded by the amorphous regions and hence melting point may increase (2) In addition, the filler may find places in between the adjacent polymer chains and thereby reduces the interaction between them which reduces the energy required for melting. In this work, all the conductive-fillers were of nano-size and may easily entrap between the polymer chains, hence, this factor is dominating over the effect of increased crystallized domains. Therefore, the melting point of the nanocomposites was found slightly less than that for control PC.

5.2.6 Electrical properties

5.2.6.1 AC electrical conductivity

As obvious, initially, the electrical conductivity of the composites was increased nominally with increasing volume fraction of the fillers. Beyond, a certain filler concentration (i.e. beyond percolation threshold), the conductivity started to increase abruptly. Figure 5.28 shows the conductivity of the Cu-PC nanocomposite which indicates the percolation at about 15 vol % of the Cu nanoparticles. The conductivity of Cu-PC was increased to the order of 10^{-5} S/cm (with 20 vol % of Cu) from 10^{-9} S/cm (for control PC). Figure 5.29 shows the conductivity as a function of vol % of both SWCNT and MWCNT in the SWCNT/MWCNT-PC nanocomposites. It was found that with SWCNT, the percolation threshold was at lower vol % (at 0.5 vol %) than that with MWCNT (at 4 vol %). The achieved conductivity order was about 10^{-4} S/cm for both types of CNTs (with 3 vol % of SWCNT and with 10 vol % of MWCNT). In the FLG-PC nanocomposite, the percolation was occurred at about 2 vol % of FLG as shown in Figure 5.30 and maximum achieved conductivity level was 10^{-2} S/cm with 4.22 vol % of FLG

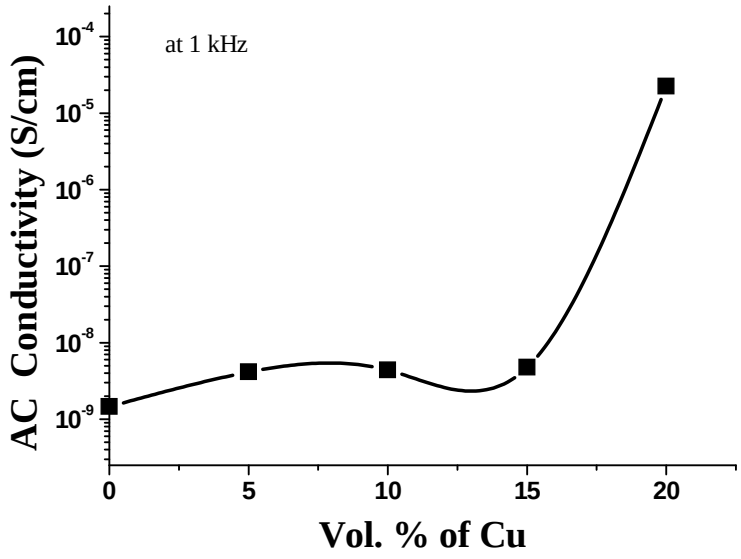

Figure 5.28. The electrical conductivity of the Cu-PC nanocomposite as a function of nano-Cu vol %.

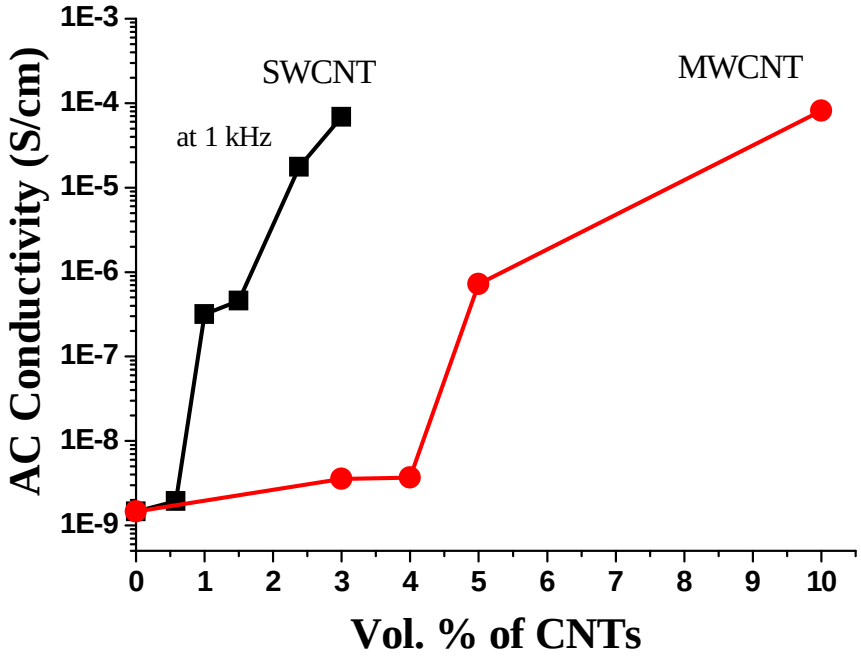

Figure 5.29. The electrical conductivity of the SWCNT/MWCNT-PC nanocomposites as a function of SWCNT/MWCNT vol %.

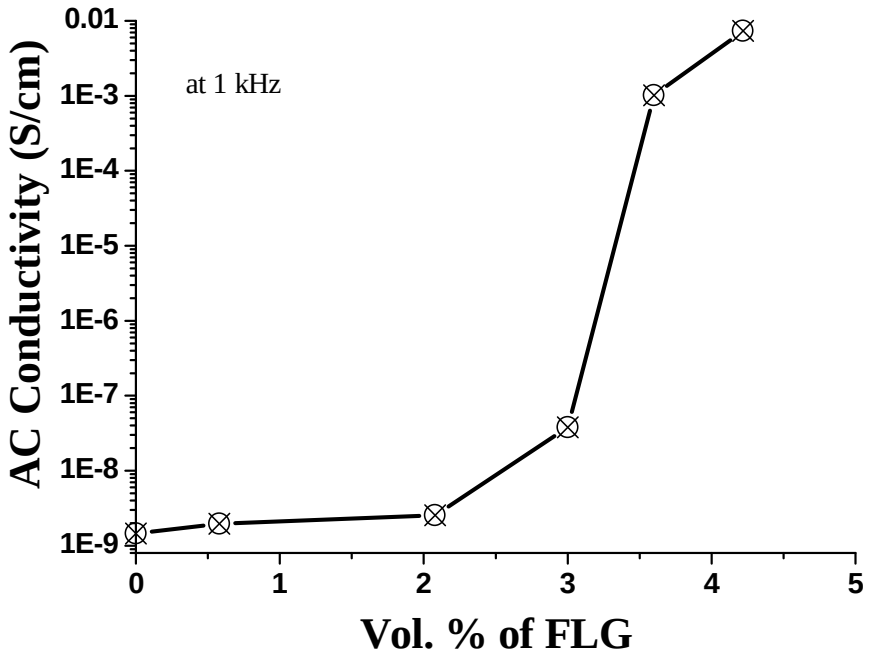

Figure 5.30. The electrical conductivity of the FLG-PC nanocomposite as a function of FLG vol %.

In such composites, the percolation occurs when the conducting particles start to interact with each other throughout the composite. The conducting particles may interact with each other by physical connections in between adjacent particles or by quantum tunnelling effect just before the physical connections between adjacent particles, when the polymer layer between the adjacent conducting particles is infinitesimal. In the above discussed nanocomposites, the percolation occurred at different vol % of fillers. Critical literature survey revealed that the percolation strongly depends on conductivity, size, shape, and aspect ratio of the filler. The aspect ratio is the most important factor that alters the percolation threshold. In Cu-PC nanocomposite, the Cu-nanoparticles are almost spherical in shape with an average size of 40 nm (as confirmed from TEM analysis). As it was reported in literature [157] that with spherical shape of metallic particles the percolation generally occurs at about 16 vol %, the experimental results are in good agreement, here. The percolation was at lower vol % in SWCNT/MWCNT-PC nanocomposites. SWCNT and MWCNT are in tubular shape and hence their aspect ratio are very high (generally greater than 1000). In comparison to SWCNTs, the MWCNTs have higher diameter. Hence, it is obvious

to find percolation at lower vol % in SWCNT-PC nanocomposite than in MWCNT-PC nanocomposite, and the experimental results are in agreement.

The percolation in FLG-PC nanocomposite was observed to occur at a lower content of filler as against in MWCNT-PC nanocomposite which can be correlated to the sheet like morphooloyg of FLG (Figure 5.23) in contrast to tube like morphology of MWCNT (Figure 5.20). However, the percolation may further vary with type of matrix, filler particle size, and method of preparation as can be noted from Tables 3.2- to 3.4.

5.2.6.2 Dielectric constant and dissipation factor

Figures 5.31 to 5.34 show the dielectric constant and dissipation factor of Cu-PC, SWCNT-PC, MWCNT-PC and FLG-PC nanocomposites, respectively. The dielectric constant increased gradually as the filler concentration increased in all the nanocomposites. Beyond percolation threshold, the dielectric constant increased greatly, as with the case of conductivity. Below percolation threshold, dissipation factor varied but remained around 0.01, but beyond percolation threshold, it increased abruptly which is not good for capacitor application point of view. Low dissipation factor is required for radio-frequency applications to avoid signal losses however much higher value of dissipation factor can be tolerated for energy storage devices [29, 158]. Hence, it is somewhat tedious to develop such polymer composite materials possessing high dielectric constant coupled with low dissipation factor. High dissipation factor is also advantageous in some applications which include EMI shielding, antistatic, flash lamps and heart actuators [36, 159-160]. For Cu-PC nanocomposites, the dielectric constant and dissipation factor measured at 1 kHz increased to 8.5 and 0.07 (for 15 vol %), respectively and thereafter increased abruptly to 10^8 and 3525, respectively, as shown in Figure 5.31.

The dielectric constant of SWCNT-PC nanocomposite was almost constant (varied from 3.4 to 3.6) up to 0.5 vol % of SWCNT and at 1 vol %, it abruptly increased to 5288 as shown in Figure 5.32. When the MWCNT was added to the PC matrix, the dielectric constant of the nanocomposites with 4 vol % and 5 vol% MWCNT was increased to 6.6 ($\tan \delta = 0.01$) and 31858, respectively (Figure 5.33).

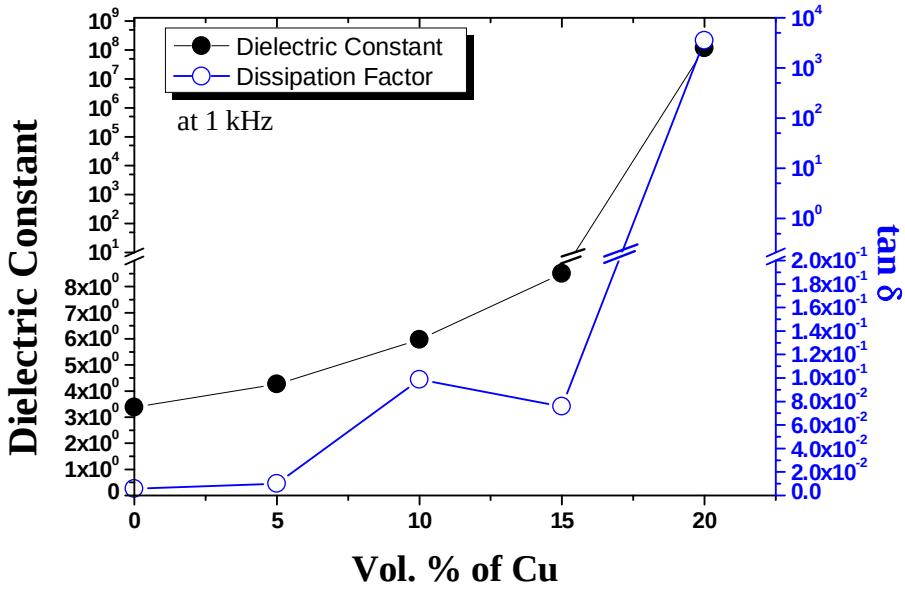

Figure 5.31. The dielectric constant and dissipation factor (tan δ) of Cu-PC nanocomposites as a function of vol % of Cu.

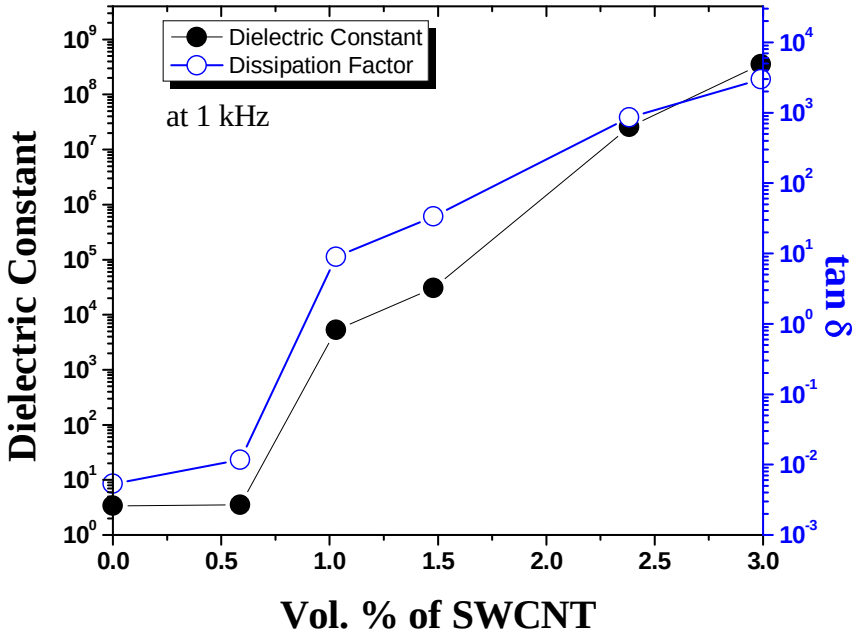

Figure 5.32. The dielectric constant and dissipation factor (tan δ) of SWCNT-PC nanocomposites as a function of SWCNT vol %.

The highest augment in the dielectric constant with moderate dissipation factor was achieved for the FLG-PC nanocomposites. For example, the dielectric constant of the FLG-PC nanocomposites with 3 vol % and 3.5 vol % of FLG was increased to about 70 (tan δ = 0.07) and 10^{10} (tan $\delta = 10^{4}$), respectively (Figure 5.34). For all the nanocomposites, the trend for increase in the dielectric constant was consistent with the trend of electrical conductivity.

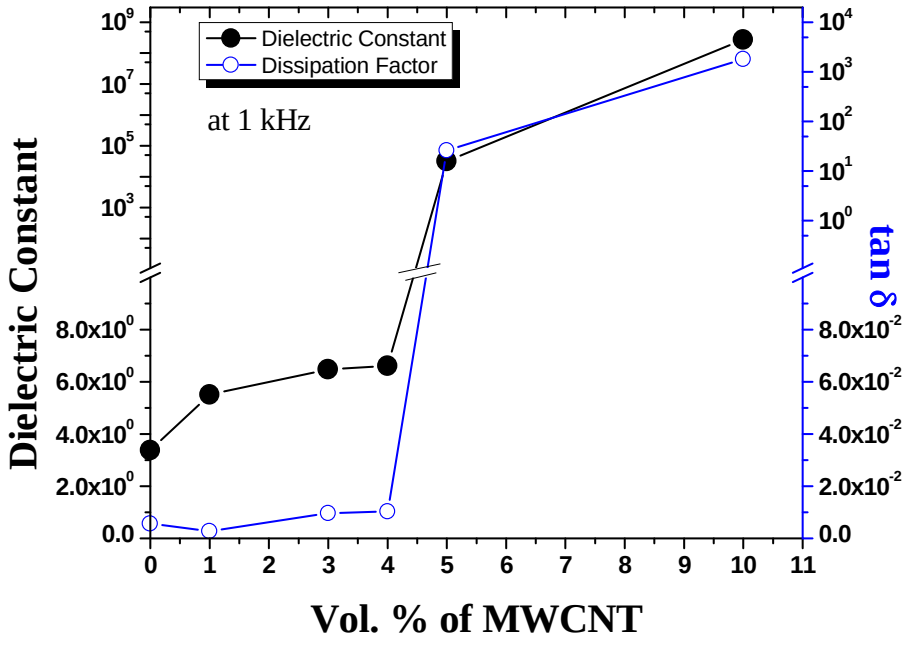

Figure 5.33. The dielectric constant and dissipation factor (tan δ) of MWCNT-PC nanocomposites as a function of MWCNT vol %.

Thus, below percolation, the highest augment in the dielectric constant was in FLG-PC nanocomposite and the lowest augment was in SWCNT-PC nanocomposite. With conductive filler, the increment in the dielectric constant should be related to the interfacial area between conductive filler and polymer matrix. This interfacial area becomes significant when the filler are inserted in good amount. As discussed in literature section, the increment in the dielectric constant is related to the formation of large number of tiny micro-capacitors in the form of filler-polymer-filler. When the polymer layer between two adjacent conducting filler (having spherical/fibrous/sheet shape) becomes infinitesimally thin with large surface area, these micro-capacitors provide high capacitance (conceptually), which results in high dielectric constant of

the composites. Due to the high aspect ratio and the tubular morphology, the CNTs make the 3-D connectivity among them at low vol % and hence percolation occurred at low vol %, consequently the dielectric constant could not increased to considerable extent.

The dielectric constant of FLG-PC nanocomposite increased to considerable extent (it was 70 with dissipation factor of 0.07 at 3 vol %). This good augment, off course, should be attributed to the large surface area of polymer film between two adjacent FLG sheets which results in the formation of micro-capacitor with good capacitance. In case of Cu-PC nanocomposites, the aspect ratio is about 1 and it was also found from XRD study that the Cu particles were covered with Cu_2O layer. Due to these reasons, the formation of micro-capacitors was not effective and hence, even with high vol % of Cu particles the increment in dielectric constant was low.

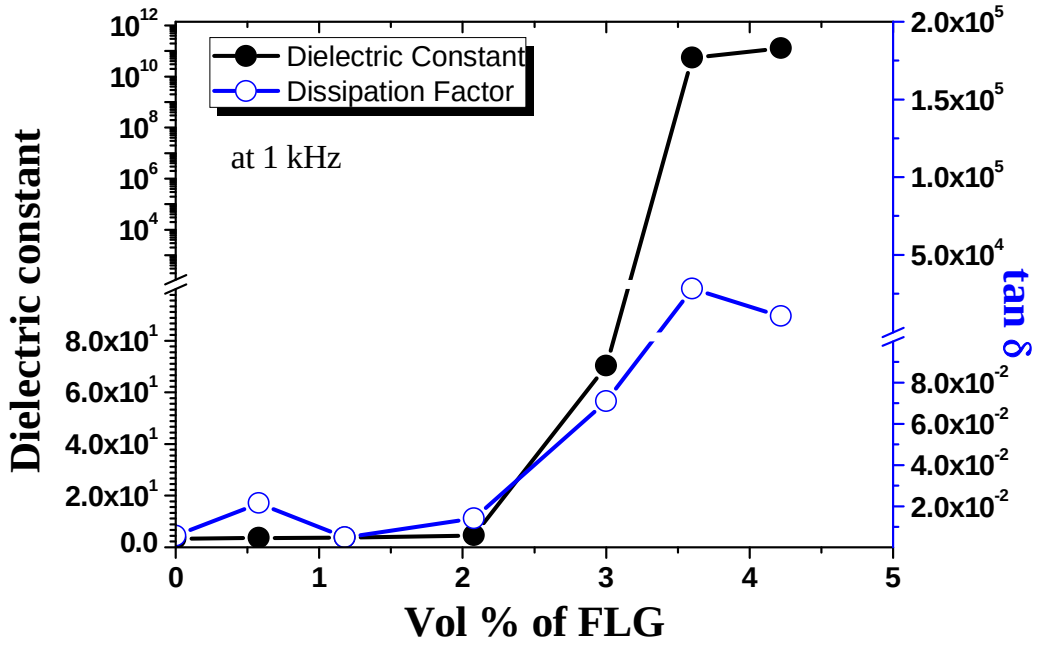

Figure 5.34. The dielectric constant and dissipation factor (tan δ) of FLG-PC nanocomposites as a function of FLG vol %.

Yousefi et al. [112] have also reported a very high value of dielectric constant (14000 at 3 wt % of rGO) in reduced graphene oxide (rGO)/epoxy nanocomposite.

However, the data for loss factor was lacking in their work. They suggested that the prepared nanocomposite can be very good candidate material for EMI shielding application through absorbing mechanism. Based on the above finding, the present FLG-PC nanocomposite appeared to be very interesting because it can, not only be used as very good EMI shield material beyond percolation but also be as good dielectric materials below percolation. The SWCNT-PC and MWCNT-PC nanocomposites, beyond percolation, can be used for EMI shielding and ESD applications.

Since the Cu particles were in oxidized condition in the Cu-PC nancomposites, this composite could also be a potential candidate for antistatic applications as suggested in previous work [161].

5.2.6.3 Effect of frequency on the dielectric constant and dissipation factor

The effects of varying frequency (10^3 to 10^6 Hz) were analyzed and the results are represented in Figures 5.35 to 5.42. It was observed that in all the cases, with increasing frequency, the dielectric constant decreases. The decrease in the dielectric constant was slow and steady up to the filler volume concentration below percolation threshold. Beyond the percolation threshold (i.e. in smearing region), the decreasing rate became more pronounced. When the system was fully percolated, the decreasing trend was almost linear. Dissipation factor also showed different behaviour with increasing frequency. Below percolation, it was showing dissipation factor with almost constant value or with slow increasing trend (except the case of Cu-PC nanocomposite system), whereas, it shows decreasing trend beyond percolation. The similar trend for both dielectric constant and dissipation factor in previously reported works by various researchers [36, 103-104] corroborate the experimental findings of this work.

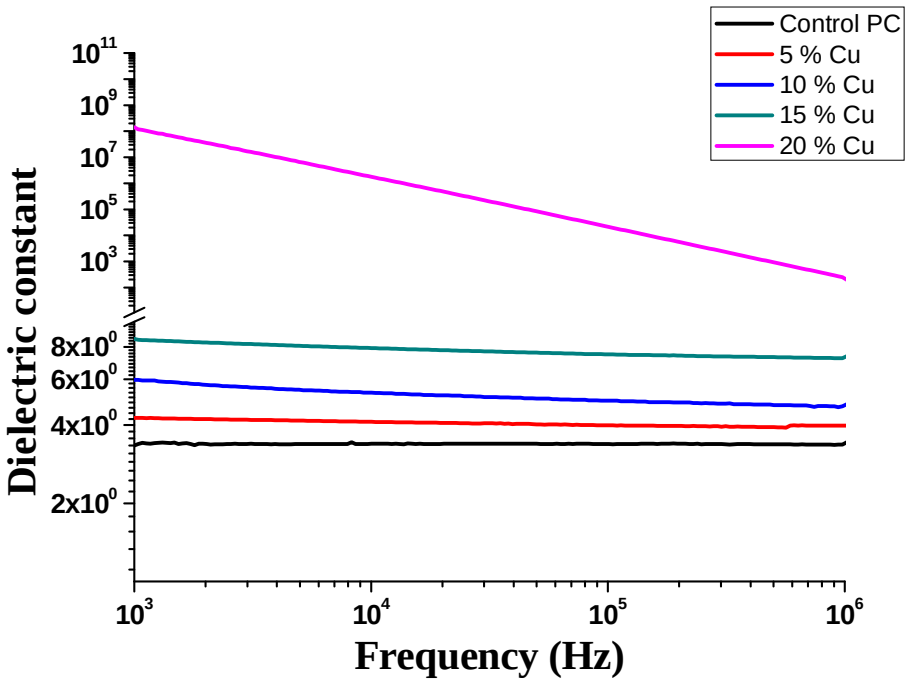

Figure 5.35. The effect of frequency on the dielectric constant of Cu-PC nanocomposites with different Cu vol %.

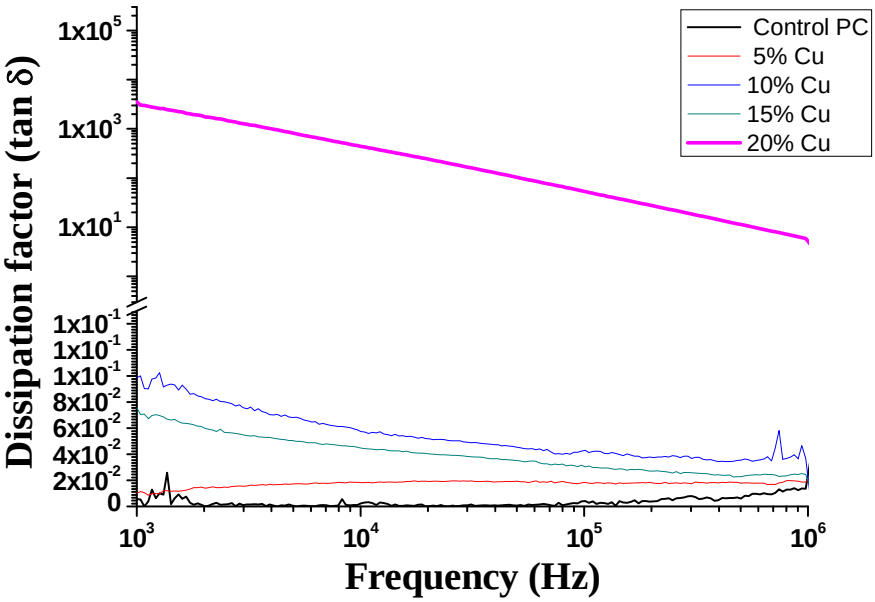

Figure 5.36. The effect of frequency on the dissipation factor (tan δ) of Cu-PC nanocomposites with different Cu vol %.

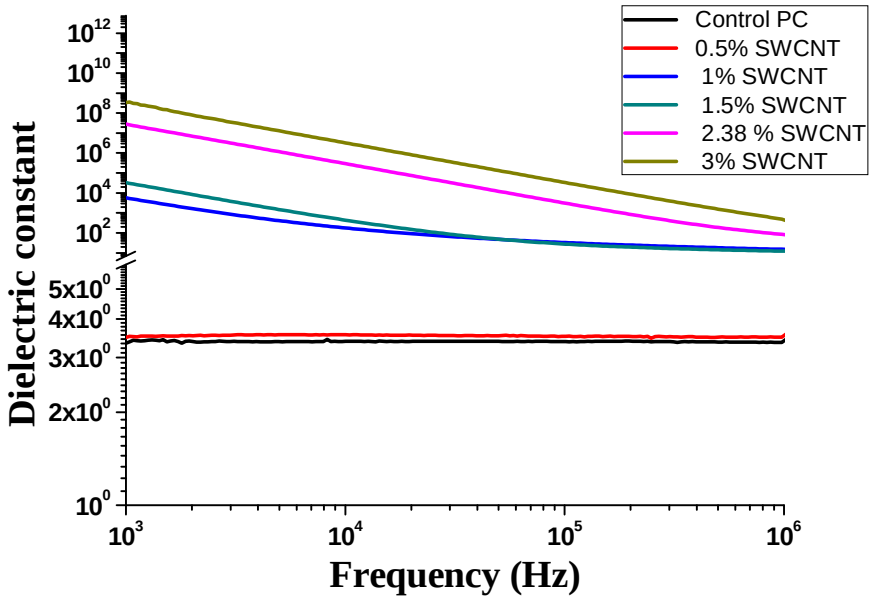

Figure 5.37. The effect of frequency on the dielectric constant of SWCNT-PC nanocomposites with different SWCNT vol %.

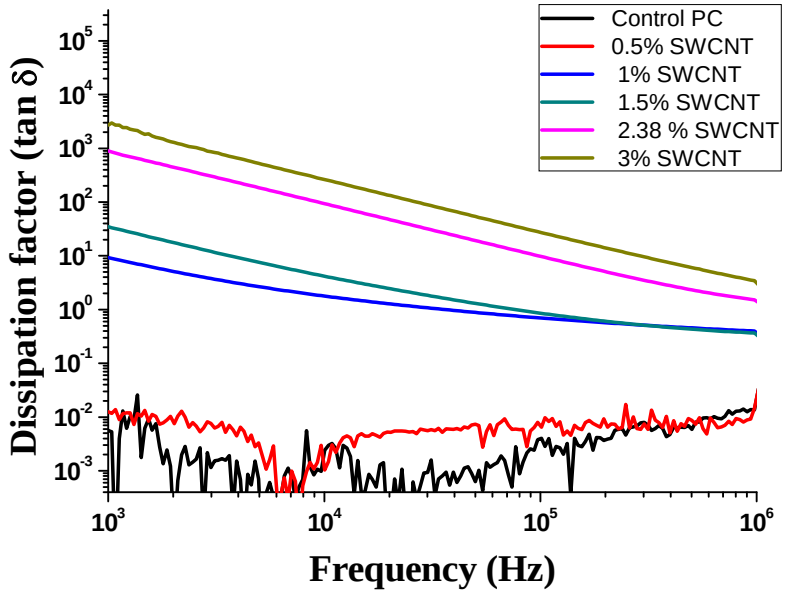

Figure 5.38. The effect of frequency on the dissipation factor (tan δ) of SWCNT-PC nanocomposites with different SWCNT vol %.

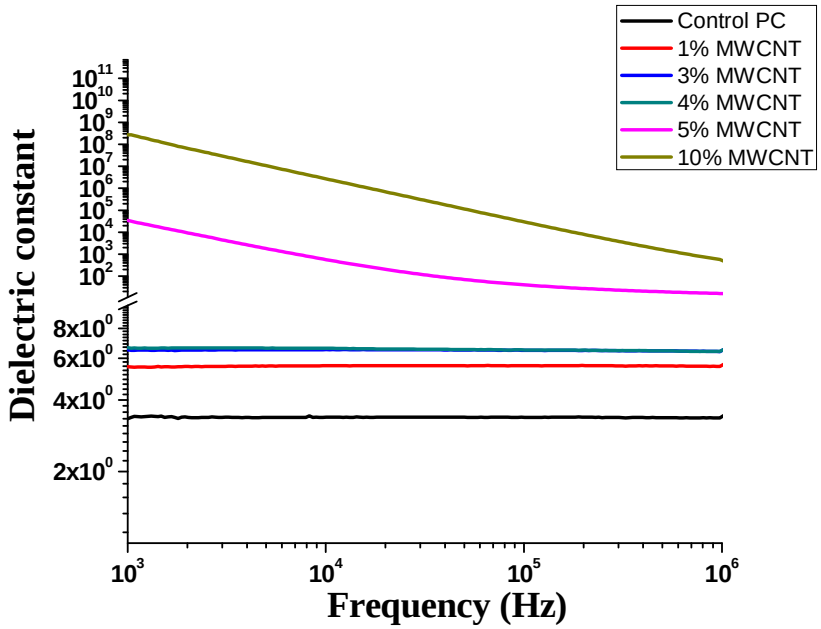

Figure 5.39. The effect of frequency on the dielectric constant of MWCNT-PC nanocomposites with different MWCNT vol %.

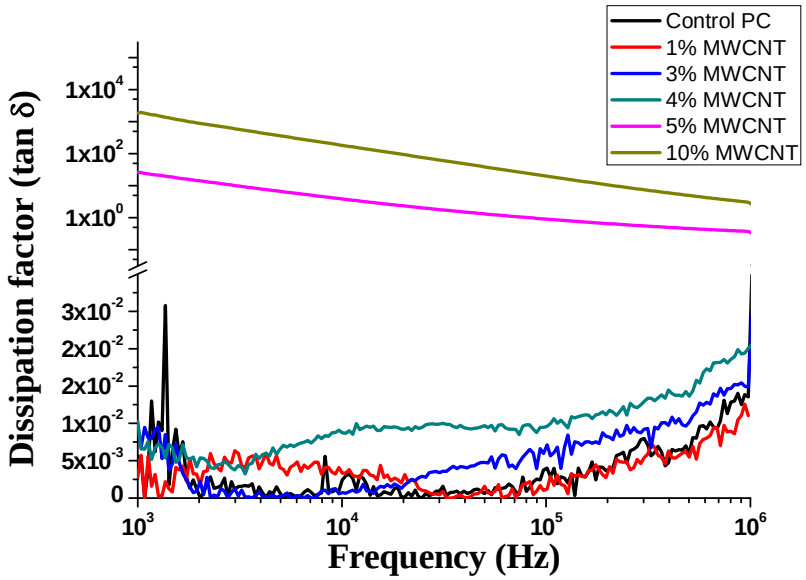

Figure 5.40. The effect of frequency on the dissipation factor (tan δ) of MWCNT-PC nanocomposites with different MWCNT vol %.

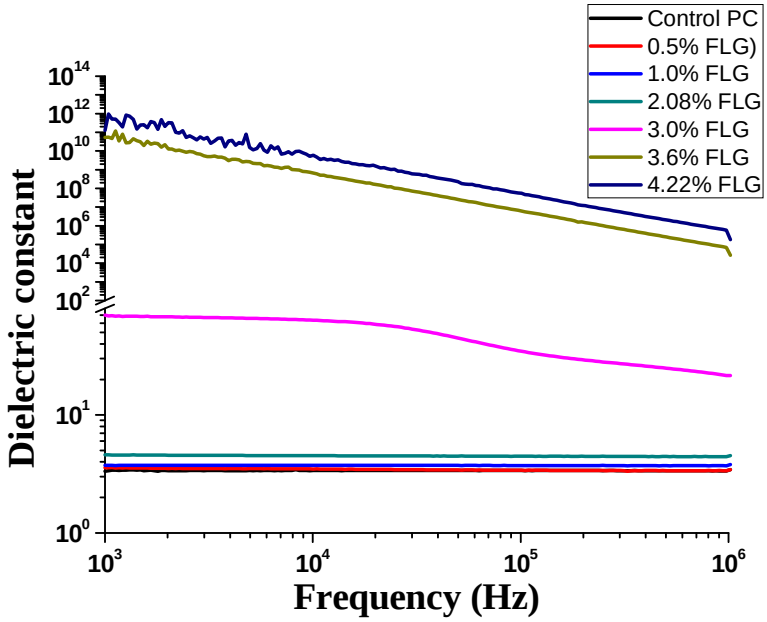

Figure 5.41. The effect of frequency on the dielectric constant of FLG-PC nanocomposites with different FLG vol %.

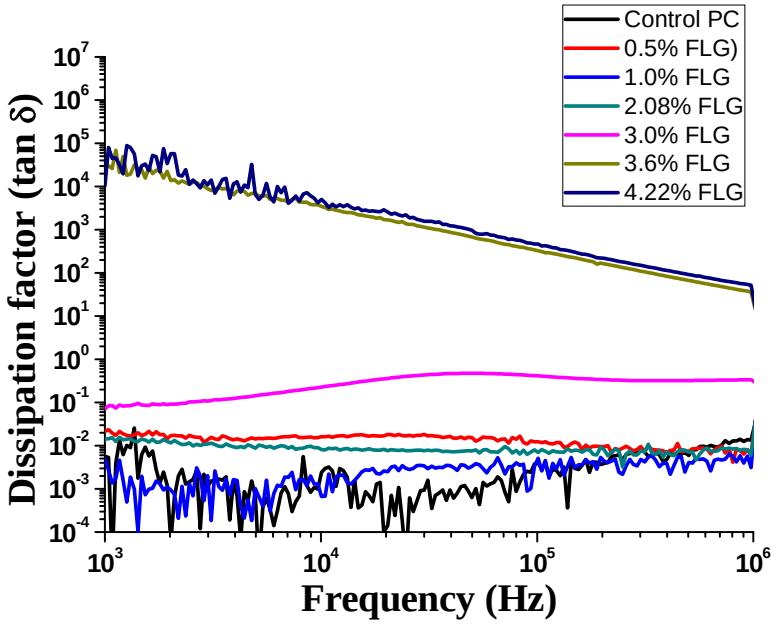

Figure 5.42. The effect of frequency on the dissipation factor (tan δ) of FLG-PC nanocomposites with different FLG vol %.

Figure 5.35 shows that in Cu-PC nanocomposite, just below percolation (15 vol %) threshold the dielectric constant was 8.5 at 1 kHz and it decreased to 7.3 as frequency increased to 1MHz. Above percolation (i.e. at 20 vol % Cu), the dielectric constant decreased almost linearly (from 10^8 to 10^2 when frequency increased from 1 kHz to 1 MHz). It is clear from Figure 5.36 that below percolation, the dissipation factor was remained below 0.1. Nanocomposite with 5 vol % Cu shows almost frequency independent dissipation factor but above 5 vol % the dissipation factor showed decreasing trend with increasing frequency. The frequency dependence of the dielectric constant and dissipation factor of the SWCNT-PC (Figures 5.37 and 5.38), MWCNT-PC (Figures 5.39 and 5.40) and FLG-PC (Figures 5.41 and 5.42) nanocomposites decreased with increasing frequency and the decreasing trend became more pronounced with increasing concentration of conductive filler.

To understand the frequency dependence of the dielectric constant one can consider the different types of polarization mechanism viz. interfacial polarization (due to the accumulation of charges at the interface between the materials having different dielectric constant and conductivity), dipole polarization (due to the orientation of dipoles), atomic polarization (due to the displacement of atoms with respect to each other in the molecule) and electronic polarization (due to the displacement of charges within the atom) [144]. The time required for a particular polarization to occur or disappear is called the *relaxation-time.* The polarization is said to be slow if the relaxation time is high and rapid if the relaxation time is small. As the frequency increases the slower polarization mechanism becomes lesser and lesser effective due to the mismatch of relaxation time and frequency of the field which result in the decreased dielectric constant with increasing frequency. The dissipation factor is related to the energy dissipated due to the friction or resistance experience by the bound charges/dipoles in forming the polarization.

All the conductive filled nanocomposites were heterogeneous systems in which the interfacial type polarization or Maxwell-Wagner-Sillars polarization, as reported in various previous works [36, 112] were dominated at lower frequencies. Hence, in all the present nanocomposites, the dielectric constant was high at lower frequencies. As the frequency increased the polarization became less dominant and hence the dielectric constant decreased with increasing frequency. As the frequency increases, due to the mismatching of relaxation time of particular polarization

mechanism and field frequency, the loss factor increases, hence the dissipation factor for the present nanocomosites showed slight increasing trend with increasing frequency. Above percolation, the rapid drop in the dielectric constant must be attributed to the large leakage current which also gives rise to high dissipation factor. This argument is in support with the finding reported in previous works [36, 104].

5.2.6.4 Effect of temperature on the dielectric constant and dissipation factor

The temperature dependency of the dielectric constant and dissipation factor for the studied nanocomposites are shown in Figures 5.43 to 5.50. The temperature dependency was analyzed for the nanocomposites below percolation. For all the nanocomposites the temperature dependency was examined at 10 kHz frequency.

The dielectric constant of the Cu (5 vol %)-PC nanocomposite was increased very slightly, beyond 100 °C, with increasing temperature, whereas, for Cu (15 vol %)-PC nanocomposite, the dielectric constant initially increased then decreased i.e. showing a broad peak expanding from room temperature to 100 °C, however the change in the dielectric constant was not significant. Beyond 100 °C, the dielectric constant again started to increase and reached to the value of about 12 at 200 °C. The dissipation factor, in both the nano Cu-filled composites, remained almost constant up to 100 °C. On further increasing the temperature, the dissipation factor was found to increase continuously.

For all the nanocomposites with carbonaceous filler i.e. SWCNT-PC (Figure 5.42 and 5.43), MWCNT-PC (Figure 5.44 and 5.45) and FLG-PC (Figure 5.46 and 5.47), the dielectric constant was almost constant (similar trend as observed for control PC) in the studied temperature range except the case of FLG (3 vol %)-PC nancomposites, in which the dielectric constant was increasing significantly beyond 120 °C and reached up to 390 at 200 °C. For all these nanocomposites, the dissipation factor exhibited a change in the form of two broad peaks, one below 120 °C and one above 130 °C.

As discussed in the literature section, two competitive factors determine the temperature dependence of dielectric behaviour of such heterogeneous composites (a) segmental mobility of the polymer chains with increasing temperature which increases

the dielectric constant and (b) different coefficient of thermal expansion of filler and polymer which disturbs the distribution of filler in the polymer and hence decreases the dielectric constant. Which factor is dominant, decides the temperature dependence of dielectric behaviour. The increment in the dissipation factor can be attributed to the increased segmental mobility (due to associated β- and α- relaxations) of polymer chains which gives rise to the increased losses.

At lower vol %, for all the nanocomposites, the dielectric constant showed almost similar trend as shown by control PC i.e. not much affected by the temperature in the studied range. However, very slight changes were observed beyond 100 °C. Such behaviour confirms that, at lower vol %, the nanocomposites structures were not much affected with increasing temperature. The slight increase in the dielectric constant, beyond 100 °C, may be correlated to the improved interfacial polarization with increasing temperature. Qi et al. [96] also observed the similar trend for dielectric constant in Ag/epoxy nanocomposites. A weak temperature dependence of dielectric constant has also been reported by Dang et al. [95] in Ag/epoxy composites which was correlated to the steady microstructure.

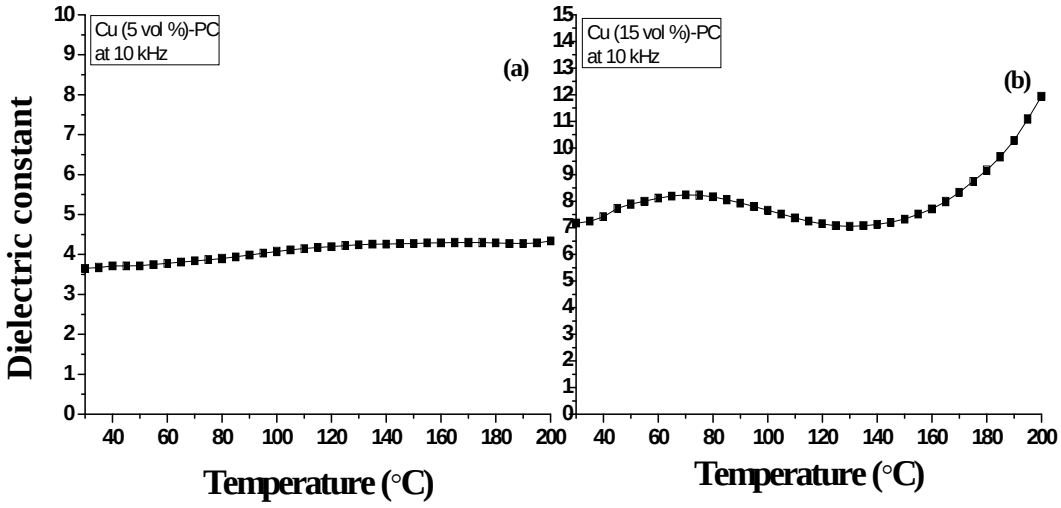

Figure 5.43. Variation in dielectric constant as a function of temperature for (a) PC-5 vol % Cu (b) PC-15 vol % Cu nanocomposites.

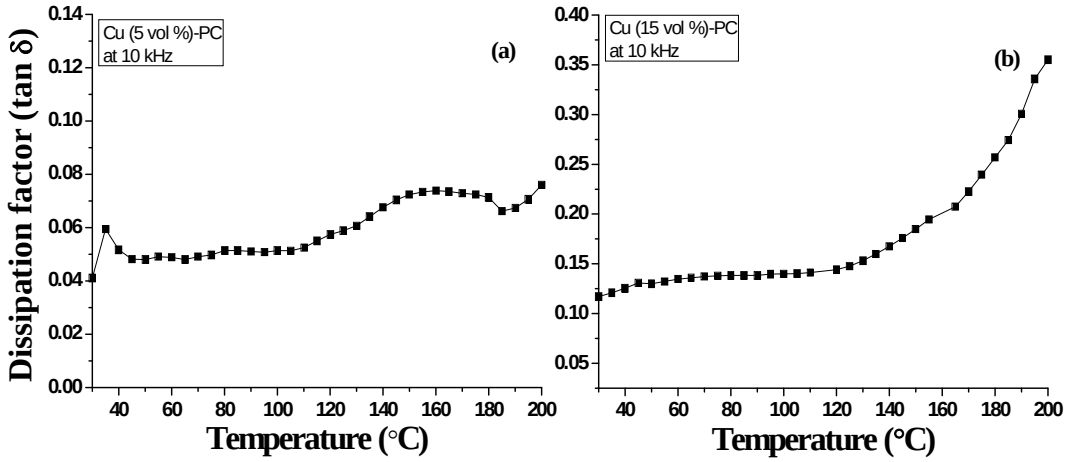

Figure 5.44. Variation in dissipation factor (tan δ) as a function of temperature for (a) PC-5 vol % Cu (b) PC-15 vol % Cu nanocomposites

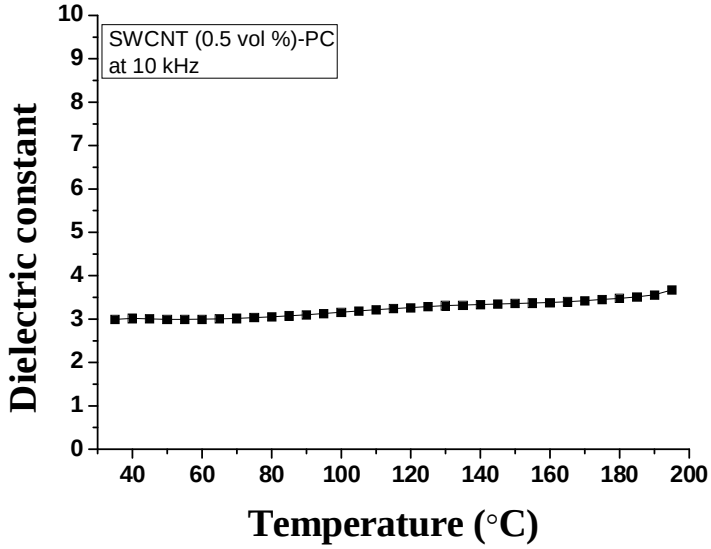

Figure 5.45. Variation in dielectric constant as a function of temperature for SWCNT (0.5%)-PC nanocomposite.

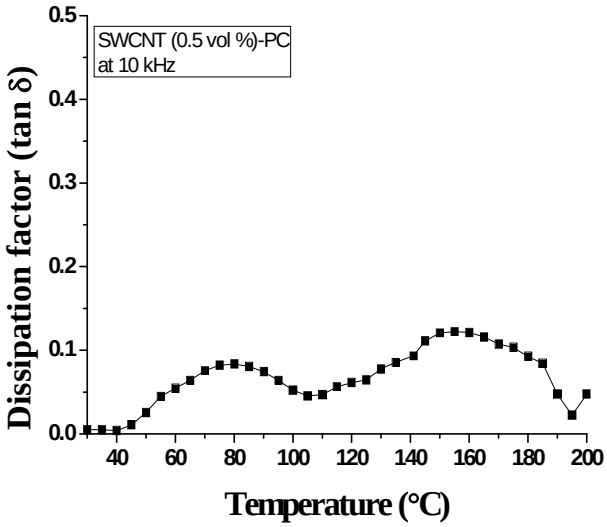

Figure 5.46. Variation in dissipation factor as a function of temperature for SWCNT (0.5 vol%)-PC nanocomposite (In case of SWCNT-PC nanocomposite, below percolation, only one composition was available and hence the temperature dependence was only analyzed for one composition).

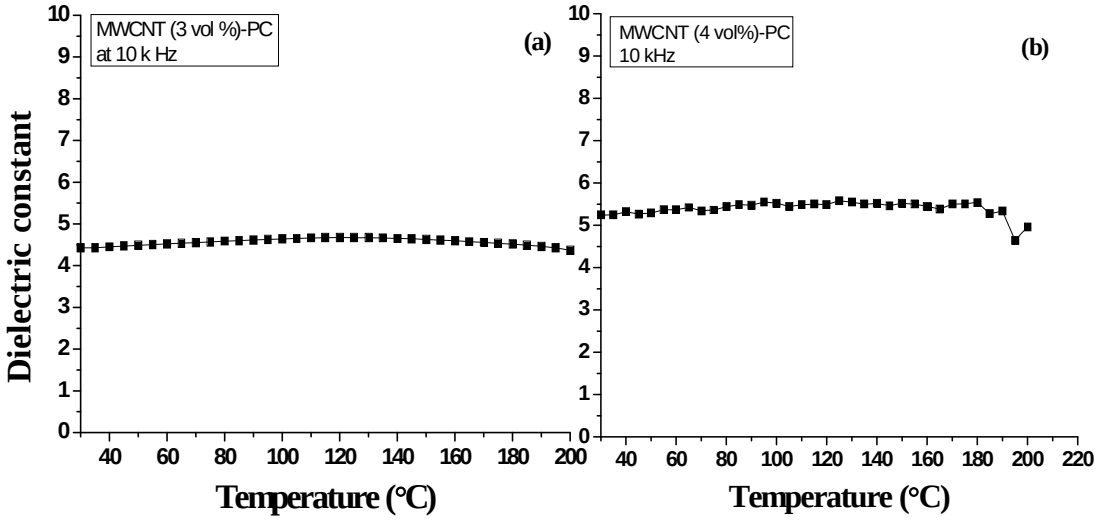

Figure 5.47. Variation in dielectric constant as a function of temperature for (a) SWCNT (3 vol %-PC) (b) MWCNT (4 vol %)-PC nanocomposites.

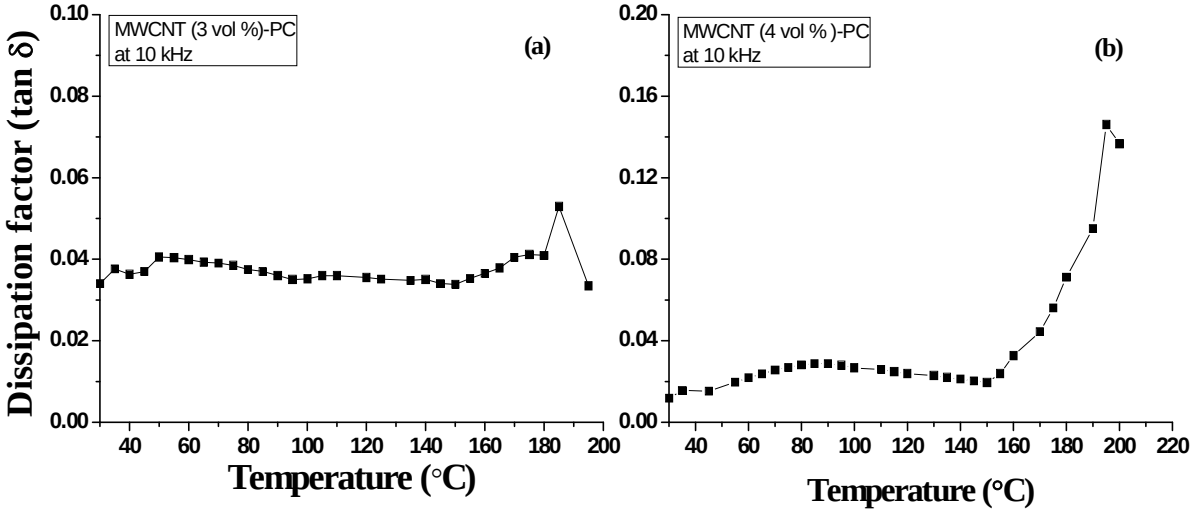

Figure 5.48. Variation in dissipation factor as a function of temperature for (a) SWCNT (3 vol %-PC) (b) MWCNT (4 vol %)-PC nanocomposites.

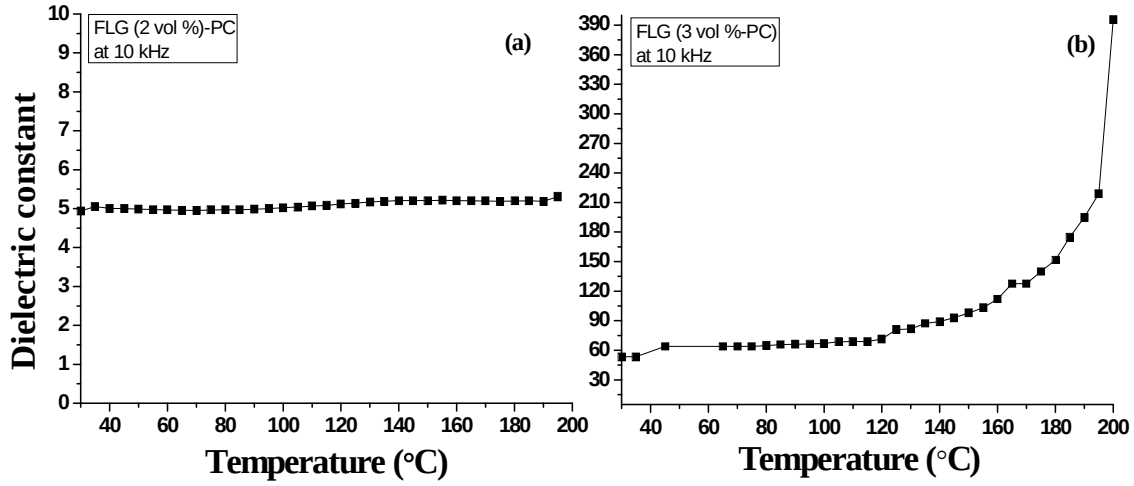

Figure 5.49. Variation in dielectric constant as a function of temperature for (a) FLG (2 vol %-PC) (b) FLG (3 vol %)-PC nanocomposites.

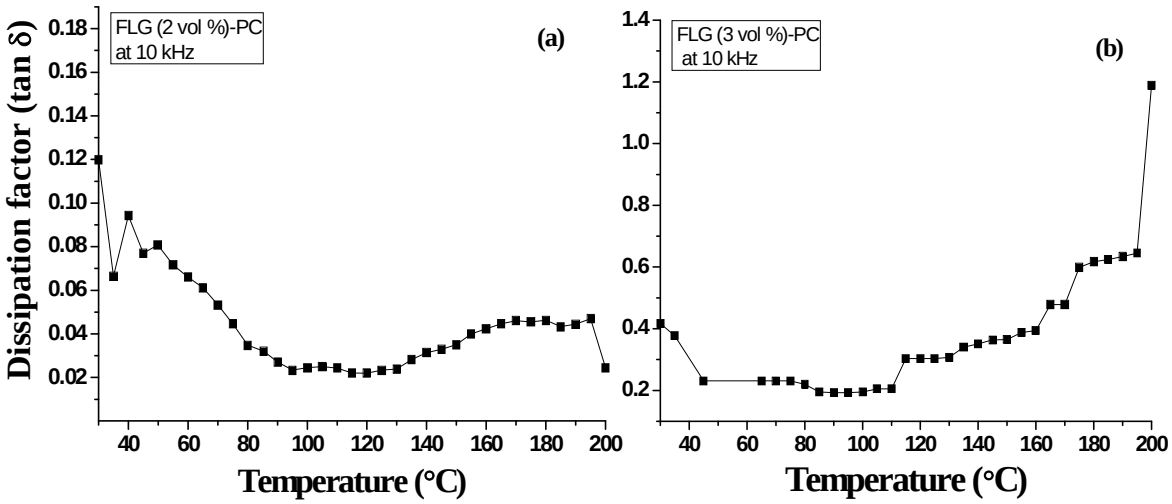

Figure 5.50. Variation in dissipation factor as a function of temperature for (a) FLG (2 vol %-PC) (b) FLG (3 vol %)-PC nanocomposites.

At low vol % of fillers, the most part of nano-sized fillers may entrap in between the adjacent polymer chains which in turn restrict mobility of filler in the matrix with increasing temperature, thereby, the micro-/nanostructure of these nanocomposites were stable with respect to temperature [35].

In case of Cu (15 vol %)-PC and FLG (3 vol %)-PC nanocomposites, the dielectric constant significantly increased beyond 100 °C. In both the cases, the filler concentrations were very close to the concentration, required for percolation, therefore, it is expected that the adjacent fillers were separated by very thin layer of polymer. At this stage, at higher temperature the charges might become more active at interface which results in the increased the interfacial polarization. Therefore, the capacitance of micro-capacitors (in the form of conducting filler-polymer-conducting filler combination) formed within the nancomposite might be increased. At the same time the chances of leakage current also increases, which ultimately appears in the form of increased dissipation factors, as observed in both the nanocomposites.

The effect of temperature on the dielectric constant and dissipation factor reveals that the studied composites (below percolation) show very good stability up to 100 °C in terms of dielectric constant value and tolerable dissipation factor. In FLG (3 vol %)-PC nanocomposites the value of dielectric constant was about 60 (at 10 kHz) up to 100 °C and increased further on increasing temperature. The dissipation factor

decreased initially with increasing temperature up to 100 °C and thereafter it increased with further increase of temperature. These data are interesting for the use of FLG-PC nanocomposites as potential dielectric materials for various commercial applications involving service temperature up to 100 °C. These nanocomposites are advantageous over previously prepared commercial polymer/ceramic hybrid films [1] due to higher dielectric constant with tolerable dissipation factor at much lower filler concentration.

CHAPTER 6

RESULTS AND DISCUSSIONS
(Three-Phase Nanocomposites)

Second filler was incorporated in two-phase (ceramic-polymer) composite so as to improve its dielectric properties and the resultant composite is termed as three-phase composite. In two-phase conductive filler-filled composites, once percolation has been achieved, it is not meaningful to increase the volume concentration of conductive filler to increase the dielectric constant, because leakage current and thereby dissipation factor also increases to a great extent. In case of three-phase micro-/nanocomposites, containing both conductive and non-conductive fillers, the presence of non conductive filler obstructs the early formation of 3-D connections among the conductive fillers. In another words one can increase the smearing region in three-phase composites. In this work two such nancomposites have been prepared: (a) Cu-PZT-PC and (b) MWCNT-PZT-PC. In both the three-phase nanocomposites the composition of PZT-PC was fixed and considered as matrix phase. Based on the results for PZT-PC composites, it was decided to use PZT (14 vol %)-PC composite as matrix and the volume concentration of Cu nano-powder and MWCNT was varied to prepare three-phase Cu-PZT-PC and MWCNT-PZT-PC nanocomposites, respectively. The criteria of selectingr PZT (14 vol %)-PC were: moderate concentration of ceramic filler (to avoid possibility of brittleness in the resultant three-phase composites), considerably enhanced dielectric constant in comparison to PC coupled with low dissipation factor (below 0.01). Due to fix composition of PZT-PC, the vol % of PZT will not be indicated while showing the composition of particular nanocomposite.

6.1 Density

The densities of the Cu-PZT-PC and MWCNT-PZT-PC nanocomposites are shown in the Figures 6.1 and 6.2. The density of the Cu-PZT-PC nanocomposite was increased with increasing Cu vol % because of the higher density of Cu. The density of the MWCNT-PZT-PC nanocomposite was almost constant with increasing MWCNT vol % which must be attributed to almost same density of MWCNT and

PZT (14 Vol %)-PC composite. However, the experimental densities were found lower than theoretical values in both the nanocomposites which may be due to the presence of pores in the composite structure. The difference was more significant in Cu-PZT-PC nancomposites as the vol % of Cu increased which might be due to the presence of Cu_2O (having the density of about 6 g/cc) in the nano-Cu filler as also discussed in previous section of two-phase composites.

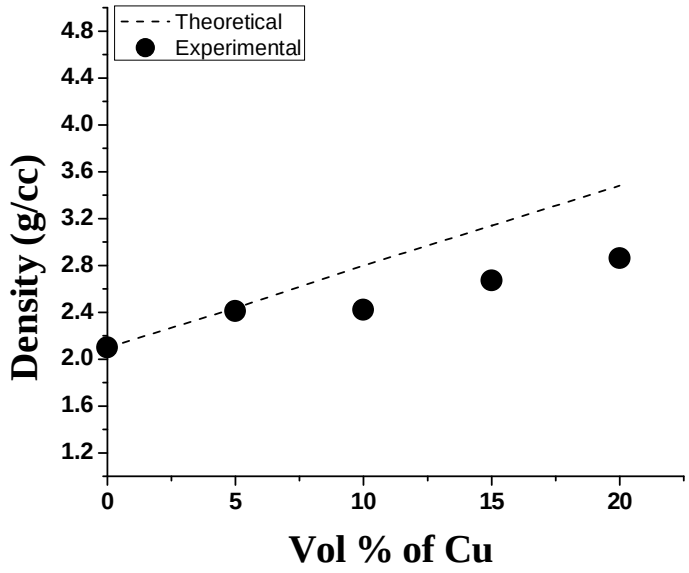

Figure 6.1. Theoretical and experimental density of the Cu-PZT-PC nanocomposites as a function of nano-Cu volume percent.

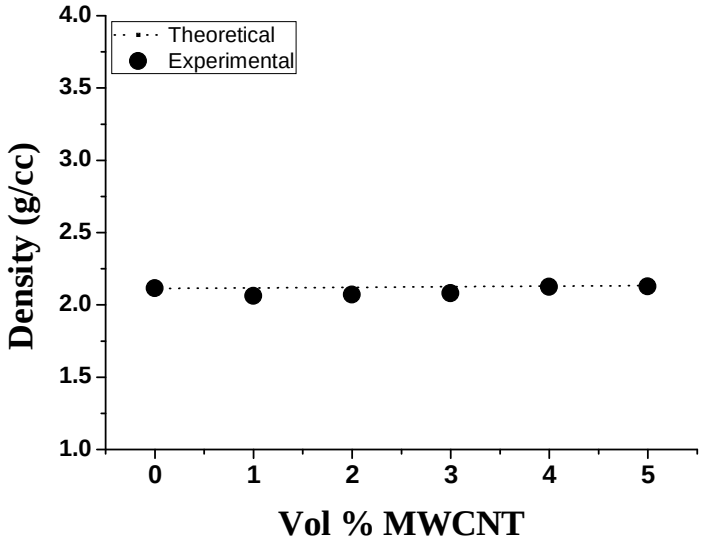

Figure 6.2. Theoretical and experimental density of the MWCNT-PZT-PC nanocomposites as a function of MWCNT volume percent.

6.2 X-ray diffractometry

The XRD patterns for both the three phase composites are shown in Figure 6.3. For better comparison the XRD traces of PC and PZT are also shown in these figures. The patterns here confirm the presence of all the three phases in the three-phase nanocomposites. The peak at around 73° is from the holder background. The peaks of PZT, Cu and Cu_2O were found in Cu-PZT-PC nanocomposite at the same positions as discussed in the previous sections of two phase composites. For MWCNT-PZT-PC nanocomposite, the peak at 26.2°, corresponding to (002) plane, confirms the presence of MWCNT, however the intensity was very low. A peak around 43.4° is also expected corresponding to (101) plane related to MWCNT, but here the peak is not apparent. The low intensity from MWCNT was due to the low volume percent (1 vol %) of the MWCNT.

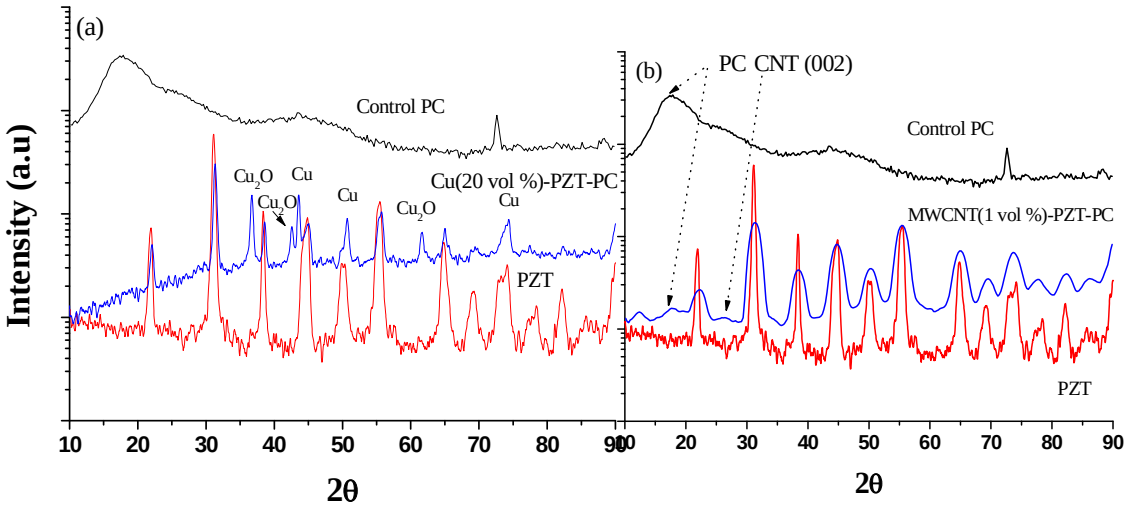

Figure 6.3. The XRD patterns for (a) Cu-PZT-PC and (b) MWCNT-PZT-PC.

6.3 Scanning electron microscopy

The SEM micrographs of the Cu-PZT-PC and MWCNT-PZT-PC are shown in the Figures 6.4 and 6.5 respectively. In Cu-ZPT-PC nanocomposites both the fillers were of particles shape (almost equiaxed faceted, but the size was different), so it was somewhat difficult to recognise them in the micrographs. To confirm their presence in the SEM micrograph, EDS analysis was also carried out.

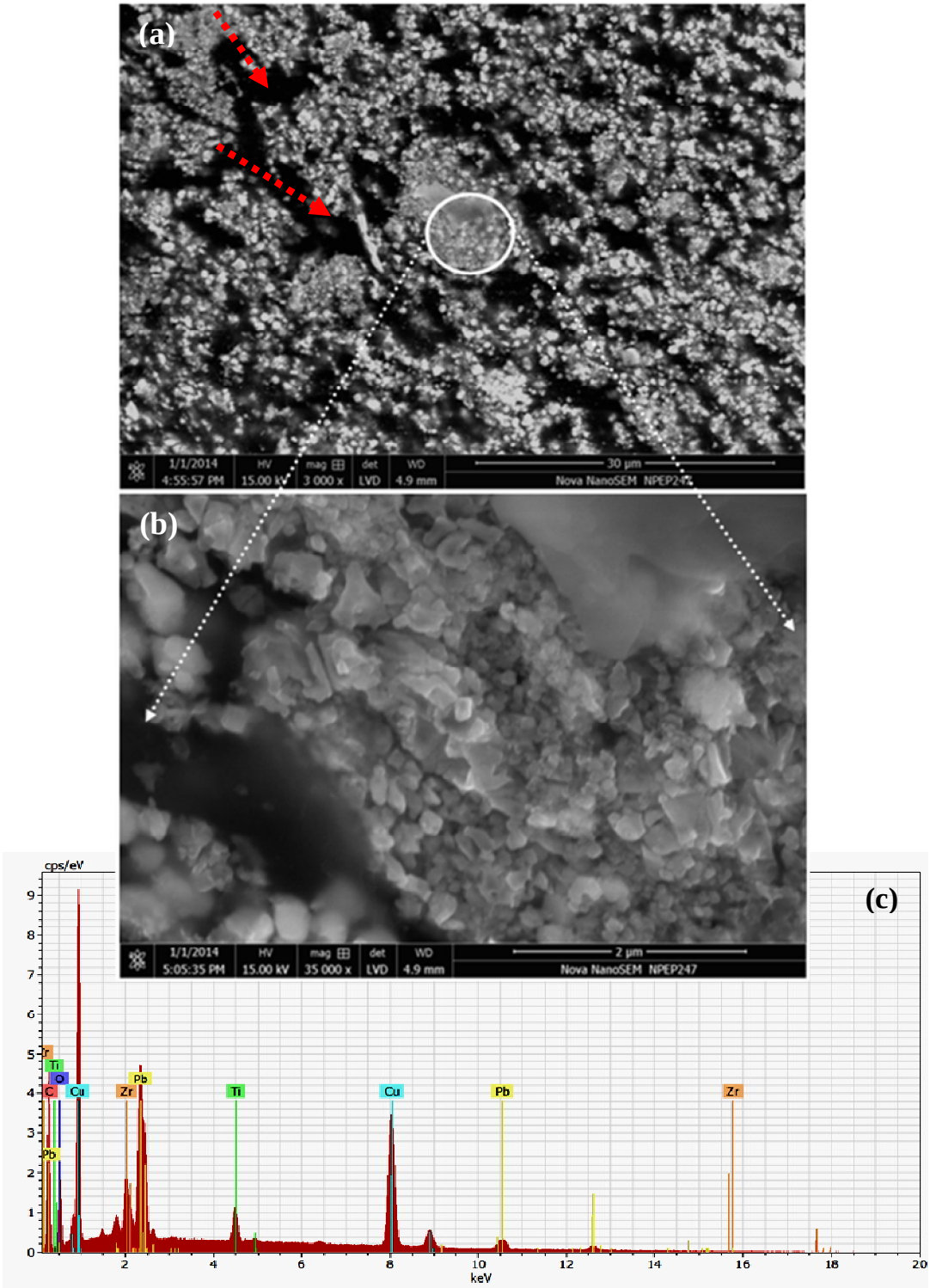

Figure 6.4. The SEM images (a) Cu (20 vol %)-PZT-PC nanocomposite (b) magnified image of the same nanocomposite; arrows are indicating the pores and (c) EDS spectrum (of the encircled area) of Cu (20 vol%)-PZT-PC nanocomposite.

The selected area is encircled in the micrograph from where the EDS spectra were taken. The EDS spectra corroborate the presence of both PZT and Cu (Cu_2O as

well). The SEM images for Cu-PZT-PC confirm the uniform dispersion of the fillers; however the formation of aggregates were also found.

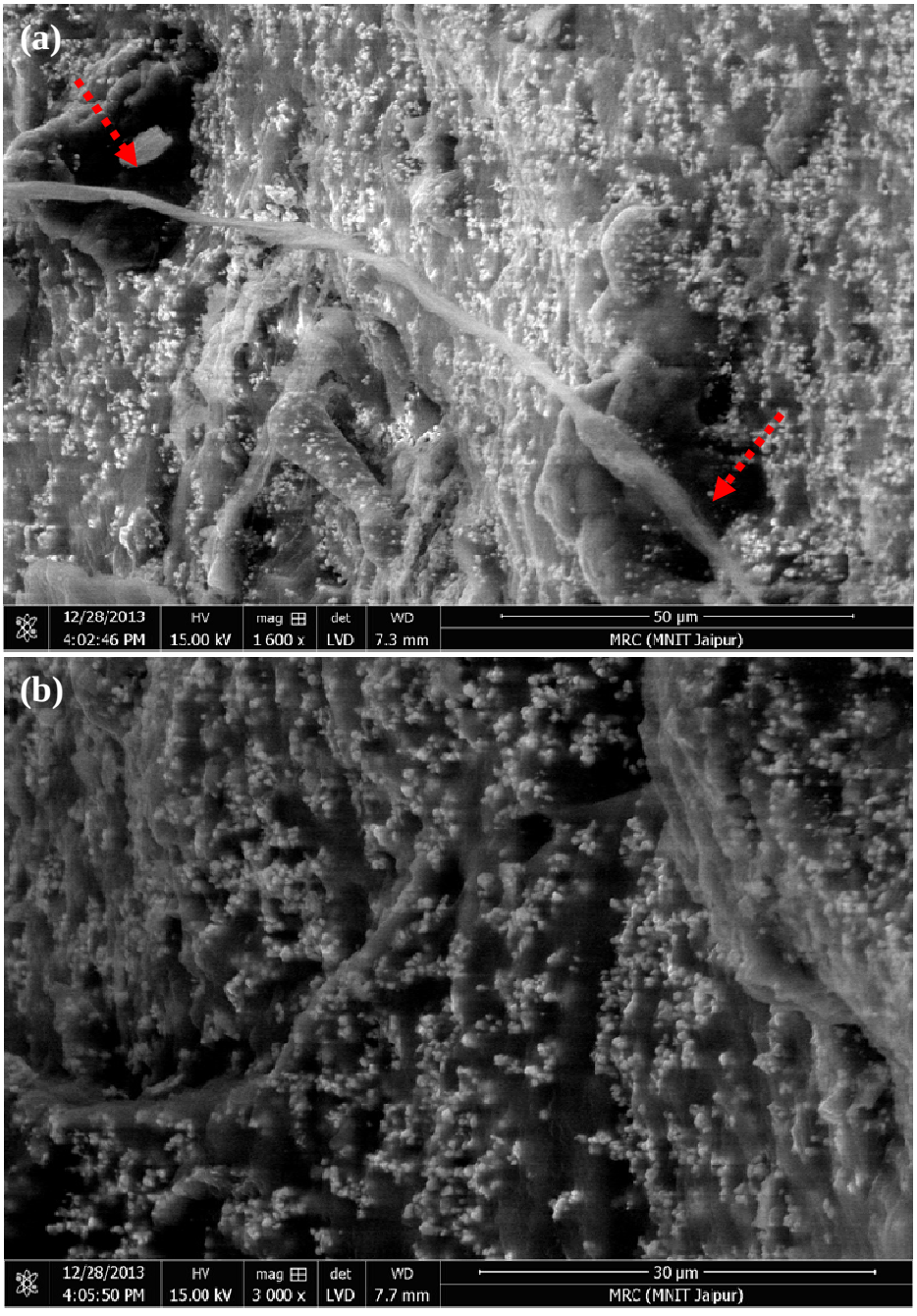

Figure 6.5. The SEM images of MWCNT (4 vol %)-PZT-PC (a) at 1600X magnification and (b) at 3000X magnification; arrows are indicating the pores.

The SEM images for MWCNT-PZT-PC clearly confirmed the presence of MWCNT and PZT particles due to their different shape morphology. As can be observed, PZT particles were embedded in the matrix disturbing the connections between MWCNTs. The arrows in the SEM images are indicating the presence of some pores.

6.4 Differential scanning calorimetry

The DSC traces for Cu-PZT-PC and MWCNT-PZT-PC are shown in the Figures 6.6 and 6.7 respectively. As found in the previous cases, due to the incorporation of nano-fillers the melting point of PC was shifted towards lower temperature side. Here, the melting point was found to be at 230.26 and 232.72 °C for Cu (20 vol %)-PZT-PC and MWCNT (5 vol %)-PZT-PC, respectively. As discussed in previous sections, the nano-sized Cu- and MWCNT-fillers might find place in between the adjacent polymer chains and thereby reduce the interaction in between these chains. Due to decreased interactions lower energy will be required for melting of the nanocomposites hence the endothermic peak for melting point shifted slightly towards lower temperature.

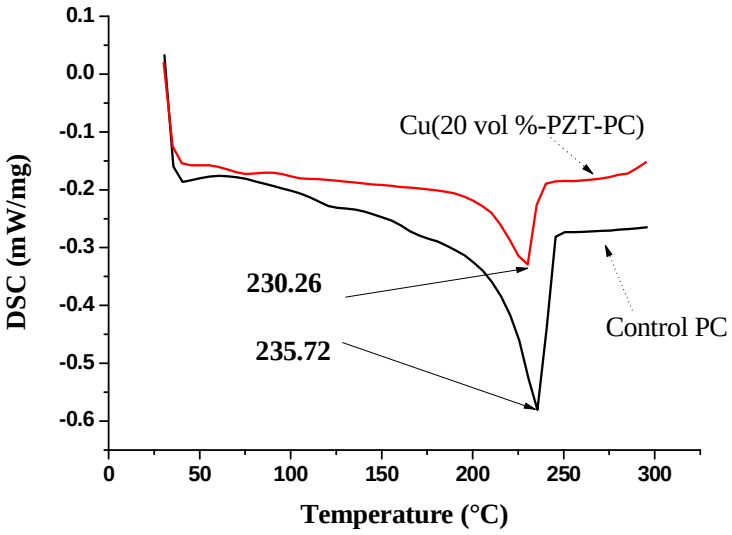

Figure 6.6. The DSC traces for control PC and Cu (20 vol %)-PZT-PC nanocomposite.

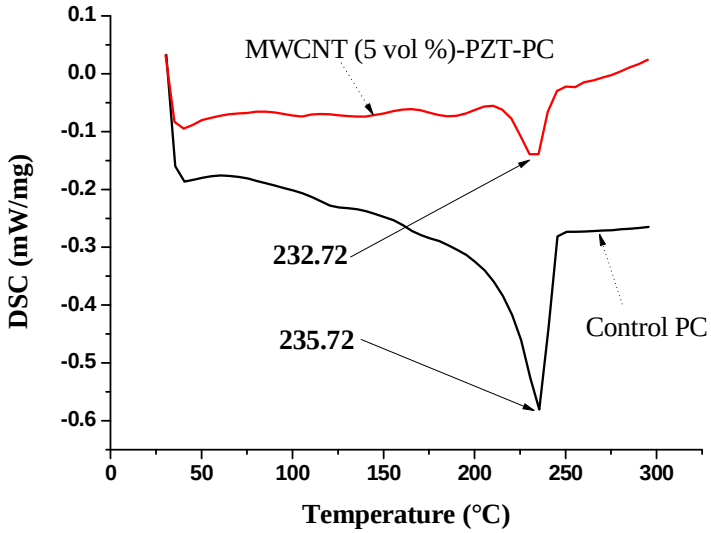

Figure 6.7. The DSC traces for control PC and MWCNT (5 vol %)-PZT-PC nanocomposite.

6.5 Electrical properties

6.5.1 AC electrical conductivity

The electrical conductivities of both the nanocomposites are shown in Figures 6.8 and 6.9.

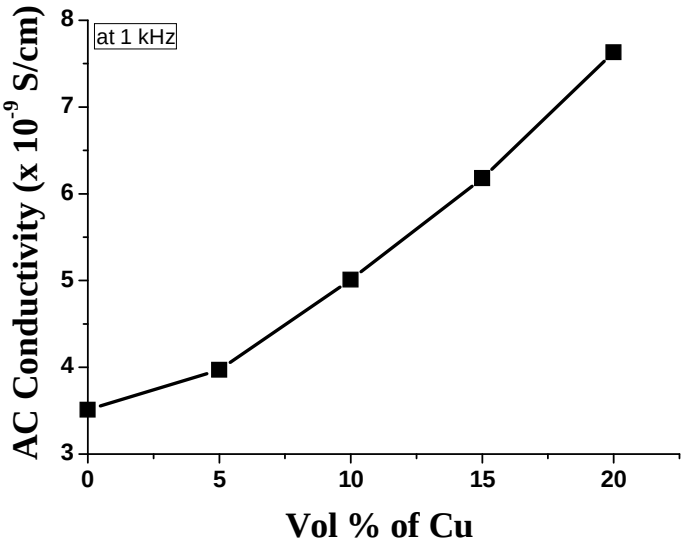

Figure 6.8. The electrical conductivity of Cu-PZT-PC nanocomposites as a function of nano-Cu filler.

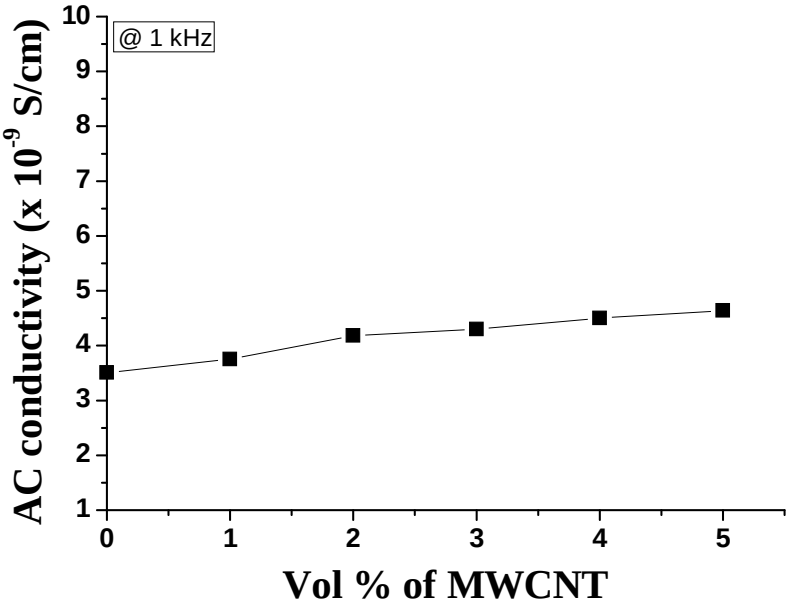

Figure 6.9. The electrical conductivity of MWCNT-PZT-PC nanocomposites as a function of MWCNT.

The observations revealed that, in three-phase composites, the electrical conductivity of the nanocomposites was slightly increased but the order of magnitude did not change. The percolation was absent in both the cases which clearly indicates that conducting fillers (i.e. Cu and MWCNT) did not able to make 3D connectivity in their three-phase nanocomposites due to the presence of PZT particles. In contrast to this, percolation was easily started in Cu-PC (with 15 vol % of Cu) and MWCNT-PC (with 4 vol % of MWCNT) nanocomposites.

6.5.2 Dielectric constant and dissipation factor

The dielectric constant of both the three-phase nanocomposites was increased continuously as shown in Figures 6.10 and 6.11. As the volume concentration of the conductive fillers increases the interfacial polarization also increases which ultimately increases the dielectric constant. Abrupt increase in the dielectric constant was not observed in the studied volume concentration window which is due to the presence of PZT particles which may inhibit the formation of effective micro-capacitors.

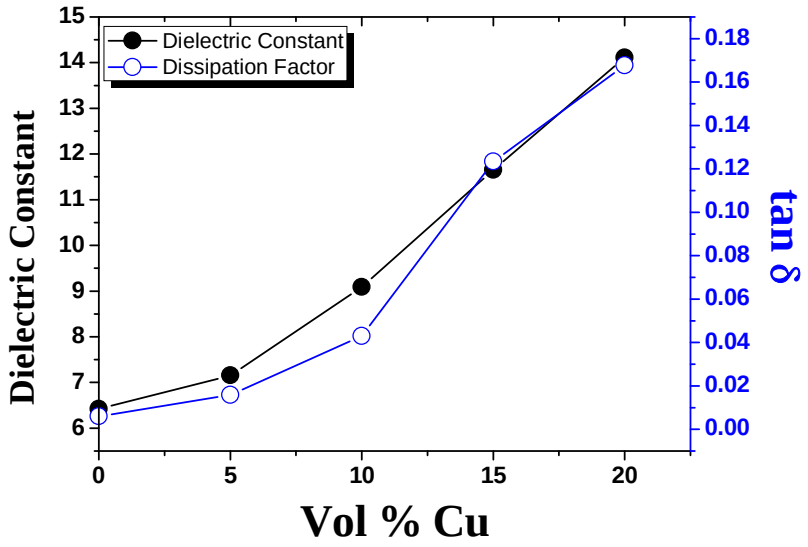

Figure 6.10. The variation in the dielectric constant and dissipation factor (tan δ) of the Cu-PZT-PC nanocomposites.

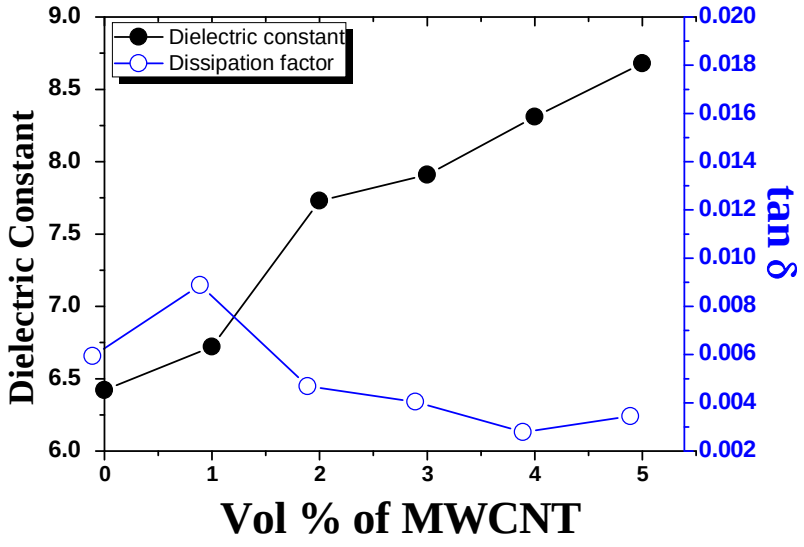

Figure 6.11. The variation in the dielectric constant and dissipation factor (tan δ) of the MWCNT-PZT-PC nanocomposites.

In case of Cu-PZT-PC nanocomposites the dissipation factor was increased continuously with increasing Cu content, whereas, in MWCNT-PZT-PC nanocomposite the dissipation factor was firstly increased and thereafter it decreased with increase of MWCNT vol %.

George and Sebastian [11] studied $Ca[(Li_{1/3}Nb_{2/3})_{0.8}Ti_{0.2}]O_{3-\delta}$ (CLNT)–epoxy–silver three-phase composite and observed that with increasing volume fraction of silver, the dissipation factor was continuously increasing, however the volume fraction was greater than 5%. Li et al. [162] also observed almost similar behaviour for three-phase composites. The similar trend for dissipation factor was observed for Cu-PZT-PC nanocomposite in present case. However, the trend for dissipation factor in MWCNT-PZT-PC was almost opposite.

Ghallabi et al. [68] studied the MWCNT containing three-phase nanocomposites and obtained very high level of dielectric constant (up to 5000), however the discussion for dissipation factor with increased MWCNT content was lacking. As reported by Zhang et al. [163], the dissipation factor in such three-phase composites depends upon the energy losses due to electron conduction, interfacial polarization process and dipole orientation process. In the present case, as the MWCNT content increased, due to fibrous morphology and awesome electronic properties, the electric field experienced by PZT particles is likely to be increased at the MWCNT/PZT interface throughout the composites. This facilitates the dipole orientation type polarization in PZT and hence the dissipation factor slightly decreased.

6.5.3 Effect of frequency on the dielectric constant and dissipation factor

In Cu-PZT-PC nanocomposites, as expected, the dielectric constant is higher (Figure 6.12) at low frequencies due to dominating interfacial polarization. As the frequency increased the dielectric constant decreased, due to the mismatching of relaxation time of polarization mechanism and field frequency. As the vol % of Cu increased in the nanocomposite, the frequency dependency was becoming more pronounced which might be attributed to the increasing interfacial polarization with increasing Cu vol %. The dissipation factor was also decreased with increasing frequency as shown in Figure 6.13. The dielectric constant for MWCNT-PZT-PC nanocomposites was almost frequency independent as shown in Figure 6.14, which is indicating that the presence of MWCNT did not alter the frequency dependence of the MWCNT-PZT-PC nanocomposites. The dissipation factor shows increasing trend above 10^5 Hz, but still remained below 0.06 as evident from Figure 6.15.

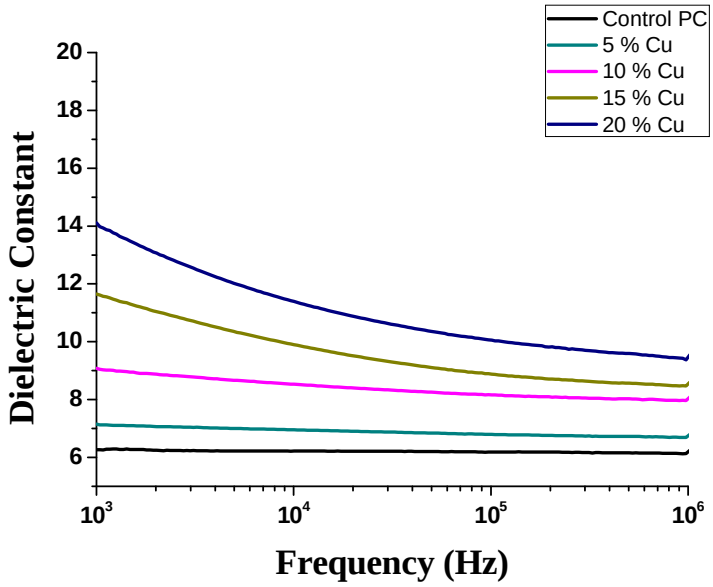

Figure 6.12. The effect of frequency of the dielectric constant of Cu-PZT-PC nanocomposites with different vol %.

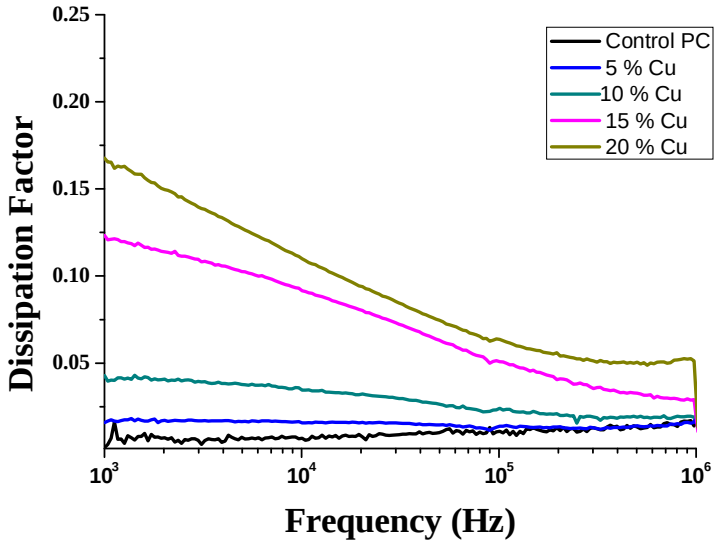

Figure 6.13. The effect of frequency of the dissipation factor of Cu-PZT-PC nanocomposites with different vol %.

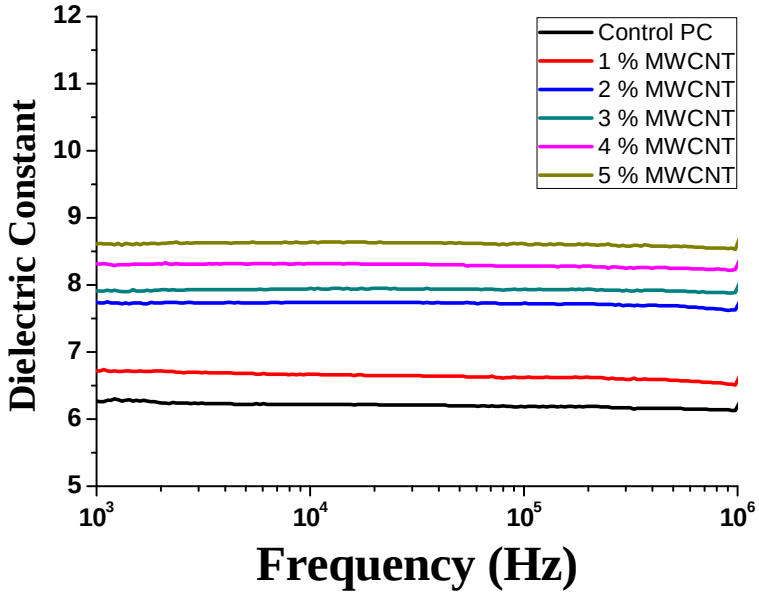

Figure 6.14. The effect of frequency of the dielectric constant of MWCNT-PZT-PC nanocomposites with different vol %.

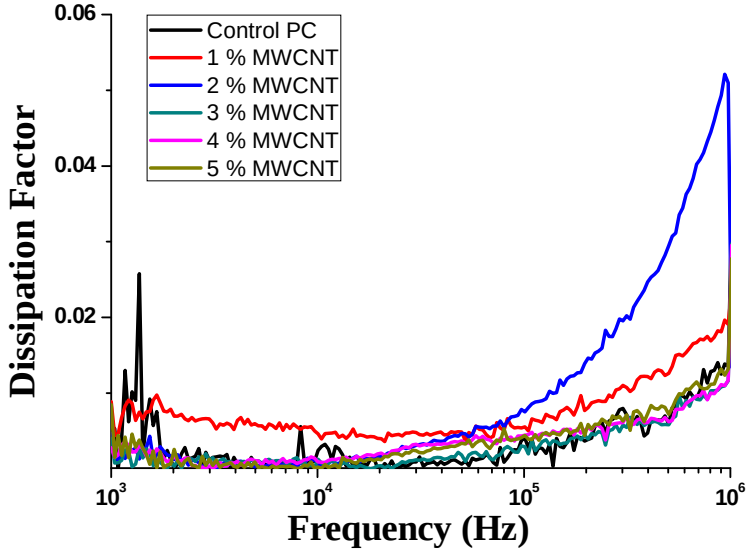

Figure 6.15. The effect of frequency of the dissipation factor of MWCNT-PZT-PC nanocomposites with different vol %.

6.5.4 Effect of temperature on the dielectric constant and dissipation factor

The temperature dependencies of the dielectric constant and dissipation factor are shown in Figures 6.16 to 6.19 for both the nanocomposites. The dielectric constant and dissipation factor of Cu (10 vol %)-PZT-PC were almost independent of temperature [Figures 6.16 (a) and 6.17 (a)]. On increasing the volume content of Cu i.e. in Cu (20 vol %)-PZT-PC nanocomposite, the dependency become pronounced. The similar trend was observed for MWCNT-PZT-PC nanocomposites (Figures 6.18 and 6.19). George and Sebastian [11] also observed the increasing temperature dependency with increasing volume content of fillers.

In the Cu(20 vol %)-PZT-PC nanocomposite, the dielectric constant firstly increased up to 80 °C then exhibited decreasing trend up to 160 °C and beyond this again increased, as evident from Figure 6.16 (b). With regard to dissipation factor, it can be seen in Figure 6.17(b) that it was continuously increased with increasing temperature. As clear from the Figure 6.18 (b), the dielectric constant of MWCNT (5 vol %)-PZT-PC nanocomposite was almost constant up to 90 °C, beyond this, it showed an abrupt drop and remained constant up to 160 °C. In case of MWCNT (5 vol %)-PZT-PC nanocomposite, two humps (first was expanding from room temperature to 80 °C and the second was expanding from 120 to 180 °C) were observed for dissipation factor, as can be observed in Figure 6.19(b).

As evident, the anomalous dielectric behaviour was observed with increasing temperature. At higher volume concentration of conductive fillers, the interfacial area among PC, PZT and Cu/or MWCNT increases. On increasing temperature, the easy facilitation of dipole orientation increases the dielectric constant. At the same time, due to the increased charges at interface and increased temperature the leakage current increases which results in the increased dissipation factor, as clearly evident in the case of Cu(20 vol %)-PZT-PC nanocomposite. However, with increasing temperature, due to the different thermal expansion coefficient of polymer matrix and fillers, the distribution of fillers in the matrix may disturb and the dominating polarization mechanisms may also change. This might be responsible for the decreasing trend of dielectric constant. The changes, observed beyond 180 °C should be attributed to the thermal agitation in the polymer segments.

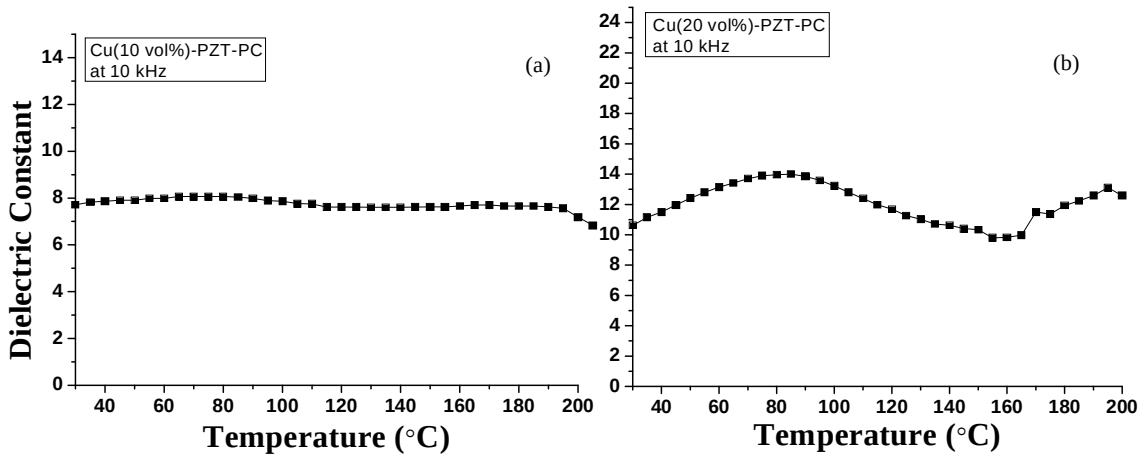

Figure 6.16. Variation in dielectric constant as a function of temperature for (a) PZT-Cu (10 vol%)-PC (b) PZT-Cu (20 vol%)-PC nanocomposites.

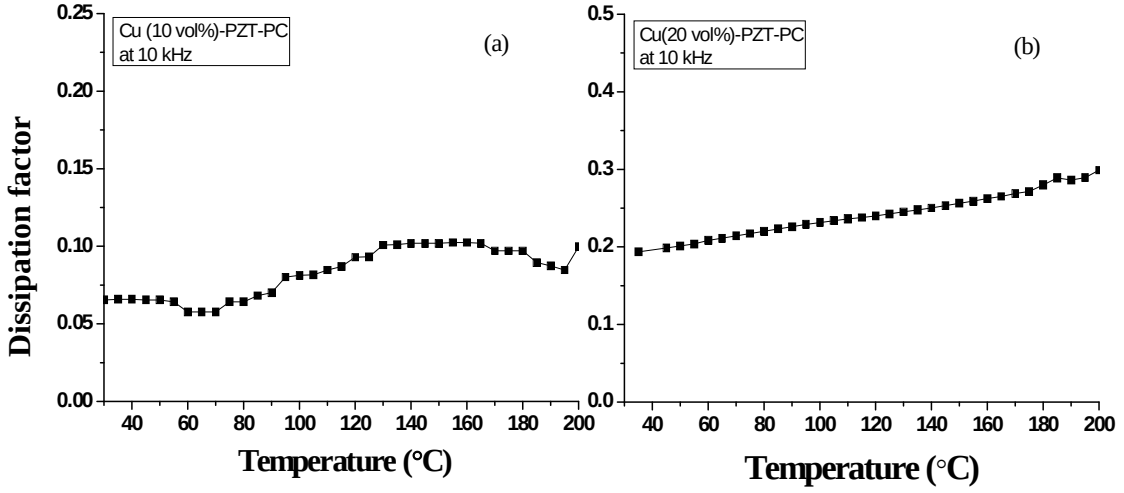

Figure 6.17. Variation in dissipation factor as a function of temperature for (a) PZT-Cu (10 vol%)-PC (b) PZT-Cu (20 vol%)-PC nanocomposites.

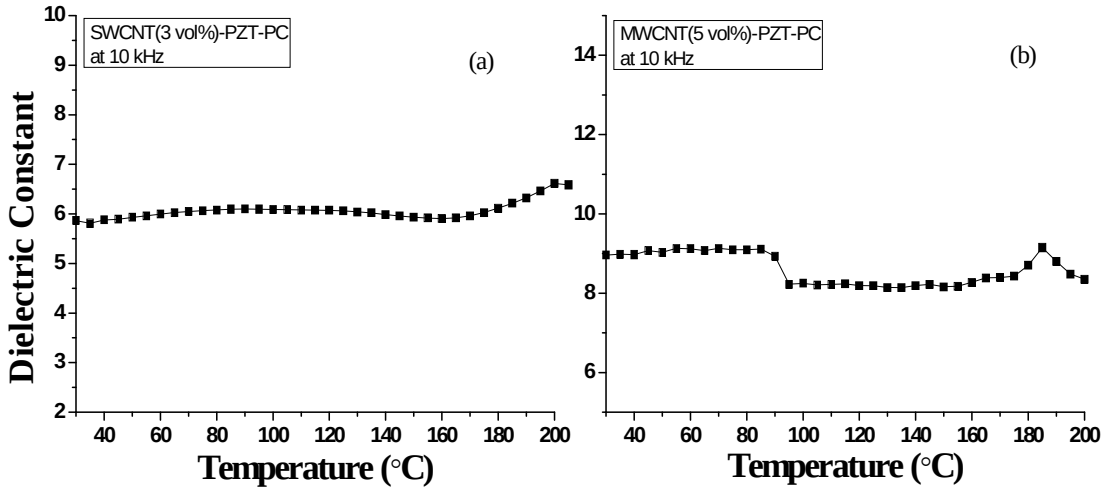

Figure 6.18. Variation in dielectric constant as a function of temperature for (a) PZT-MWCNT (3 vol%)-PC (b) PZT-MWCNT (5 vol%)-PC nanocomposites.

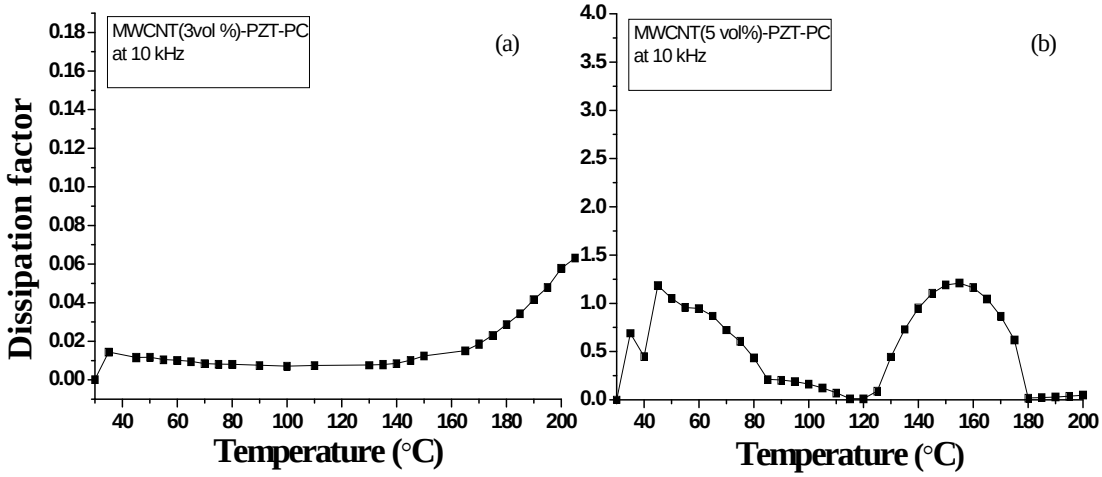

Figure 6.19. Variation in dissipation factor as a function of temperature for (a) PZT-MWCNT (3 vol%)-PC (b) PZT-MWCNT (5 vol%)-PC nanocomposites.

CHAPTER 7

CONCLUSIONS

The research work on preparation and studies on polycarbonate based nanocomposite for electronic applications has been successfully carried out. Based on the finding from density measurements, XRD analysis, microscopic studies, DSC analysis and electrical measurements, the following conclusions can be made.

- Two-phase composites namely, PZT-PC, Cu-PC, SWCNT-PC, MWCNT-PC and FLG-PC, have been successfully prepared and studied.
- Two phase composite based on PC containing about 14 vol % (50 wt %) PZT was considered as matrix for preparing three-phase nanocomposites. Three-phase nanocomposites namely, Cu-PZT-PC and MWCNT-PZT-PC have been prepared and studied.
- The densities of the micro- and nanocomposites were found close to the theoretical values except the cases of Cu-PC and Cu-PZT-PC nanocomposites. In case of Cu-filled nanocomposites, the presence of Cu_2O is probably the cause of lower experimental densities than those of theoretical densities.
- The XRD study confirmed the induced crystallinity in PC due to the solution effect and nucleating effect of fillers. XRD studies also confirmed the presence of fillers in the micro-and nanocomposites.
- Scanning electron microscopy confirmed good dispersion of fillers in the PC matrix. Raman spectroscopy confirmed the formation of few-layer graphene in the prepared sample.
- DSC analysis confirmed that PC dissolved in THF is crystallized and showed sharp melting point while as received PC was amorphous and showed a sharp glass transition temperature.
- Among the studied conductive filler-filled nanocomposites, lowest percolation threshold was observed for the SWCNT-PC nanocomposite and the maximum

achieved electrical conductivity was 10^{-4} S/cm. The dielectric constant was increased up to 10^3 with the dissipation factor of about 9 (at 1 vol % of SWCNT).

- The highest dielectric constant of 70 (i.e., about 20 times higher than that of pure PC) with dissipation factor of 0.07 was found for FLG-PC nanocomposite. It is very interesting from the application point of view. However, on further increasing the FLG in the PC matrix, the dissipation factor was found to increase significantly. The highest electrical conductivity of this nanocomposite containing 4.2 vol % FLG was 10^{-2} S/cm.

- In three-phase Cu-PZT-PC and MWCNT-PZT-PC nanocomposites, the percolation was not observed in the studied volume range of conductive filler. The maximum achieved dielectric constant was about 14 ($\tan \delta = 0.17$) and 8.5 ($\tan \delta = 0.004$) in Cu-PZT-PC and MWCNT-PZT-PC nanocomposites, respectively.

- Insignificant change in the dielectric constant was found for the PZT-PC composites and MWCNT-PZT-PC nanocompoistes with increasing frequency while there was decreasing trend in the dielectric constant for the other nanocomposites containing conductive fillers particularly above the percolation threshold. The dielectric constant and dissipation factor were found to be stable up to 100 ^{0}C.

- The FLG-PC nanocomposite, below percolation, could be a potential dielectric material to be useful for the embedded capacitors because its dielectric constant values fall in the range of dielectric constant (i.e., > 15) of the commercial products with tolerable dissipation factor.

- Cu-PC, SWCNT-PC, MWCNT-PC and FLG-PC nanocomposites, beyond percolation, may be useful for electromagnetic interference shielding/electro static dissipation (ESD).

REFERENCES

[1] H. J. Park, S. M. Hong, S.-S. Lee, J. Kim, M. Park, "Effects of CNT/BaTiO3 composite particles prepared by mechanical process on dielectric properties of epoxy hybrid films", IEEE Transactions on Advanced Packaging, Vol. 31 (2), 2008, 417-422.

[2] P. Thomas, K. T. Varughese, K. Dwarakanath, K.B.R. Varma, "Dielectric properties of poly(vinylidene fluoride)/CaCu3Ti4O12 composites" Composite Science and Technology, Vol. 70 (3), 2010, 539-545.

[3] V. Stancu, M. Lisca, I. Boerasu, L. Pintilie, M. Kosec, "Effects of porosity on ferroelectric properties of $Pb(Zr_{0.2}Ti_{0.8})O_3$ films" Thin solid film, Vol. 15 (16), 2007, 6557-6561.

[4] Q. Y. Peng, P. H. Cong, X. J. Liu, T. X. Liu, S. Huang, T. S. Li, "The preparation of PVDF/clay nanocomposites and the investigation of their tribological properties" Wear, Vol. 266 (7-8), 2009, 713-720.

[5] D. Shah, P. Maiti , E Gunn, D Schmidt, D Jiang, C Batt and E. P. Giannelis, "Dramatic enhancements in toughness of polyvinylidene fluoride nanocomposites via nanoclay-directed crystal structure and morphology" Advanced Materials, Vol. 16 (14), 2004, 1173-1177.

[6] S. Qu, S. C. Wong "Piezoresistive behavior of polymer reinforced by expanded graphite" Composites Science and Technology Vol. 67(2), 2007, 231-237.

[7] J. Xua, M. J. Dapino, D. G. Perezb, D Hansford, "Microphone based on polyvinylidene fluoride (PVDF) micro-pillarsand patterned electrodes" Sensors and Actuators A: Physical, Vol. 153 (1), 2009, 24-32.

[8] R. K. Goyal, V. V. Madav, P. R. Pakankar, S. P. Butee, "Fabrication and properties of novel polyetheretherketone/barium titanate composites with low dielectric loss", Journal of Electronic Materials, Vol. 40 (11), 2011, 2240-2247.

[9] K. W. Paik, S. D. Cho, J. Y. Lee, and L. G. Hyun, “Low tolerance Epoxy/BaTi03 composite embedded capacitor films (ECFs)”, Int’l Symposium on Electronic Materials and Packaging, 2002, 341-347.

[10] W. Liu, B. Zhu, S. Xie, Z. Xu, “Dielectric property of polyimide/barium titanate composites and its influence factors (II)” Frontier Chemical Engineering in China, Vol. 2 (4), 2008, 417-421.

[11] S. George, M. T. Sebastian, “Three-phase polymer–ceramic–metal composite for embedded capacitor applications”, Composite Science and Technology, Vol. 69, 2009, 1298–302.

[12] R. K. Goyal and A. B. Kulkarni, “Electrical properties of novel three-phase polymer nanocomposites with a high dielectric constant”, Journal of Physics D: Applied Physics, Vol. 45, 2012, 465302, 1-9.

[13] E. S. Lim, J. C. Lee, J. J. Kim, E. T. Park, Y. K. Chung H. Y. Lee, “Dielectric characteristics of polymer-ceramic-metal composites for the application of embedded passive devices”, Integrated Ferroelectrics, Vol. 74, 2005, 53–60.

[14] Q Li, Q. Xue, Q. Zheng, L. Hao, X. Gao, “Large dielectric constant of the chemically purified carbon nanotube/polymer composites”, Materials Letters, Vol. 62 2008, 4229–4231.

[15] L. Ramajo, M. S. Castro, M. M. Reboredo, “Dielectric response of Ag/BaTiO3/epoxy nanocomposites”, Journal of Mater Science., Vol. 45, 2010, 106–111.

[16] S. Banerjee, K. A. Cook-Chennault, “Influence of Al particle size and lead zirconate titanate (PZT) volume fraction on the dielectric properties of PZT-Epoxy-Aluminum composites, Journal of Engineering Materials and Technology, Vol. 133, 2011, 041016-1-6.

17] H. K. Charles Jr., Miniaturized Electronics, Johns Hopkins Apl Technical Digest, Vol. 26 (4), 2005, 402-413.

[18] Y. Rao, S. Ogitani, P. Kohl, C. P. Wong, “High dielectric Constant polymer-ceramic composite for embedded capacitor application”, International Symposium on Advanced Packaging Materials, 2000, 32-37.

[19] J. G. Hyun, S. Lee, S. D. Cho, K. W. Paik, “Frequency and temperature dependence of dielectric constant of epoxy/$BaTiO_3$ composite embedded capacitor films (ECFs) for organic substrate” Electronic Components and Technology Conference, 2005, 1241-1247.

[20] J. R. Yoon, J. W. Han, K. M. Lee, H. Y. Lee, “Dielectric properties of polymer-ceramic composites for embedded capacitors”, Transactions on Electrical and Electronic Materials, Vol. 10 (4), August 25, 2009, 116-120.

[21] J. Xu, C. P. Wong, “Effect of the polymer matrices on the dielectric behavior of a percolative high-k polymer composite for embedded capacitor applications” Journal of Electronic Materials, Vol. 35 (5), 2006, 1087-1094.

[22] V. Stancu, M. Lisca, I. Boerasu, L. Pintilie, M. Kosec, “Effects of porosity on ferroelectric properties of $Pb(Zr_{0.2}Ti_{0.8})O_3$ films” Thin Solid Film, Vol. 15 (16), 6557-6561.

[23] Q.-Y. Peng, P-H Cong, X.-J. Liu, Tian-Xi Liu, Shu Huang, Tong-Sheng Li, “The preparation of PVDF/clay nanocomposites and the investigation of their tribological properties” Wear, Vol. 266 (7-8), 2009, 713-720.

[24] D. Shah, P Maiti , E Gunn, D Schmidt, D Jiang, C Batt and E. P. Giannelis, “Dramatic enhancements in toughness of polyvinylidene fluoride nanocomposites via nanoclay-directed crystal structure and morphology” Advanced Materials, Vol. 16 (14), 2004, 1173-1177.

[25] S. Qu, S. C. Wong “Piezoresistive behavior of polymer reinforced by expanded graphite” Composites Science and Technology, Vol. 67(2), 2007, 231-237.

[26] J. Xua, M. J. Dapino, D. G. Perezb, D Hansford, “Microphone based on polyvinylidene fluoride (PVDF) micro-pillarsand patterned electrodes” Sensors and Actuators A: Physical, Vol. 153 (1), 2009, 24-32.

[27] P. Thomas; K. T. Varughese, K. Dwarakanath, K.B.R. Varma, “Dielectric properties of poly(vinylidene fluoride)/$CaCu_3Ti_4O_{12}$ composites” Composite Science and Technology, Vol. 70 (3), 2010, 539-545.

[28] D. Zhou, H. Wang, L.-X. Pang, C. A. Randall, X. Yao, “Bi_2O_3–MoO_3 Binary System: An Alternative Ultralow Sintering Temperature Microwave Dielectric” Journal of the American Ceramic Society, 2009, Vol. 92(10), 2242-2246.

[29] J. Lu, Ph.D. Thesis, “High dielectric constant polymer nanocomposites for embedded capacitor applications”, School of Materials Science and Engineering, Georgia Institute of Technology, December 2008.

[30] D. D. L. Chung, “Electromagnetic interference shielding effectiveness of carbon material” Carbon, 39, 2001, 279-285.

[31] D. D. L. Chung, “Materials for Electromagnetic interference shielding” Journal of Materials Engineering and Performance, Vol. 9(3), 2000, 350-354.

[31a] P. Saini, M. Arora, “Microwave absorption and EMI shielding behavior of nanocomposites based on intrinsically conducting polymers, graphene and carbon Nanotubes” Chapter 3, Intech open science, 2012, 71-112.

[32] M. S. Han, Y. K. Lee, W. N. Kim, H. S. Lee, J. S. Joo, M. Park, Y. J. Lee, C. R. Park, “Effect of multi-walled carbon nanotube dispersion on the electrical, morphological and rheological properties of polycarbonate/multi-walled carbon nanotube composite” Macromolecular Research, Vol. 17 (11), 2009, 863-869.

[33] M. Wan, 2008, “Conducting polymers with micro or nanometer structure”, Tsinghua University Press, Beijing and Springer-Verlag GmbH Berlin Heidelberg.

[34] Z. M. Dang, Y F Yu, H P Xu, J Bai, “Study on microstructure and dielectric properties of the $BaTiO_3$/epoxy resin composites” Composite Science and Technology, Vol. 68, 2008, 171-177.

[35] Z. M. Dang, J. K. Yuan, J. W Zha, T. Zhou, S. T. Li, G. H. Hud, "Fundamentals, processes and applications of high-permittivity polymer–matrix composites" Progress in Materials Science, Vol. 57, 2012, 660-723.

[36] R. K. Goyal, A. Kadam, "Polyphenylene sulphide/graphite composites for EMI shielding applications", Advanced Materials Letters, Vol. 1 (2), 2010, 143-147.

[37] G. C. Psarras, "Hoping conductivity in polymer matrix-metal particle composites", Composites: Part A, Vol. 37, 2006, 1545-1553.

[38] S. Liang, S. R. Chong, and E. P. Giannelis, "Barium Titanate/epoxy composite dielectric materials for integrated thin film capacitors" Electronic Components and Technology Conference, 1998, 171-175.

[39] D. Balaraman, P. M. Raj, S. Bhattacharya, R. R. Tummala, "Novel hydrothermal processing (>100 ºC) of ceramic-polymer composites for integral capacitor applications", Electronic Components and Technology Conference, 2002, 1699-1703.

[40] K. W. Paik, S. D Cho, J. Y. Lee, and L. G. Hyun, "low tolerance epoxy/BaTi03 composite embedded capacitor films (ECFs)", Int'l Symposium on Electronic Materials and Packaging, 2002, 341-347.

[41] S. D. Cho, K. W. Jang, J. G Hyun, S. Lee, K. W. Paik, H. Kim, J. H. Kim, "Epoxy/BaTiO3 composite films and pastes for high dielectric constant and low-tolerance embedded capacitors fabrication in organic substrates", IEEE Transactions on Electronics Packaging Manufacturing, Vol. 28 (4), 2005, 297-303.

[42] R. N. Das, F D. Egitto, J. M. Lauffer, V. R. Markovich, "Laser micromachining of nanocomposite-based flexible embedded capacitors" Electronic Components and Technology Conference, 2007, 435-441.

[43] B. Carlberg, J Norberg, J Liu, "Electrospun nano-fibrous polymer films with barium titanate nanoparticles for embedded capacitor applications" Electronic Components and Technology Conference, 2007, 1019-1026.

[44] R. N. Das, F. D. Egitto, J. M. Lauffer, V. R. Markovich, “laser micromachining of barium titanate (BaTiO3)-epoxy nanocomposite-based flexible/rollable capacitors: New approach for making library of capacitors” IEEE Transactions on Electronics Packaging Manufacturing, Vol. 31 (2), 2008, 978-103.

[45] J. G. Hyun, K. W. Paik, J. S. Pak, “Characterization of epoxy/BaTiO3 composite embedded capacitors for high frequency behaviors” Electronic Components and Technology Conference, 2009, 2046-2050.

[46] J. G Hyun, S. Dong Cho, K. W. Paik, “A study on the temperature dependence of epoxy/$BaTiO_3$ composite embedded capacitor films”, Journal of Electronic Materials, Vol. 34 (9), 2005, 1264-1269.

[47] W. Liu, B. Zhu, S. Xie, Z. Xu, “Dielectric property of polyimide/barium titanate composites and its influence factors (II)” Frontier of Chemical Engineering in China, Vol. 2 (4), 2008, 417-421.

[48] P. Thomas, S. Satapathy, K. Dwarakanath, K. B. R. Varma, “Dielectric properties of poly(vinylidene fluoride)/$CaCu_3Ti_4O_{12}$ nanocrystal composite thick films”, eXPRESS Polymer Letters, Vol. 4 (10), 2010, 632–643.

[49] R. K. Goyal, A. N. Tiwari, U. P. Mulik, Y. S. Negi, “Novel high performance Al_2O_3/poly(ether ether ketone) nanocomposites for electronics applications”, Composites Science and Technology, Vol. 67, 2007, 1802–1812.

[50] T. Hanemann, H. Gesswein, B. Schumacher, “Development of new polymer–BaTiO3-composites with improved permittivity for embedded capacitors”, Microsystem Technologies, Vol. 17, 2011, 195–201.

[51] L. A. Ramajo, M. M. Reboredo, M. S. Castro, “Characterisation of epoxy/BaTiO3 composites processed by dipping for integral capacitor films (ICF)” Journal of Materials Science, Vol. 42, 2007, 3685–3691.

[52] F. Chao, G. Liang, W. Kong, Z. Zhang, J. Wang, “Dielectric properties of polymer/ceramic composites based on thermosetting polymers”, Polymer Bulletin, Vol. 60, 2008, 129–136.

[53] J. Xu, S. Bhattacharya, K. Moon, J. Lu, B. Englert and C.P. Wong, “Large-area processable high-κ nanocomposite-based embedded capacitors”, Electronic Components and Technology Conference, 2006, 1520-1532.

[54] R. Kota, A F. Ali, B. I. Lee, M. M. Sychov, “Dielectric constant of barium titanate/cyanoethyl ester of polyvinyl alcohol composite in comparison with the existing theoretical models” Microelectronic Engineering, Vol. 84, 2007, 2853–2858.

[55] A. Qureshi, A. Mergen, M. S. Eroğlu, N. L. Singh, A. Güllüoğlu, “dielectric properties of polymer composites filled with different metals” Journal of Macromolecular Science, Part A: Pure and Applied Chemistry, Vol. 45, 2008, 462–469.

[56] J. Lu, C.P. Wong, “nanoparticle-based high-*k* dielectric composites: opportunities and challenges”, Nanopackaging: Nanotechnologies and Electronics Packaging, 2008, 121-137.

[57] W. Zheng, S. C. Wong, “Electrical conductivity and dielectric properties of PMMA/expanded graphite composites”, Composites Science and Technology, Vol. 63 2003, 225–235.

[58] C. A. Martin, J. K. W. Sandler, M. S. P. Shaffer, M. -K. Schwarz, W. Bauhofer, K. Schulte, A. H. Windle, “Formation of percolating networks in multi-wall carbon-nanotube–epoxy composites”, Composites Science and Technology, Vol. 64, 2004, 2309–2316.

[59] T. K. Das, S. Prusty, “Review on conducting polymers and their applications” Polymer-Plastics Technology and Engineering, Vol. 51, 2012, 1487–1500.

[60] P. Pötschke, S. M. Dudkin, I. Alig, “Dielectric spectroscopy on melt processed polycarbonate—multiwalled carbon nanotube composites”, Polymer, Vol. 44, 2003, 5023–5030.

[61] G. Pandey, E. T. Thostenson, “carbon nanotube-based multifunctional polymer nanocomposites” Polymer Reviews, Vol. 52, 2012, 355–416.

[62] Q Li, Q. Xue, Q. Zheng, L. Hao, X. Gao, “Large dielectric constant of the chemically purified carbon nanotube/polymer composites”, Materials Letters, Vol. 62 2008, 4229–4231.

[63] J. R. Potts, D. R. Dreyer, C. W. Bielawski, R. S. Ruoff, “Graphene-based polymer nanocomposites”, Vol. 52 (1) Polymer, 2011, 5-25.

[64] L. Cui, X. Lu, D. Chao, H. Liu, Y. Li C. Wang, “Graphene-based composite materials with high dielectric permittivity via an in situ reduction method” Physica Status Solidi A, Vol. 208 (2), 2011, 459–461.

[65] J Xu, K. S. Moon, C. Tison, C. P. Wong, “A novel aluminum-filled composite dielectric for embedded passive applications”, IEEE Transactions on Advanced Packaging, Vol. 29 (2), 2006, 295-306.

[66] F. Hussain, M. Hojjati, M. Okamoto, R. E. Gorga, “Review article: Polymer-matrix nanocomposites, processing, manufacturing, and application: An overview”, Journal of Composite Materials, Vol. 40 (17), 2006, 1511-1575.

[67] V. Singh, A. R. Kulkarni, T. R. Rama Mohan, “Dielectric properties of aluminum–epoxy composites”, Journal of Applied Polymer Science, Vol. 90, 2003, 3602–3608.

[68] Z. Ghallabi, M. Arous, A. Kallel, I. Royaud, G. Boiteux, G. Seytre, “Giant permittivity in three-phase PVDF composites” International Conference on Solid Dielectrics, Potsdam, Germany, July 4-9, 2010, 1-3.

[69] Z.-M. Dang, L.-Z. Fan, Y. Shen, C.-W. Nan, “Dielectric behavior of novel three-phase MWNTs/BaTiO3/PVDF composites”, Materials Science and Engineering B, Vol. 103, 2003, 140-144.

[70] L. Ramajo, M. S. Castro, M. M. Reboredo, “Dielectric response of Ag/BaTiO3/epoxy nanocomposites”, Journal Materials Science, Vol. 45, 2010, 106–111.

[71] S. Banerjee, K. A. Cook-Chennault, “Influence of Al particle size and lead zirconate titanate (PZT) volume fraction on the dielectric properties of PZT-

epoxy-aluminum composites, Journal of Engineering Materials and Technology, Vol. 133, 2011, 041016-1-6.

[72] S. Banerjee, K. A. Cook-Chennault, “An analytical model for the effective dielectric constant of a 0-3-0 composite”, Journal of Engineering Materials and Technology, Vol. 133, 2011, 041005-1-5.

[73] J. R. Ramsden, “Applied nanotechnology” Micro and Nano Technology Series, Elsevier, 2009, 8.

[74] D. K. Das-Gupta, K. Doughty, “Polymer-ceramic composite materials with high dielectric constants”, Thin Solid Films, Vol. 158, 1988, 93-105.

[75] A.V. Goncharenko, V.Z. Lozovski, E.F. Venger, “Lichtenecker’s equation: applicability and limitations”, Optics Communications, Vol. 174, 2000, 19–32.

[76] Y. Wu, X. Zhao, F. Li, Z. Fan, “Evaluation of mixing rules for dielectric constants of composite dielectrics by MC-FEM calculation on 3D cubic lattice”, Journal of Electroceramics, Vol. 11, 2003, 227–239.

[77] T. Zakri, J. P. Laurent, M. Vauclin, “Theoretical evidence for ‘Lichtenecker’s mixture formulae’ based on the effective medium theory”, Journal of Physics D: Applied Physics, Vol. 31, 1998, 1589–1594.

[78] M. T. Sebastian, H. Jantunen, “polymer-ceramic composites of 0-3 connectivity for circuits in electronics: A Review”, International Journal of Applied Ceramic Technology, Vol. 7 (4), 2010, 415-434.

[79] S. D. Cho, S. Y. Lee, J. G. Hyun, K. W. Paik, “Comparison of theoretical Predictions and experimental values of the dielectric constant of epoxy/$BaTiO_3$ composite embedded capacitor films”, Journal of Materials Science: Materials in Electronics, Vol. 16, 2005, 77-84.

[80] M. Olszowy, “Dielectric and pyroelectric properties of the composites of ferroelectric ceramic and poly(vinyl chloride)” Condensed Matter Physics, Vol. 6, 2(34), 2003, 307-313.

[81] G. Subodh, V. Deepu, P. Mohanan, M. T. Sebastian, “Dielectric response of high permittivity polymer ceramic composite with low loss tangent” Applied Physics Letters, Vol. 95, 2009, 062903-1-3.

[82] I. Vrejoiu1, J. D. Pedarnig, M. Dinescu, S. B. Gogonea, D. Bäuerle, “Flexible ceramic–polymer composite films with temperature-insensitive and tunable dielectric permittivity”, Applied Physics A, Vol. 74, 2002, 407–409.

[83] Z.-M. Dang, J. K. Yuan, J. W. Zha, T. Zhou, S. T. Li, G. H. Hud, “Fundamentals, processes and applications of high-permittivity polymer–matrix composites”, Progress in Materials Science, Vol. 57, 2012, 660–723.

[84] C. K. Chiang, R. Popielarz, “Polymer composites with high dielectric constant”, Ferroelectrics, Vol. 275, 2002, 1–9.

[85] Z. M. Dang, Y. F. Yu, H. P. Xu, J. Bai, “Study on microstructure and dielectric property of the $BaTiO_3$/epoxy resin composite”, Composite Science and Technology, Vol. 68, 2008, 171-177.

[86] J. G. Hyun, S. D. Cho, K. W. Paik, “A study on the temperature dependence of epoxy/$BaTiO_3$ composite embedded capacitor films”, Journal of Electronic Materials, Vol. 34 (9), 2005, 1264-1269.

[87] T. Onho, D. Suzuki, H. Suzuki, T. Ida, “Size effect for barium titanate nano-particles”, Kona, Vol. 22, 2004, 195-201.

[88] J. R. Yoon, J. W. Han, K. M. Lee, “Dielectric properties of polymer-ceramic composites for embedded capacitors” Transactions on Electrical and Electronic Materials, Vol. 10(4), 2009, 116-120.

[89] S. D. Cho, J. Y. Lee, K. W. Paik, “Effects of particle size on dielectric constant and leakage current of epoxy/barium titanate (BaTi03) composite films for embedded capacitors”, Int'l Symposium on Electronic Materials and Packaging, 2001, 63-68.

[90] K. Uchino, E. Sadanaga, T. Hirose, “Dependence of the crystal structure on particle size in barium titanate”, Journal of American Ceramic Society, Vol. 72 (8), 1989, 1555-1558.

[91] C. W. Nan, Y. Shen, J. Ma, “Physical properties of composite near percolation”, Annual Review of Materials Research, Vol. 40, 2010, 131-151.

[92] V. I. Roldughin, V. V. Vysotskii, “Percolation properties of metal-filled polymer films, structure and mechanisms of conductivity”, Progress in Organic Coatings, Vol. 39, 2000, 81-100.

[93] F. Carmona, Conducting filled polymers, Physica A, Vol. 157, 1989, 461-469.

[94] M. G. Kulthe, R. K. Goyal, Microhardness and electrical properties of PVC/Cu composites prepared by ball mill, Advanced Materials Letters, Vol. 3(3), 2012, 246-249.

[95] Z. M. Dang, B. Peng, D. Xie, S. H. Yao, M. J. Jiang, J. Bai, “High dielectric permittivity silver/polyimide composite films with excellent thermal stability”, Applied Physics Letters, Vol. 92, 2008, 112910-1-3.

[96] L. Oi, B. I. Lee, S. Chen, W. D. Samuels, G. J. Exarhos, “”High-Dielectric-Constant Silver-Epoxy-Composites as Embedded Dielectrics” Advanced Materials, Vol. 17, 2005, 1777-1781.

[97] B. S. Prakash, K. B. R. Varma, “Dielectric behavior of CCTO/epoxy and Al-CCTO/epoxy composites”, Composites Science and Technology, Vol. 67, 2007, 2363–2368.

[98] W. Bauhofer, J. Z. Kovacs, “A review and analysis of electrical percolation in carbon nanotube polymer composites”, Composites Science and Technology, Vol. 69, 2009, 1486–1498.

[99] N. G. Sahoo, S. Rana, J. W. Cho, L. Li, S. H. Chan, “Polymer nanocomposites based on functionalized carbon nanotubes” Progress in Polymer Science, Vol. 35, 2010, 837–867.

[100] B. P. Grady, 2011, Carbon nanotube–polymer composites: Manufacture, properties, and applications, John Wiley & Sons, Inc, 249-275.

[101] A. Allaoui, S. Baia, H. M. Cheng, J.B. Bai, “Mechanical and electrical properties of a MWNT/epoxy composite”, Composites Science and Technology, Vol. 62, 2002, 1993–1998.

[102] R. K. Goyal, S. D. Samant, A. K. Thakar, A. Kadam, “Electrical properties of polymer/expanded graphite nanocomposites with low percolation”, Journal of Physics D: Applied Physics., Vol. 43, 2010, 365404, 1-7.

[103] X. Huang, P. Jiang, C. Kim, Q. Ke, G. Wang, “Preparation, microstructure and properties of polyethylene aluminum nanocomposite dielectrics”, Composites Science and Technology, Vol. 68, 2008, 2134–2140.

[104] Y. J. Li, M. Xu, J. Q. Feng, “Dielectric behavior of a metal-polymer composite with low percolation threshold”, Applied Physics Letters, Vol. 89, 2006, 072902-1-3.

[105] A. Boudenne, L. Ibos, M. Fois, J.C. Majeste, E. Ge´hin, “Electrical and thermal behavior of polypropylene filled with copper particles”, Composites: Part A, Vol. 36, 2005, 1545–1554.

[106] A.S. Luyt, J.A. Molefi, H. Krump, “Thermal, mechanical and electrical properties of copper powder filled low-density and linear low-density polyethylene composites”, Polymer Degradation and Stability, Vol. 91, 2006, 1629-1636.

[107] I. Moreno, N. Navascues, S. Irusta, J. Santamaría, “Silver nanowires/polycarbonate composites for conductive films”, IOP Conf. Series: Materials Science and Engineering, Vol. 40, 2012, 012001, 1-6.

[108] P. Pötschke, A. R. Bhattacharyya , A. Janke, “Carbon nanotube-filled polycarbonate composites producedby melt mixing and their use in blends with polyethylene”, Carbon, Vol. 42, 2004, 965–969.

[109] Y. Zhu, S. Murali, M. D. Stoller, K. J. Ganesh, W. Cai, P. J. Ferreira, A. Pirkle, R. M. Wallace, K. A. Cychosz, M. Thommes, D. Su, E. A. Stach, R. S. Ruoff, “Carbon-Based Supercapacitors Produced by Activation of Graphene” Reports, Science, Vol. 332, 2011, 1537-1541.

[110] S. Stankovich, D. A. Dikin, G. H. B. Dommett, K. M. Kohlhaas, E. J. Zimney, E. A. Stach, R. D. Piner, S. T. Nguyen, R. S. Ruoff, “Graphene-based composite materials” Nature, Letters, Vol. 442, 2006, 282-286.

[111] H. Kim, A. A. Abdala, C. W. Macosko, “Graphene/polymer nanocomposites”, Macromolecules, Vol. 43, 2010, 6515–6530.

[112] N. Yousefi , X. Sun , X. Lin , X. Shen , J. J. , B. Zhang , B. Tang, M. Chan, J. K. Kim, “Highly aligned graphene/polymer nanocomposites with excellent dielectric properties for high-performance electromagnetic interference shielding”, Advanced Materials, Vol. 26, 2014, 5480–5487.

[113] J. T.Bendler, D. A. Boyles, C. A. Edmondson, T. Filipova, J. J. Fontanella, M. A. Westgate, M. C. Wintersgill, “Dielectric properties of bisphenol a polycarbonate and its tethered nitrile analogue ”, Macromolecules, Vol. 46, 2013, 4024−4033.

[114] J. J. Fontanella, D. A. Boyles, T. S. Filipova, S. Awwad, C. A. Edmondson, J. T. Bendler, M. C. Wintersgill, J. F. Lomax, M. J. Schroeder, “Dielectric studies of tetraaryl and triaryl polycarbonates and comparisons with bisphenol A-polycarbonate”, Journal of Polymer Science Part B: Polymer Physics, Vol. 50, 2012, 289–304.

[115] J. A. Brydson, 1999, “Plastics materials” Chapter 20, Seventh Edition, Butterworth-Heinemann.

[116] A. K. Bhargava, 2012, Engineering Materials, Polymers Ceramics and Composites, Chapter 2, PHI Learning, New Delhi.

[117] B. A. Higgins, W. J. Brittain, “Polycarbonate carbon nanofiber composites”, European Polymer Journal, Vol. 41, 2005, 889–893.

[118] P. Pötschke, G. M Abdel, I. Alig, S. Dudkin, D. Lellinger, “Rheological and dielectrical characterization of melt mixed polycarbonate-multiwalled carbon nanotube composites, Polymer, Vol. 45(26), 2004, 8863–8870.

[119] L. Chen, X. J. Pang, Z. L. Yu, “Study on polycarbonate/multi-walled carbon nanotubes composite produced by melt processing”, Materials Science and Engineering A, Vol. 457(1-2), 2007, 287-291.

[120] B. Hornbostel, P. Pötschke, J. Kotz, S. Roth, “Single-walled carbon nanotubes/ polycarbonate composites: basic electrical and mechanical properties”, Physica Status Solidi B, Vol. 243 (13), 2006, 3445–3451.

[121] P. Pötschke, T. D. Fornes, D. R. Paul, “Rheological behavior of multiwalled carbon nanotube/polycarbonate composites, Polymer, Vol. 43(11), 2002, 3247–3255.

[122] S. P. S. Yen and C. R. Lewis, “Structure and morphology on thermal and electrical properties of polycarbonate film capacitors” Institute of Electrical and Electronics Engineers conference, IEEE, 1990, 387-391.

[123] C.A. Harper (Editor), 2000, “Modern plastic handbook”, Chapter 1, McGraw-Hill New York San Francisco, Washington.

[124] D. E. Hudgin (funding editor), D. G. LeGrand, J. T. Bendler (Eds.), 2000, “Handbook of polycarbonate science and technology”, Chapter 13, Marcel Dekker, Inc., New York.

[125] A. Chamola, H. Singh, U.C. Naithani, S. Sharma, U. Prabhat, P. Devi, A. Malik, A. Srivastava, R.K. Sharma, “Structural, dielectric and electrical properties of Lead zirconate titanate and $CaCu_3Ti_4O_{12}$ ceramic composite”, Advanced Materials Letters, Vol. 2(1), 2011, 26-31.

[126] F. M. Pontes, E. R. Leite, M. S. J. Nunes, D. S. L. Pontes, E. Longo, R. Magnani, P. S. Pizani, J. A. Varela, “Preparation of $Pb(Zr,Ti)O_3$ thin films by soft chemical route”, Journal of the European Ceramic Society, Vol. 24, 2004, 2969–2976.

[127] L Jin, Ph.D Thesis, “Broadband Dielectric Response in Hard and Soft PZT: Understanding Softening and Hardening Mechanisms” Swiss Federal Institute of Technology, Lausanne, Switzerland, 2011, 4–5.

[128] V. D. Parvanova, M. M. Nadoliisky, “Polarization process in PZT ceramics”, Bulgarian Journal of Physics, Vol. 32, 2005, 45-50.

[129] D. M. Guldi, N. Martin (Eds.), 2010, “Carbon nanotubes and related structures: Synthesis, characterization, Fictionalization and Applications”, Chapter 1, Wiley-VCH Verlag GmbH & Co. KGaA, Weinheim.

[130] R. Ramasubramaniam, J Chen, H. Liu, “Homogeneous carbon nanotube/polymer composites for electrical applications. Applied Physics Letters Vol. 83 (14), 2003, 2928-30.

[131] P. Pötschke, B. Hornbostel, S. Roth, U. Vohrer, S. M. Dudkin, I. Alig, “Purification and percolation-unexpected phenomena in nanotube polymer composites”, In AIP conference proceedings Vol (786), Electronic Properties of Novel Nanostructures, Kirchberg, Tirol, Austria, 2005, 596-601

[132] M. M. Gallego, M. M. Bernal, M. Hernandez, R. Verdejo, M. A. Lopez-Manchado, “Comparison of filler percolation and mechanical properties in graphene and carbon nanotubes filled epoxy nanocomposites” European Polymer Journa, 2013, (Article in press), 1-7.

[133] S. Vadukumpully, J. Paul, N. Mahanta, S. Valiyaveettil, “Flexible conductive graphene/poly(vinylchloride) composite thin films with high mechanical strength and thermal stability”, Carbon, Vol. 49, 2011, 198 – 205

[134] N. K. Srivastava, R. M. Mehra, “Study of structural, electrical, and dielectric properties of polystyrene/foliated graphite nanocomposite developed via in situ polymerization”, Journal of Applied Polymer Science, Vol. 109, 2008, 3991-3999.

[135] S. Ansari, E. P. Giannelis, “Functionalized graphene sheet—poly(vinylidenefluoride)conductive nanocomposites”, Journal of Polymer Science: Part B: Polymer Physics, Vol. 47, 2009, 888–897.

[136] H.-B. Zhang, W.-G. Zheng, Q. Yan, Y. Yang, J.-W. Wang, Z.-H. Lu, G.-Y. Ji, Z.-Z. Yu, “Electrically conductive polyethylene terephthalate/graphene nanocomposites prepared by melt compounding” Polymer, Vol. 51, 2010, 1191-1196.

[137] G. Chen, W. Weng, D. Wu, C. Wu, “PMMA/graphite nanosheets composite and its conducting properties” European Polymer Journal, Vol. 39, 2003, 2329–2335.

[138] Y. P. Mamunya, V. V. Davydenko, P. Pissis, E. V. Lebedev, “Electrical and thermal conductivity of polymers filled with metal powders”, European Polymer Journal, Vol. 38, 2002, 1887-1897.

[139] A. Chakrabarti, J. Lu, J. C. Skrabutenas, T. Xu, Z. Xiao, J. A. Maguire and N. S. Hosmane, “Conversion of carbon dioxide to few-layer graphene”, Journal of Materials Chemistry, Vol. 21, 2011, 9491-9493.

[140] G. Thomas, 1962, “Transmission electron microscopy of metals” Appendix A, Wiley, New York: London.

[141] H. Schorn H, M Heβ, R Kosfeld, Solution Induced Crystallization of Polycarbonate by Thf, Integration of Fundamental Polymer Science and Technology-2. ed P J Lemstra and L. A. Kleintjens (Eindhoven: Springer), 1988, 385-388.

[142] J. Lehmann, “The observation of the crystallization of high polymer substances from the solution by nuclear magnetic resonance” Colloid and Polymer Science, Vol. 212, 1966, 167-168.

[143] R. Ranjan, R. Kumar, B. Behera, R. N. P. Choudhary, “Effect of Sm on structural, dielectric and conductivity properties of PZTceramics” Materials Chemistry and Physics, Vol. 115, 2009, 473-477.

[144] E. J. Murphy, S. O. Morgan, “The dielectric properties of insulating materials” Bell System Technical Journal, 493-512.

[145] H. Yin, S. Napolitano, A. Schönhals, “Molecular Mobility and Glass Transition of Thin Films of Poly(bisphenol A carbonate)”, Macromolecules, Vol. 45, 2012,1652−1662.

[146] Z. Ahmad, “Polymeric dielectric materials”, Intech Open Science, Chapter 1, 2012, 1-26.

[147] W. C. Liu, A. D. Li, J. Tan, H. Ye, N. B. Ming, "Prepartion and characterization of poled nanocrystal and polymer composite PZT/PC films", Applied Physics A, Vol. 81, 2005, 543-547.

[148] A. Schönhals, "Dielectric spectroscopy on the dynamics of amorphous polymer systems", Application Note Dielectric, Novocontrol GmbH, 1998, 1-17.

[149] C. V. Chanmal, J. P. Jog, "Dielectric relaxations in PVDF/$BaTiO_3$ nanocomposites", Express Polymer Letters, Vol. 2 (4), 2008, 294-301.

[150] C. Pirlot, I. Willems, A. Fonseca, J. B. Nagy, J. Delhalle, "Preparation and characterization of carbon nanotube/polycrylonitrile composites" Advanced Engineering. Materials, Vol. 4 (03), 2002, 1-11.

[151] J. Al-Osaimi, N. Alhosiny, Ali Badawi, S. Abdallah, "The effects of cnts types on the structural and electrical properties of CNTs/PMMA nanocomposite films", International Journal of Engineering & Technology IJET-IJENS Vol. 13 (02), 77-79.

[152] Z. Ni, Y. Wang, T. Yu, Z. Shen, "Raman spectroscopy and Imaging of graphene", Nano Research, Vol. 1, 2008, 273-291.

[153] H. M. Heise, R. Kuckuk, A. K. Ojha, A. Srivastava,V. Srivastava B.P.Asthana, "Charactrization of carbonaceous materials using Raman spectroscopy": a comparison of carbon nanotube filter, single- and multi- walled nanotubes, graphitised porous carbon and graphite" Journal of Raman Spectroscopy, Vol. 40, 2009, 344-353.

[154] R. A. DiLeo, B. J. Landi, R. P. Raffaelle, "Purity assessment of multiwalled carbon nanotubes by Raman spectroscopy", Journal of Applied Physics., Vol. 101, 2007, 064307-1-5.

[155] C. Journet, W. K. Maser, P. Bernier, A. Loiseau, M. L. Chapelle, S. Lefrant, P. Deniard, R. Leek, J. E. Fischer, "Large-scale production of single-walled carbon nanotubes by the electric-arc technique", Nature, Vol. 388, 1997, 756-758.

[156] L. Song, L. Ci, L. Lv, Z. Zhou, X. Yan, D. Liu, H, Yuan, Y. Gao, J. Wang, L. Liu, X. Zhao, Z. Zhang, X. Dou, W. Zhou, G. Wang, C. Wang, S. Xie, "Direct synthesis of a macroscale single-walled carbon nanotube non-woven material" Advanced Materials, Vol. 16 (17), 2004, 1529-1534.

[157] L. Dai, 2004, "Conducting polymers", Chapter 2, Intelligent Macromolecules for Smart Devices, 41-81.

[158] S. Paul, T. K. Sindhu, "Development of epoxy-aluminum nanocomposite dielectric material with low filler concentration", IEEE Transactions on Dielectrics and Electrical Insulation, Vol. 21 (2), 2014, 460-466.

[159] Y. Yang, M. C. Gupta, K. L. Dudley, R. W. Lawrence, "Conductive carbon nanofibre polymer foam structure", Advanced Materials, Vol. 17, 2005, 1999-2003.

[160] R. K. Goyal, P. A. Jagadale, U. P. Mulik, "Thermal, Mechanical, and Dielectric Properties of Polystyrene/Expanded Graphite Nanocomposites", Journal of Applied Polymer Science, Vol. 111**,** 2009**,** 2071-77.

[161] M. Kovich, G. R. Rowland Jr., "Antistatic polycarbonate/copper oxide composite" A technical report, Johnson Space Center.

[162] M. Li, Y. Deng, Y. Wang, Y. Zhang, J. Bai, "High dielectric properties in a three-phase polymer composite induced by parallel structure", Materials Chemistry and Physics, Vol. 139, 2013, 865-870.

[163] Z. Zhang, Y. Gu, S. Wang, M. Li, J. Bi, Z. Zhang, "Enhancement of dielectric and electrical properties in BT/SiC/PVDFthree-phase composite through microstructure tailoring", Composites: Part A, Vol. 74, 2015, 88–95.

BIO-DATA OF THE AUTHOR

Pramod Kumar Sain was born on 22 September, 1984. He completed B.Sc. from University of Kota, Kota, Rajasthan in 2006. He did M.Sc. (Physics) from department of Physics, University of Rajasthan in 2008. In 2010, he completed M.Tech. in Metallurgical and Materials Engineering with Gold Medal from Malaviya National Institute of Technology Jaipur.

He has been pursuing Ph.D. since July, 2010 at Malaviya National Institute of Technology. He has been working in the field of polymer nanocomposites and having the Ph.D. title “Preparation and Studies on Polycarbonate Matrix Nanocomposites for Electronic Applications”.

He has published 2 conference and 1 International SCI research papers from his M.Tech. work. So far, from Ph.D. work, he has published 3 International SCI research articles. He also presented a paper in National Seminar.

Presently he is lecturer of Physics, in Government Polytechnic College, Bharatpur, Rajasthan.